DEVELOPMENT OF INDIUM TIN OXIDE (ITO) NANOPARTICLE INCORPORATED TRANSPARENT CONDUCTIVE OXIDE THIN FILMS

A THESIS SUBMITTED TO
THE GRADUATE SCHOOL OF NATURAL AND APPLIED SCIENCES
OF
MIDDLE EAST TECHNICAL UNIVERSITY

BY

HAKAN YAVAŞ

IN PARTIAL FULFILLMENT OF THE REQUIREMENTS
FOR
THE DEGREE OF MASTER OF SCIENCE
IN
METALLURGICAL AND MATERIALS ENGINEERING

JULY 2012

Approval of the thesis:

DEVELOPMENT OF INDIUM TIN OXIDE (ITO) NANOPARTICLE INCORPORATED TRANSPARENT CONDUCTIVE OXIDE THIN FILMS

submitted by **HAKAN YAVAŞ** in partial fulfillment of the requirements for the degree of **Master of Science in Metallurgical and Materials Engineering, Middle East Technical University** by

Prof. Dr. Canan Özgen
Dean, Graduate School of **Natural and Applied Sciences** ___________

Prof. Dr. C. Hakan Gür
Head of Department, **Metallurgical and Materials Engineering** ___________

Assoc. Prof. Dr. Caner Durucan
Supervisor, **Metallurgical and Materials Eng. Dept., METU** ___________

Examining Committee Members:

Prof. Dr. M. Vedat Akdeniz
Metallurgical and Materials Engineering Dept., METU ________________

Assoc. Prof. Dr. Caner Durucan
Metallurgical and Materials Engineering Dept., METU ________________

Prof. Dr. Kadri Aydınol
Metallurgical and Materials Engineering Dept., METU ________________

Assoc. Prof. Dr. Burcu Akata Kurç
Department of Micro and Nanotechnology, METU ________________

Assist. Prof. Dr. H. Emrah Ünalan
Metallurgical and Materials Engineering Dept., METU ________________

Date: 03.07.2012

I hereby declare that all information in this document has been obtained and presented in accordance with academic rules and ethical conduct. I also declare that, as required by these rules and conduct, I have fully cited and referenced all material and results that are not original to this work.

Name, Last Name : Hakan YAVAŞ

Signature :

ABSTRACT

DEVELOPMENT OF INDIUM TIN OXIDE (ITO) NANOPARTICLE INCORPORATED TRANSPARENT CONDUCTIVE OXIDE THIN FILMS

Yavaş, Hakan
M.Sc., Department of Metallurgical and Materials Engineering
Supervisor: Assoc. Prof. Dr. Caner Durucan

July 2012, 108 pages

Indium tin oxide (ITO) thin films have been used as transparent electrodes in many technological applications such as display panels, solar cells, touch screens and electrochromic devices. Commercial grade ITO thin films are usually deposited by sputtering. Solution-based coating methods, such as sol-gel however, can be simple and economic alternative method for obtaining oxide films and also ITO. In this thesis, “ITO sols” and “ITO nanoparticle-incorporated hybrid ITO coating sols” were prepared using indium chloride ($InCl_3{\cdot}4H_2O$) or indium nitrate ($InNO_3{\cdot}xH_2O$) and tin nitrate ($SnCl_4{\cdot}5H_2O$) precursors in order to form transparent conductive films on glass. The specific objectives of the study were two-fold. The first objective was to investigate the effect of sol-gel processing variables; heat treatment temperature (350º-600 ºC), spin coating process parameters (rate and time), number of coating operations (1, 2, 4, 7 and 10 layers) and sol aging on the electrical/optical/microstructural properties of ITO thin films (*plain ITO thin films*). The results showed that, highly transparent (97 % in the visible region) and moderately conductive (1.2 kΩ/sqr) ITO thin films can be obtained after calcination in air at 550 ºC by optimization of the coating sol concentration. The surface coverage and thickness of thin films can be controlled by spin rate-time and number of coatings. In addition, it was found that, induce-aging (at temperatures < 100 °C, for several hours) of the premature coating sol prior to deposition can be a practical tool for controlling/modifying the physical properties of the plain ITO films. In the second part of the study, the effect of nanoparticle incorporation into the ITO sols at different extent on optoelectronic and microstructural properties of ITO thin films were reported (*hybrid ITO thin films*). Initially, parametric colloidal chemistry studies were performed in defining the conditions for obtaining stable ITO suspensions that can incorporated into the ITO sol. Then, the reasons and structural/chemical controlling factors leading to improvements in the functional properties for these hybrid films are presented and thoroughly discussed, compared to the properties of their plain (unmodified) counterparts.

Keywords: sol-gel, optoelectronics, ITO thin films, transparent conductive oxides

ÖZ

İNDİYUM KALAY OKSİT (ITO) NANOPARÇACIK KATKILI ŞEFFAF İLETKEN İNCE FİLMLERİN GELİŞTİRİLMESİ

Yavaş, Hakan
Yüksek Lisans, Metalurji ve Malzeme Mühendisliği Bölümü
Tez Yöneticisi: Doç. Dr. Caner Durucan

Temmuz 2012, 108 sayfa

İndiyum kalay oksit (ITO) ince filmler görüntü ekranları, güneş hücreleri, dokunmatik ekranlar ve elektrokromik cihazlar gibi pek çok teknolojik uygulamada şeffaf elektrot olarak kullanılmaktadır. ITO ince filmler ticari kullanım amaçlı olarak genellikle sıçratma tekniği ile üretilmektedir. Öte yandan, sol-jel gibi sıvı bazlı kaplama teknikleri, oksit ve ITO filmlerin üretiminde basit ve alternatif bir teknik olarak öne çıkmaktadır. Bu tez çalışmasında, cam üzerinde şeffaf-iletken filmler oluşturmak için indiyum klorür ($InCl_3 \cdot 4H_2O$) ya da indiyum nitrat ($In(NO_3)_3 \cdot xH_2O$) ve kalay klorür ($SnCl_4 \cdot 5H_2O$) kullanılarak yalın ITO ve melez ITO nanoparçacık eklentisi yapılmış kaplama çözeltileri hazırlanmıştır. Çalışmanın özelleştirilmiş hedefleri iki yönlüdür. İlk amaç, ısıl işlem sıcaklığı (350 º- 600 ºC), döndürmeli kaplama süreç değişkenleri (hız ve süre), kaplama işlem sayısı (1, 2, 4, 7 ve 10 kat) ve çözelti yaşlanması sol-jel süreç değişkenlerinin ITO ince filmlerin (yalın ITO ince filmler) elektriksel/optik/mikroyapısal özellikleri üzerine etkisi incelenmiştir. Sonuçlar yüksek şeffaflıkta (görünür bölgede % 97) ve orta derecede iletkenlik (yaprak direnci: 1.2 kΩ/sqr) gösteren ITO ince filmlerin, kaplama çözeltisi kontrol edilerel

550 ºC hava ortamında işlem sonucunda sonucunda üretilebildiğini göstermektedir. Üretilen filmlerin yüzey kaplama özellikleri ve kalınlığı, döndürmeli kaplama hızı-süresi ve kaplama işlem sayısı ile kontrol edilebilmiştir. Buna ek olarak, uyarılmış-yaşlandırma işleminin (farklı sürelerde 100 ºC altındaki sıcaklılarda) yalın ITO ince filmlerin fiziksel özelliklerini iyileştirmek/kontrol etmek için pratik bir yöntem olduğu saptanmıştır. Çalışmanın ikinci bölümünde, ITO kaplama çözeltisi içerisine farklı miktarlarda ITO nanoparçacık eklentisinin ITO ince filmlerin (melez ITO ince filmler) optik-elektronik ve mikroyapısal özellikleri üzerine olan etkisi sunulmuştur. Öncelikle, ITO kaplama çözeltisi içerisine eklenecek olan ITO nanoparçacık süspansiyonlarının durağanlık koşullarının belirlenmesi amacıyla bir dizi koloid kimyası araştırması yapılmıştır. Sonra, bu melez filmlerin fonksiyonel özellıklerinde ıyıleşmelere yol açan yapısal ve kimyasal faktörler tartışılmış ve yalın (eklenti yapılmamış) muadilleri ile karşılaştırılmıştır.

Anahtar kelimeler: sol-jel, optoelektronik, ITO ince filmler, şeffaf iletken oksitler

To my family...

I am to wait, though waiting so be hell;

Not blame your pleasure, be it or well…

W.S.

ACKNOWLEDGEMENTS

First of all, I would like to express my gratitude to Dr. Caner Durucan for giving me the opportunity to realize this study under his guidance, also for his support and patience with friendly attitude. I could not get through this task without his help, comments...

I extend my sincere thanks to Dr. Emrah Ünalan for his intense help and friendship and Dr. Vedat Akdeniz for allowing me to use his lab facilities.

I would like to thank Dr. İbrahim Çam at METU Central Laboratory for his help in AFM analysis.

I owe my deepest gratitude to my colleagues – Özlem Altıntaş Yıldırım, Tümerkan Kesim, Gözde Alkan, Onur Rauf Bingöl and Özgecan Dervişoğlu. I will never forget the chats, laughs, discussions. The atmosphere has always been a perfect source of motivation.

I also would like to show my gratitude to Fatih Pişkin, Şahin Çoşkun, Emre Mülazımoğlu, Nihat Ali Işıtman and Murat Güneş who were always willing to help and discuss.

Special thanks to Damla Dilber, Sezgi Kumru and Caner Erdem for their endless encouragement and support.

I want to thank Tuğçe Yıldız for her understanding and support during all the years of my study. *I couldn't have done it without you…*

Lastly and most important, my everlasting gratitude goes to my father, mother, sister and brother for their continuous support and love. This thesis is dedicated to them.

TABLE OF CONTENTS

CHAPTERS

LIST OF FIGURES

FIGURES

LIST OF TABLES

TABLES

LIST OF ABBREVIATIONS

Abbreviation	
4-pt	Four point
N	Carrier concentration
μ	Mobility
AcAc	Acetylacetone
$\mathbf{E_g}$	Band energy
HCl	Hydrochloric acid
ITO	Indium tin oxide
ITONP	Indium tin oxide nanoparticle
JCPDS	Joint Committee on Powder Diffraction Standards
kΩ/sqr	Kilo ohm per square
M	Molarity
PVD	Physical vapor deposition
rpm	Rate per minute
SEM	Scanning electron microscopy
SLS	Soda-lime-silicate
TCO	Transparent conductive oxide
UV-Vis	Ultra violet visible
XRD	X-ray diffraction

CHAPTER 1

INTRODUCTION

1.1. General introduction and rationale of the thesis

Transparent conductive oxides (TCOs) have been used in many applications and devices that we use every day. TCOs offer unique features of optical transparency in the visible range and high electrical conductivity. These applications are mostly in photovoltaics, light emitting diodes (LEDs) flat panel displays (FPDs) and smart windows. In the last fifty years, there have been many processing efforts for enhancing optical and electrical performance of TCOs. However, there is a still a demanding need for TCOs with better optical and electrical properties. That is particularly due to need in high mass production of flat panel displays and smart phones with economically feasible production costs. This has been motivated many researchers to carry out studies to explore more economical production techniques and alternative processing approaches for making TCOs.

Conventional TCOs are oxide ceramics, such as, In_2O_3, ZnO, SnO_2 and CdO. All these materials are wide band gap semiconductors and the electrical properties of these materials can be modified by alloying and doping. Indium or tin doped cadmium oxide is the highest electrically conductive TCOs. However, due to toxicity of cadmium oxide or cadmium based oxides, the use of these materials are avoided in consumer products. Currently, indium tin oxide (ITO) thin films are most extensively used TCOs due to its wide band gap (approximately 4.0 eV), high electrical conductivity and optical transparency. ITO is generally used as electrode material, especially in large area flat panel displays.

Commercial grade ITO thin films are usually produced by vacuum-based deposition techniques (sputtering, thermal evaporation, etc.) and wet/aqueous techniques. Sputtering is the most preferred production technique leading to an optical transparency in the order of 95 % and minimum electrical resistivity 4×10^{-5} Ωcm. However, sputtering is expensive due to use of sophisticated instruments, high vacuum need. It is also applicable to only planar substrates. Therefore, optoelectronic industries are searching for alternative low cost and competitive methods to fabricate ITO thin films. Among alternative fabrication methods, sol-gel processing is a promising candidate for its easiness, low cost and ability to coat different geometrically shaped substrates. This method is based on transformation of liquid solution *(sol)* to a dense solid oxide layer *(gel)* via hydrolysis-condensation reactions at around room temperature followed by relatively low (~400- 500 ºC) thermal treatments for maturing the product.

For sol-gel processing, coating methods (spray, dip and spin coating), coating thickness, heat treatment temperature and coating sol molarity are some of the important parameters which may affect the performance of ITO thin films. In addition, chemical stability and modification of sol can also lead microstructural variations in the ITO thin films which can be also critical for the final properites.

The basic objectives of this thesis are;

i. Establishing correlations between selected sol-gel processing variables including the spin coating parameters, number of coating operations, heat treatment temperature, sol molarity and sol aging on the electrical/optical/microstructural properties of sol-gel derived ITO films.

ii. Establishing novel processing routes for making hybrid ITO thin films. This was realized by physical incorporation of ITO nanoparticles into ITO sols. These studies included developing and understanding mechanisms for obtaining stable ITO nanoparticle suspensions in organic solvents. Thereafter, adding these suspensions into ITO sol and investigation of electrical/optical/microstructural properties of these nanoparticle:sol dual nature films have been accomplished.

Various analytical techniques were employed for characterization of sol-gel ITO thin films. The optical properties of ITO thin films are measured by UV-Vis spectrophotometer. The surface morphology and microstructure of thin films was examined by SEM and AFM. The electrical resistivity of thin films was tested by four-point probe testing equipment. Meanwhile, the structural/phase properties were investigated by XRD.

1.2. Structure of thesis

There are five chapters in this thesis. In the *first chapter –Introduction-* the general motivation, objective and structure of the thesis has been described.

In C*hapter 2,* the history, the technical knowledge and the related literature on TCOs are presented. The market figures, emerging applications and electrical and optical properties of TCOs are introduced. The TCO film formation methods such as, chemical vapor deposition (CVD), physical vapor deposition (PVD) and solution-based processing techniques of TCOs are discussed.

Chapter 3 is firstly presents brief information on properties of ITO thin films, and then some important performance-defining processing parameters for sol-gel ITO thin films are discussed. In the following section of this chapter experimental details for processing of plain ITO coatings are given. The analytical characterization equipments and the details of characterization techniques are also introduced in this section. Furthermore, the results and details of the effects of spin coating rate, spin coating time, number of coatings, post coating heat treatment temperature, sol molarity and induce aging on optical, electrical and microstructural properties of thin films are presented and discussed.

Chapter 4 is on ITO nanoparticle-incorporated hybrid ITO thin films. First, gives information and background on colloidal stabilization techniques and literature review of ITO nanoparticle incorporation into ITO sol. In following section, details of experimental procedures and analytical characterization techniques are described. At the end, the effect of ITO nanoparticle incorporation on optical, electrical and structural properties of ITO thin films discussed.

Finally, the conclusions are presented in *Chapter 5.*

CHAPTER 2

TRANSPARENT CONDUCTIVE OXIDES

2.1. General introduction: transparent conductive oxides

The transparent conductive oxide (TCO) thin films have high optical transmittance, higher than 80 % in the visible range (400- 700 nm) and high electrical conductivity (resistivity values around 10^{-3}- 10^{-4} Ωcm). Both electrical conductivity and optical transparency are key properties for the TCOs and can these be achieved by two material groups. A few atomic layer thin (about 10 nm) metallic thin films can be defined as *first group*. Silver, gold, iron, copper are some dominant materials in this group. The optical transparency is reached maximum 50 % and can be improved by antireflective thin film coatings [1]. The electrical conductivity is related with thin film thickness and decreases with decreasing film thickness where optical transparency reaches maximum. The wide band gap semiconductor thin films are the *second group.* Visible light is a kind of electromagnetic radiation. In 400- 700 nm wavelength part of the spectrum, energy range is between 3.1 to 1.8 eV. This energy range directly influences the materials optical properties. If materials band gap energy is less than 1.8 eV it will be opaque to that radiation (visible light). In this case, light will be absorbed by electron transitions from the valence band to conduction band. If materials band gap energy is higher than 3.1 eV it will be transparent to light. However, in this case due to large band gap, material has no or little electrical conductivity. The solution for obtaining conductive and transparent material therefore is degenerating high band gap material by appropriate dopants. In 1907, Badeker et al. reported optical transparency and electrical conductivity in cadmium oxide [2]. Badeker sputtered cadmium oxide coating and heat treated at ambient conditions. The heat treatment process led to formation of oxygen vacancies $(V_O^{\bullet\bullet})$ in the cadmium oxide lattice. This oxygen defects formed energy levels which led to generation of conduction band. This system was the first experimental study on n-type TCOs.

The first TCO patents were filed for doped and un-doped tin oxide in 1931 [3] and 1942 [4]. TCO products were first used in World War II as aircraft windshield deicers [5]. In following decades indium-based and zinc-based TCOs have been produced. In 1971 indium tin oxide (ITO) and aluminum doped zinc oxide (AZO) thin films were developed. After that time there have been tremendous efforts in improving the performance of tin oxide, indium oxide and zinc oxide thin films. In the last decade many binary [6-8] and ternary [8,9] complex TCO compositions have been investigated as new alternatives. Typical binary oxides are; SnO_2, In_2O_3, ZnO, CdO, Ga_2O_3, Tl_2O_3, Pb_2O_3, and Sb_2O_5. Typical ternary and quaternary oxides are; $CdSnO_4$, $CdSnO_3$, $CdInO_4$, $ZnSnO_4$, $MgInO_4$, $CdSb_2O_6$:Y, $GaInO_3$, $Zn_2In_2O_5$ and $In_4Sn_3O_{12}$. The basic compositional space for oxide-based TCOs is shown in Figure 2.1.

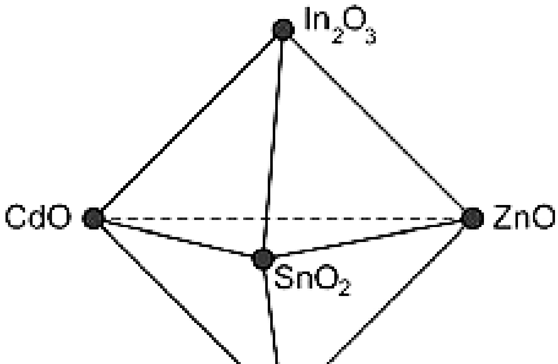

Figure 2.1 Basic compositional space of conventional TCOs [10].

Many of these materials mentioned above are n-type (metal type conductivity) semocinductors. Mostly, TCOs are n-type enabling oxygen vacancies or cation interstitials in their lattice [11]. Alternatively, development of p-type TCOs with reasonable electrical conductivities has been another major research challenge. In 1990s Kawazoe and Hosono were studied Cu based $CuAlO_2$ [12] and $SrCu_2O$ [13]. These two oxides were p-type but their doping level ($N< 10^{18}/cm^3$) and mobilities ($\mu< 1cm^2/V$) were relatively lower than their n-type counterparts. Early 2000s many research groups started to study novel p-type TCOs which based on making ZnO p-type and act as a high performance optoelectronic material similar to GaAs [14,15]. However there are still problems in fabricating p-type TCOs in a reproducible manner. Nowadays many research groups are still working in this topic and trying to control the band gap by addition of magnesium, cadmium and cobalt. Finally, Tsukazaki et.al. have developed p-type nitrogen doped ZnO [16] by laser molecular beam epitaxy technique which shows relatively better optoelectronic performance. In literature many of n-type and p-type TCOs were reported with different processing routes and optical and electrical properties. In Table 2.1 selected critical properties of some TCOs are listed.

Currently tin doped indium oxide (In_2O_3) or indium tin oxide (In_2O_3:Sn or ITO), fluorine doped tin oxide (SnO_2:F or FTO) and aluminum doped zinc oxide (ZnO:Al or AZO) thin films are typically used in many applications. These materials uses extrinsic dopant species for generating n-type electrical conduction, in particular ITO is the first and mostly used modern TCOs which was discovered in 1954 by Rupperecht [17].

Besides oxide based TCOs emerging interest is in organic transparent conductors driven by optoelectronic community. The new polymeric TCO candidates are; intrinsically conducting polymers [18], charge transfer polymers, such as PEDOT: PSS [19,20], carbon nanotubes (CNTs) [21,22]. These materials have significant importance for the OLED, flexible electronic and polymer photovoltaic industries because of the potential efficient processing conditions and high optoelectronic performance. The typical electrical conductivities for organic TCOs are in the range of 2- 1200 S/cm.

Table 2.1 Functional properties of TCOs. (Reproduced from [23])

TCO	DOPE TYPE	COATING METHOD	P (Ωcm)	T (%)	E_g (eV)	n (cm^{-3})	μ ($cm^2/s/V$)
SnO_2	n-type	Spray	$4.3x10^{-3}$	97	4.11		
SnO_2	n-type	Sputtering	$6.1x10^{-3}$	95	4.13	$1.3x10^{20}$	7.7
SnO_2:F	n-type	Spray	$5x10^{-4}$	80	4.41	$4.6x10^{20}$	28
SnO_2:Mo	n-type	Reactive Ev.	$5x10^{-4}$	85	4.10	$8x10^{20}$	10
SnO_2:Sb	n-type	Spray	10-^{3}	85	3.75	$2x10^{20}$	10
Cd_2SnO_4	n-type	Sputtering	$5x10^{-4}$	80		$5x10^{20}$	40
Cd_2SnO_4	n-type	Sputtering	$5x10^{-4}$	93	2.7	$5x10^{20}$	22
$CdIn_2O_4$	n-type	Sputtering	$2.7x10^{-4}$	90	3.24	$4x10^{20}$	57
$In_4Sn_3O_{12}$	n-type	Sputtering	$3.5x10^{-4}$	80	3.5	$7x10^{20}$	11.5
In_2O_3	n-type	Thermal Ev.	$2x10^{-4}$	90	3.56	$4x10^{20}$	70
In_2O_3	n-type	PLD	$2x10^{-4}$	86		$9x10^{20}$	37
In_2O_3:F	n-type	CVD	$2.9x10^{-4}$	85	3.5		
$GaInO_3$	n-type	Sputtering	$2.5x10^{-3}$	90		$4x10^{20}$	10
ITO	n-type	E-Beam Ev.	$2.4x10^{-4}$	90	3.85	$8x10^{20}$	30
ITO	n-type	CVD	$1.7x10^{-4}$	90	3.9	$8.8x10^{20}$	43
ITO	n-type	Sputtering	$2.4x10^{-4}$	95	4	$1x10^{20}$	12
ITO	n-type	PLD	$8.5x10^{-5}$	85		$1.4x10^{21}$	53.5
ITO	n-type	Sol-Gel	$5x10^{-3}$			$1.9x10^{20}$	12
ITO:F	n-type	Sputtering	$6.7x10^{-4}$	80		$6x10^{20}$	16
In_2O_3:Mo	n-type	Sputtering	$5.9x10^{-4}$	90	4.3	$5.2x10^{20}$	20.2
ZnO	n-type	Reactive Ev.	10^{-3}	88	3.3	10^{20}	10
ZnO	n-type	Sputtering	$2x10^{-3}$	80		$1.2x10^{20}$	16
ZnO:Al	n-type	Sputtering	10^{-2}	90	3.52	$4.7x10^{20}$	1.47
ZnO:Al	n-type	CVD	$3.3x10^{-4}$	85		$8x10^{20}$	35
ZnO:Al	n-type	PLD	$3.7x10^{-4}$	90	3.8	$8x10^{20}$	18
ZnO:Ga	n-type	Sputtering	10^{-3}	85	3.59	$10x10^{20}$	10
ZnO:In	n-type	Sputtering	$2x10^{-2}$	80	3.29	$7x10^{19}$	1.9
$Zn_3In_2O_6$	n-type	PLD	$1x10^{-3}$	85	3.4	$4x10^{20}$	20
$ZnSnO_3$	n-type	Sputtering	$4x10^{-3}$	80		10^{20}	10
$CuAlO_2$	p-type	PLD		70	3.5	$2.7x10^{19}$	0.13
$CuAlO_2$	p-type	CVD		70	3.75	$1.8x10^{19}$	0.16
$SrCuO_2$	p-type	PLD		75	3.3	$6.1x10^{17}$	0.46
$CuYO_2$:Ca	p-type	Thermal Ev.		50	3.5		1
$AgCoO_2$	p-type	Sputtering		50	4.15		
$CuGaO_2$	p-type	PLD		80	3.2	$1.7x10^{18}$	0.23
ZnO:P	p-type	Sputtering		80	3.35	10^{17}	0.53
ZnO:N	p-type	PLD		85		$6x10^{18}$	0.1

P: electrical resistivity, T: optical transmittance, E_g: band energy, n: carrier concentration and μ: mobility

2.2. TCO market

The commercial TCOs are restricted to only small group of oxides i.e. ITO, FTO and AZO. The current dominant markets for TCOs are; functional window applications such as smart windows, flat panel displays and photovoltaics industry. Energy efficient windows are efficient in preventing radiative heat loss and generally produced by tin oxide coatings. Due to their low thermal emittance these type of windows are ideal for daily use in cold environments/climates [24]. In 2007, the annual demand for energy efficient windows in Europe was 60x10^6 m^2 and increased every following year [25]. Same year in China this demand was reached to 97 x10^6 m^2 but domestic production capacity was only 50 x10^6 m^2. Additionally, demands from automotive, photovoltaic and display industries also increases production capacity stress on low thermal emittance windows [26].

The flat panel display market is another dominant market with high annual production volume. World Flat Panel Display Markets community demonstrated that market revenue reaches to 125.32 billion US dollars in 2012 as shown in Figure 2.2 [27].

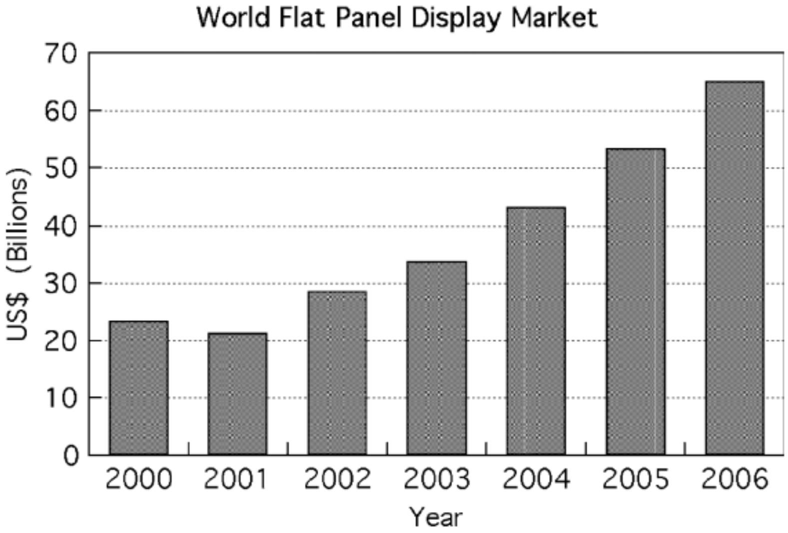

Figure 2.2 Total world FPD market revenue [27].

The third and fastest growing market is solar cells or photovoltaics. For single crystal and polycrystalline solar cell applications which represent about 93 % of whole photovoltaic industry, TCOs are very important. For example, in typical heterojunction photovoltaic cells (Figure 2.3) both front and back contacts are made by TCOs. Figure 2.4 shows projected market growth of photovoltaic industry with a growing rate of 15- 30 % per year. In 2007, this market shows 50 % growing rate without showing any decline.

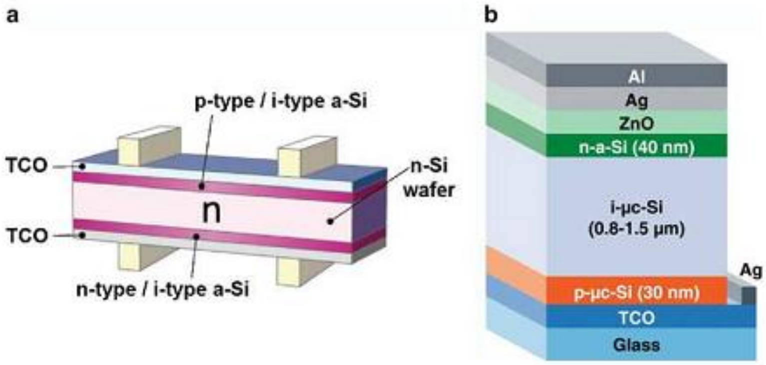

Figure 2.3 Multilayered formation of typical heterojunction photovoltaic cell [26].

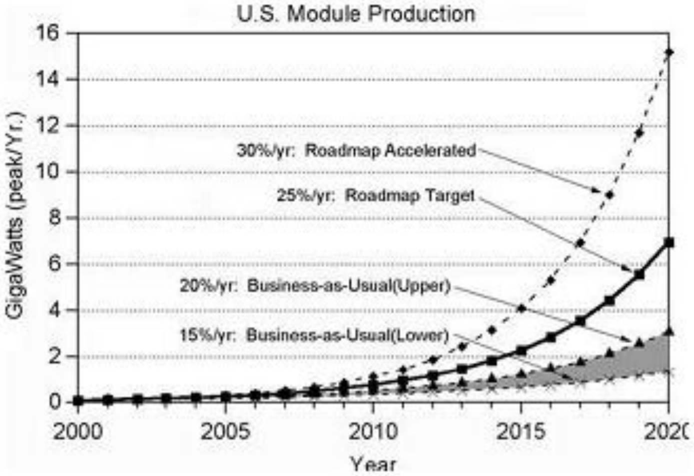

Figure 2.4 Total world flat panel display (FPD) market revenue [26].

2.3. Applications and technological uses of TCOs

In the last decades TCO has extraordinary impact on many different technological applications and today these materials are used in numerous practical systems. These applications are mostly related with solar cells, display technologies (high-definition televisions including liquid crystal displays (LCD), plasma and organic light emitting diode based displays) flat screens for portable smart computers, energy-efficient low-emittance windows, electrochromic windows and touch screens (smart phones and displays).

The applications of the TCOs can be classified into two main categories.

1) The applications of transparent thin films electrodes, heat mirror glazings and photovoltaics where high electrical conductivity and optical transparency is required.

2) The photocatalysis and gas sensor applications depending on the nature of semiconducting materials where the population of free electron in the conduction band is not significant.

2.3.1. Photovoltaics

TCOs are used to satisfy the potential demand for thin film electrodes in the photovoltaic industry. The typical commercial solar cells are amorphous silicon solar cells, dye sensitized solar cells (DSSC) and polymer-based solar cells [29,30]. Crystalline silicon solar cells have large crystal grains and comparatively few imperfections; therefore, high electron mobilities can be achieved in the core layer. Because crystalline silicon solar cells have high mobility, thin metal wires can be evaluated as the top electrode on the solar cells. On the other hand, electron mobility is reduced with development of the new generation of polycrystalline or amorphous thin films [31]. This lower mobility reduces the usability by reason of the increment in lateral resistance on the surface of solar cell. Such thin films have transparent conducting thin films electrode used as the top layer on solar cells. These highly conductive thin films maintain the high transmittance of the light while preventing lateral resistive losses on the top electrode surface layer of the solar cell. [32]. The representative structure of a photovoltaic cell is given in Figure 2.5.

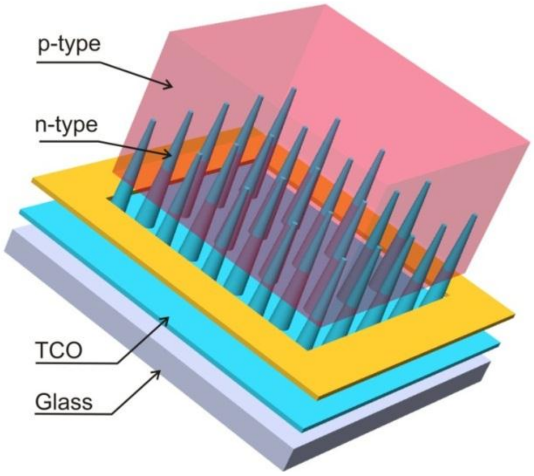

Figure 2.5 Representative structure of a photovoltaic cell build on a TCO-coated glass [33].

2.3.2. Gas sensors

A chemical gas sensor is the device which reacts according to impulse reaction of chemical stimulus. The change in chemical conductivity is the basic working mechanism of an electrical semiconducting gas sensor which can detect changes in the chemical environment. These semiconducting materials can detect differences in composition of the atmosphere and react according to electrical circuit measurement. The resulting in a change of resistance is then used for response of device. The critical parameter to enhance the performance of gas sensor is choosing the adequate semiconductor material depending on the specific application.

The conductivity need to be satisfied under some specific properties like response stability, sensitivity and selectivity, and lastly it should be able to show large conductance change once the gas species are adsorbed. As well as the material selection, morphology is critical parameter in order to control the quality of device. According to these parameters, ZnO, SnO_2, TiO_2 and In_2O_3, WO_3 and MoO_3 are the metal oxide gas sensors which show high performance [34].

2.3.3. Touch screens

Touch screens (also called touch panels) are another application of optoelectronic devices. Electrical conduction is obtained through mechanically attaching two conducting panes. Such electrical and transparent switches are important devices which control the electrical transport in some applications such as railway and air traffic control systems, and automatic ticket-vending machines (ATVMs) [35]. For these applications, the requirement of the sheet resistance and transmittance for coating deposits are expected to be < 1 kΩ and >80 %, respectively. Two important features which are high mechanical durability and easy to etch come forward in order to evaluate low-cost transparent conduction materials. Representative layered structure of touch screen panels is given in Figure 2.6.

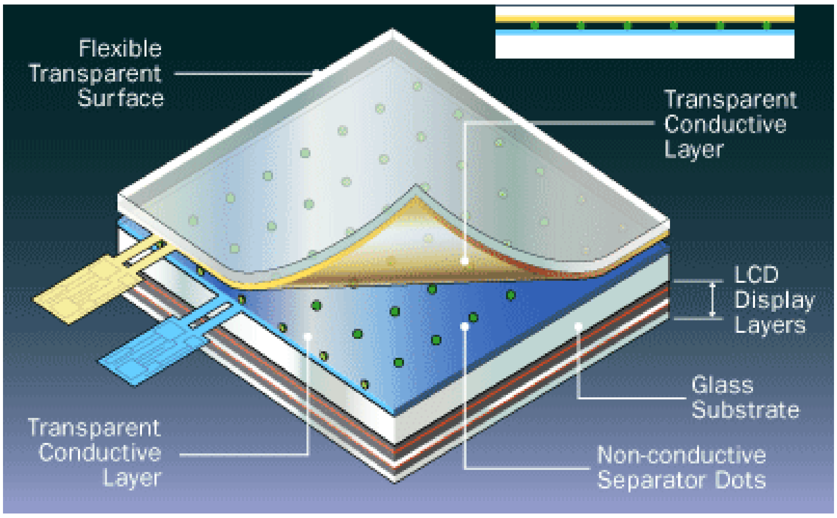

Figure 2.6 Multi-layered structure of touch screen panel constructed on TCO-coated glass substrate [36].

2.3.4. Functional glasses

The other application area for TCOs is functional glasses which are used for thermal management in architectural, automotive and aerospace applications. Thermal management is an important design factor based on the electrically activation of window glass which is called electrochromic (EC) windows. TCOs provide heat efficiency by acting as a filter that blocks the infrared. It remains transparency while reflects the infrared. TCO-coated windows reflect heat back during winter season and absorb the heat in hot climates. As well as the heat efficiency, TCO-coated windows (also called low-emissivity glass) are beneficial because of its cost-effectiveness comparing to double glazing. Operation stages of electrochromic windows is given in Figure 2.7. Despite the several developments of TCOs, SnO_2 is the one advantageous choice due to the lower cost of direct-spray pyrolysis of tin chloride. On the other hand, ITO has more thermal benefits for high-value aircraft applications, and offers additional functions such as de-misting and de-icing windows, and anti-glaring

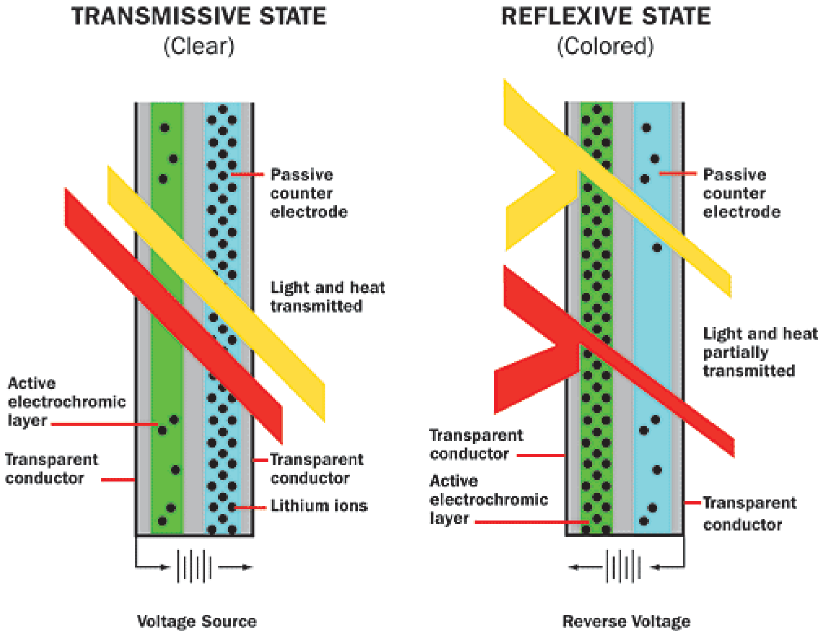

Figure 2.7 Operation modes of typical electrochromic window [37].

2.3.5. Flat panel displays

Flat panel displays (FPDs) are offered in a variety of application, such as instrument panels for airplanes and automobiles, electronics, phones, video displays systems, displays for the medical and military industry. The design of device and optical enhancements should be combined well to meet the diverse requirements of different applications. TCO has the significant role in all application, and used as a transparent conducting electrode which is transmitting each pixel on the screen. The function of TCO is basically same and is used for same purpose in spite of the variety of display types. Figure 2.8 shows the schematic illustration of typical FPDs [38].

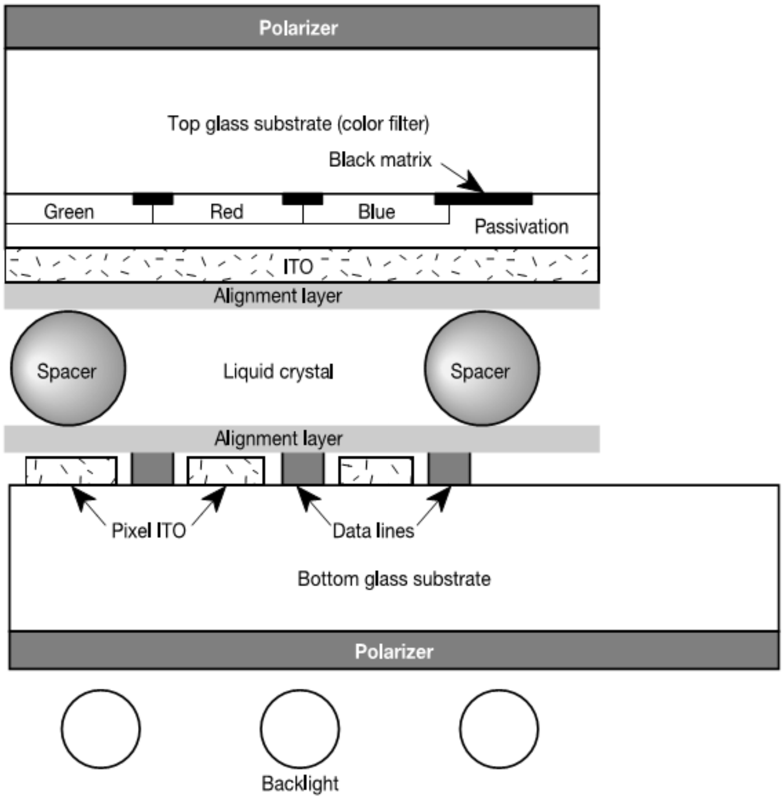

Figure 2.8 The schematic representation of basic elements of FPD [38].

2.3.6. Electromagnetic shielding

The electromagnetic shielding which used for video display terminals is one of the promising applications for TCOs. Shielding properties are considered according to requirements of industry standards [39]. High transmissivity and modest resistivity (2000 ohm/sqr) are demanded for such application. However, the resistivity requirements for electromagnetic shielding which may need to be considered during design process in order to add benefit on the anti-static function are reduced due to these standards [40]. The technologies of sputtering, polymer lamination, and spin-coating of a water-based ITO powder suspension can be used for production of these multilayer thin films. Multi-layered structure of electromagnetic shielding film is given in Figure 2.9.

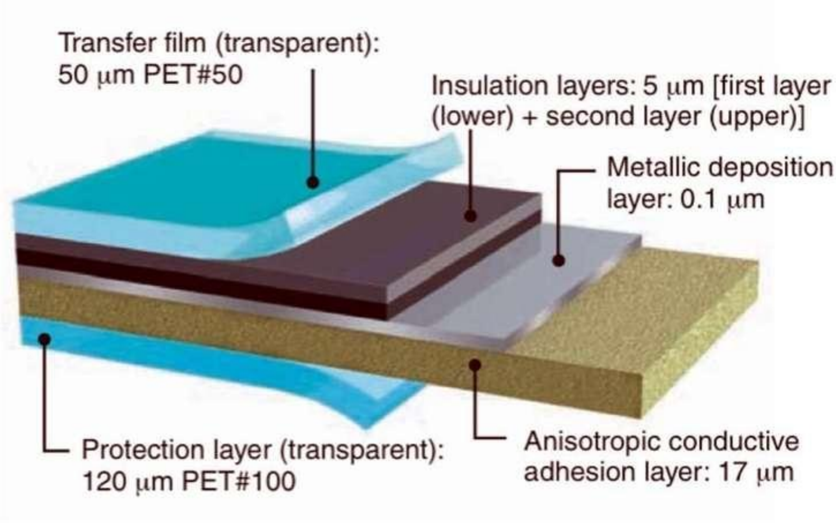

Figure 2.9 Multi-layered structure of electromagnetic shielding film [41].

2.4. Properties of transparent conducting oxides

2.4.1. Optical properties

The main requirement of all TCOs is high optical transparency (higher than 80%) in the visible range of electromagnetic light spectrum. The optical properties of TCOs strongly depends on band structure, impurity levels, localized defects, lattice vibrations, processing technique, microstructure and so on. As it mentioned above wide band gap semiconductors satisfy this optical requirement due to largely ionic nature of the metal-oxide bonds that terminates the accumulation of ionized acceptors [42]. Furthermore, charge carrier concentration and mobility are other significant factors for optical performance of TCOs and together with possibility in manipulation of the plasma absorption edge and infrared (IR) transparency. The absorption edge is an important feature because it determines the critical frequency level at which electrons can react to applied electric field. Above critical frequency the material shows a transparent characteristic but at lower frequencies (below critical frequency) the material will reflect or absorb incident radiation. It is well known that the plasma absorption frequency is proportional to square root of carrier concentration. For example, SnO_2 has a relatively lower electron concentration than ITO and ZnO. The plasma wavelength of SnO_2 is on the order of 1.6 µm but this value decreases to 1.0 and 1.3 µm for ITO and ZnO [43].

The typical spectral dependence of optical properties of transparent conducting oxide materials is given in Figure 2.10. In that figure it is clearly seen that optical transparency is defined by two non-transparent regions. In the first region where energy of the light (photon) is higher than band gap of the material (at low wavelengths) the band gap dominated absorption will occur. The energy of photons is absorbed and transformed to band transitions and material behaves like non-transparent. In the second region where energy of the light is lower than band gap of the material (in the near infrared part of the electromagnetic spectrum) no light is transmitted due to the plasma absorption edge effect [44].

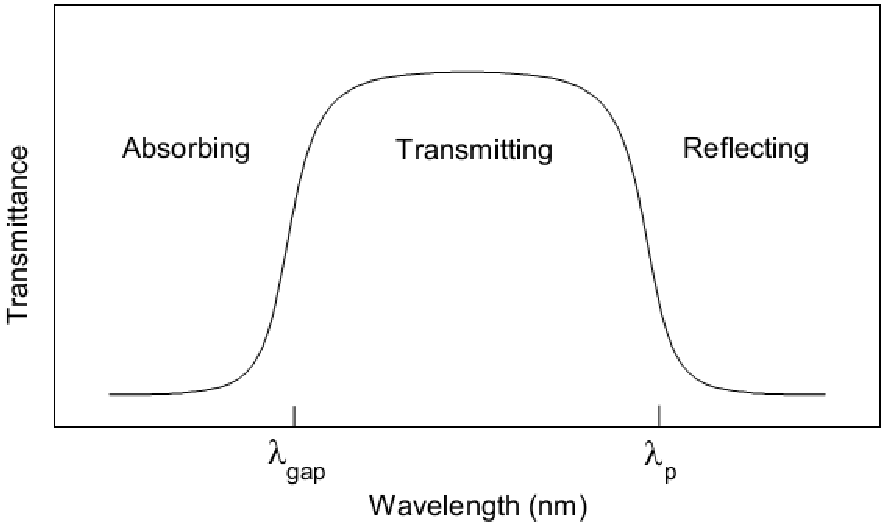

Figure 2.10 Spectral dependence of transparent conducting oxides. λ_{gap}: wavelength of band gap absorption takes place, λ_p: wavelength of plasma absorption takes place [45].

2.4.2. Electrical properties

The electrical conductivity is mainly controlled by the electrical charges; electrons, holes and ions in an applied electric field. The electrical conductivity of n-type semiconductors or transparent conducting oxides can be defined with the following equation:

$$\sigma = \rho^{-1} = ne\mu \tag{1}$$

where σ is the electrical conductivity (in *Siemens/meter, S/m*), ρ is the specific resistivity, n is the number of charge carriers, e is the electric charge and μ is the charge mobility [46]. It is clearly seen that, high electrical conductivity can be achieved with high electron concentration and high charge mobility.

The electrical conductivity of high performance TCOs such as, ITO and doped-ZnO, depend on dopant materials. The selection criteria for proper dopant is related with electronic structure of host material. The energy levels of valence electrons, unoccupied conduction band energy levels and effect of dopant atoms on energy levels of host matrix, must be examined.

In order to enhance electrical conductivity, the first possible way is increasing mobility. However mobility is directly linked to materials intrinsic scattering mechanisms which are; grain boundary scattering, ionized impurity scattering, lattice scattering and electron- electron scattering. These mechanisms restrict the carrier mobility and therefore cannot control in an orderly manner.

Another possible way to enhance electrical conductivity is increasing charge carrier concentration by doping. According to host material type this can be done by substitutional doping, formation of vacancies or formation of interstitials. There are some basic requirements for selecting proper dopant:

i. The doping cation should have higher valence electrons than host material. For example, for ITO system Sn^{4+} is substitute with In^{3+} in the host lattice. The substitution of In atom with high valence electron atom (Sn) causes the formation of free electrons which enhances the electrical conductivity (n-type). Otherwise, if the dopant cation has a lower valence, the vacancy formation will occur and behaves like an electrical trapping site which decreases conductivity. Alternatively, if the doping anion has lower valence electrons than oxygen, electrical conductivity will increase. SnO_2:F system is a good example for this kind of doping [47]. The representative band structures of typical n-type and p-type semiconductors are given in the Figure 2.11.

ii. The radius of doping ion should be equal or lower than the host material ion. If not, these large ions act as a scattering center.

iii. Any intermetallic compounds or solid solutions between doping and host ions should not form during doping step.

iv. For all doped-metal oxide systems there is a critical dopant concentration value. If this critical is exceeded electrical conductivity will decrease due to excess occupation interstitial positions and formation of unpredictable defects and impurities [48].

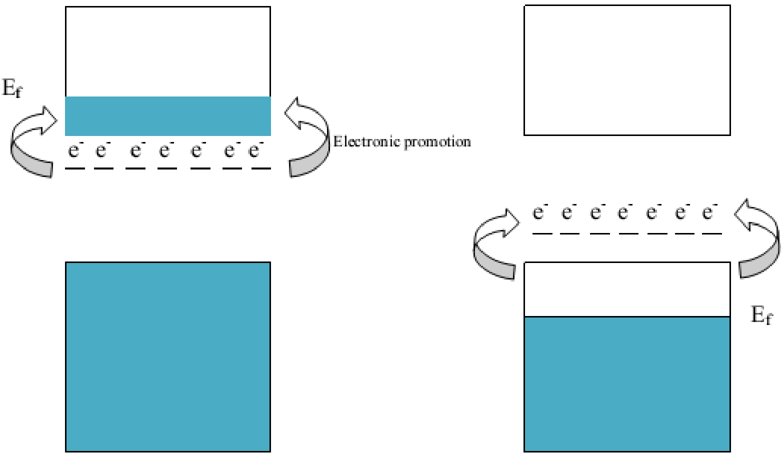

n-type doping

p-type doping

Figure 2.11 Typical band structure diagrams of n-type and p-type semiconductors. E_f is the Fermi level which is the highest electronically occupied energy level [49].

2.4.3. Sheet resistance

The electrical sheet resistance of the TCO thin films is a helpful measurement index to determine electrical performance which defines the resistance of a square layer area. The correlation between sheet resistance and specific resistivity can be calculated with the following equation:

$$R_\square = \rho/t \tag{2}$$

where $R_\square$ is the sheet resistance (in *ohm/square*, Ω/sqr) of TCO thin film, ρ is the specific resistivity and t is the thickness.

The sheet resistance of the thin films can be measured by four-point probe technique. The probe has four tips with controlled spacing. The current is applied through outer probes and voltage measured by two inner probes. During measurement, tip contact load can be arranged by controller springs in order to minimize thin film surface damage. The representative scheme of four-point probe configuration is given in the Figure 2.12.

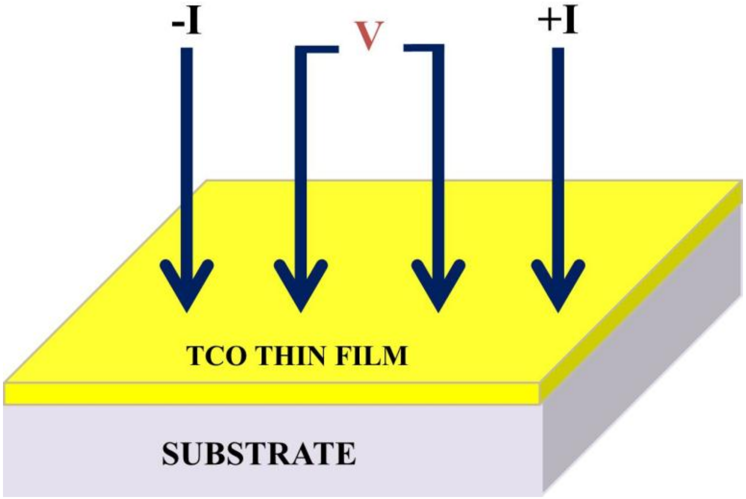

Figure 2.12 Scheme of four-point probe set-up.

2.5. TCO coating/film formation techniques

Many different thin film deposition techniques have been developed fabricate transparent conducting oxide thin films. Each technique directly affects the final electrical, optical, morphological and structural properties. These techniques can be divided into two main subgroups: *i) vapor phase deposition techniques*, *ii) solution based deposition techniques*. Each process has unique processing conditions and can be controlled with several parameters like deposition rate, deposition atmosphere, substrate temperature, etc.

2.5.1. Vapor phase deposition techniques

Vapor phase deposition techniques can be divided into two main groups:

i) Chemical vapor deposition (CVD)
ii) Physical vapor deposition (PVD)

2.5.1.1. Chemical vapor deposition (CVD)

Chemical vapor deposition is a technique based on reaction of reactive gaseous precursors at the surface of a substrate [50]. Processing conditions are selected according to specific substrate surface to promote pyrolysis, reduction and oxidation reactions. There are many types of CVD precursors such as, gases, volatile liquids, solids or hybrid compositions of these material groups. Melting point of these precursors should be lower than substrate material and they should be stable at room temperature. CVD method makes possible deposition of high melting temperature materials with a high growth rates but some complex processing equipments may be required. CVD method is widely used for fabricating different types of crystalline or amorphous state functional coatings with a high purity. Schematic representation of CVD technique is given in the Figure 2.13.

The most commonly used CVD techniques are; *thermal-CVD* [51], *plasma-CVD* (PCVD) [52] and *laser-CVD* (LCVD) [53]. Generally, LCVD and thermal-CVD techniques are used at high temperature processing conditions due to chemical nature of the precursor materials. In contrary, PCVD can be used relatively lower temperatures due to creation of plasma which forces activation of the chemical reactions. Therefore, soft or low melting temperature materials can be coat with high deposition rates at low temperatures.

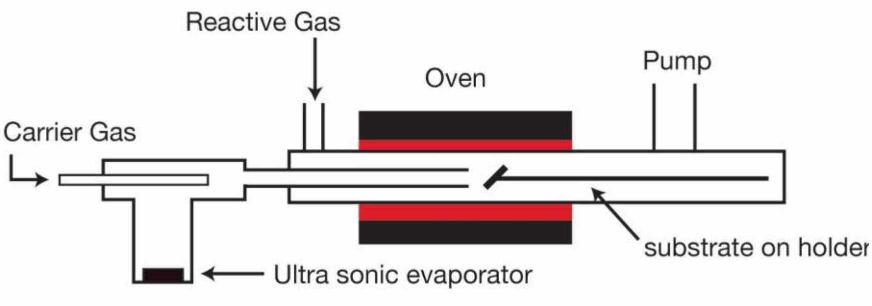

Figure 2.13 Schematic illustration of CVD process [54].

2.5.1.2. Physical vapor deposition (PVD)

Physical vapor deposition is a general name of techniques which are based on evaporation of a precursor material subsequent deposition onto a substrate. These reactions take place under low pressure-vacuum conditions or controlled atmosphere in a chamber. Generally, evaporation and formation of vapor phase can be achieved thermally (thermal evaporation) or bombardment of precursor material by high energetic particles, mostly Ar ions (sputtering) [55].

Specifically, in thermal evaporation, the precursor material is heated to high to allow vaporization which then condenses on cooled substrate surface to form a film layer. The vaporizer equipment is generally made of resistance-heated device such as, sublimation oven, heated crucible, e-beam evaporation device or a tungsten wire resistance [56].

In sputtering whole process takes place in a vacuum chamber. The basic principle of this technique is based on sputtering of target material by ionized argon ions then condensation onto a substrate. The negative potential in maintained at target material and argon ions charged positively. The positively charged argon ions accelerated and striking the target material with an appropriate force to remove target atoms from its surface. The ejected atoms are formed a thin film on a substrate material. Schematic representation of sputtering technique is given in the Figure 2.14. If a chemical reaction takes place during sputtering, the process is called as *reactive sputtering*. The major advantages of sputtering process are; coating high melting temperature materials at relatively low temperatures, better adhesion to the substrate and easy to control deposited film composition with target material.

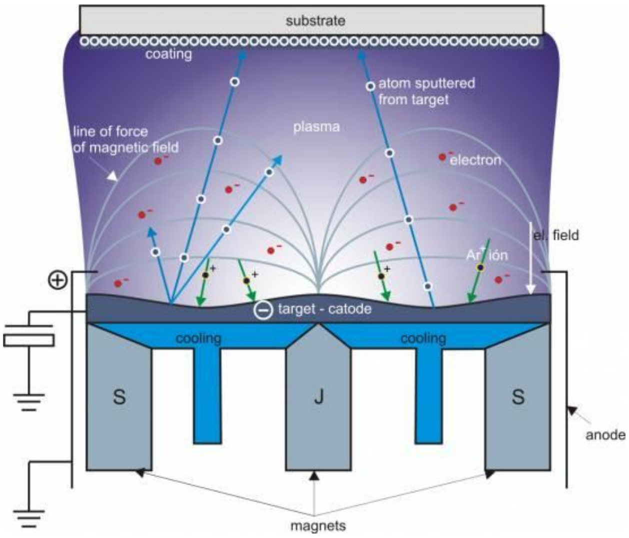

Figure 2.14 Schematic illustration of sputtering process [57].

There are three main sputtering classes, which are;

i. DC sputtering
ii. RF sputtering
iii. Magnetron sputtering

2.5.1.2.1. DC sputtering

The substrate material is set as the anode and target material is the cathode. The chamber is pumped down to high vacuum conditions and generally filled by argon gas. A high DC voltage is applied between anode and the cathode and plasma created. The advantages of this technique are: simple, easy to control homogeneity of the film thickness and large surface area coatings might be possible. However, only electrically conductive materials are generally used in this technique. Electrically insulator materials quickly lose their negative potential which is required accelerating positive ions. This is the main drawback of this technique [58].

2.5.1.2.2. RF sputtering

A high frequency alternating voltage (generally in a range of 10- 15 MHz) is applied between anode and the cathode. Due to the effect of high frequency voltage levels, the electrons are starts to oscillate which is called as *negative glow*. As a result of this oscillation behavior electrons acquire required energy for ionization. The major advantage of this technique is, possibility in using electrically conducting and non-conducting (insulator) target materials [59].

2.5.1.2.3. Magnetron sputtering

A magnetic field is applied on the electric field which is close to the target material [al dahoudi -7]. As a result of applied magnetic field, the possibility of formation of ionizing collisions increase and also it helps to limit high energy electrons near target surface. The major advantages of this technique are; high deposition rates can be obtained at low vacuum conditions and coating of low melting temperature substrates (such as polymers) is possible. This technique has been industrially scaled up for large plain substrates (up to 4 meter width substrates).

2.5.2. Solution based deposition techniques

Solution based deposition techniques are basically based on dispersion of different species (ions, particles, etc.) in a liquid medium. The high optical quality and homogenous coatings can be formed on transparent substrates like glass and polymer and as well as non-transparent substrates. Once the green coatings (wet coated layer) are formed, they are heated to (calcined) relatively high temperatures. However, calcination at lower temperatures (couple hundred ºC) is possible which is related with the solution chemistry.

There are four important solution chemistry and physics dependent requirements for obtaining homogenous and continuous coatings with a high optical quality [60]:

i. The solubility of the precursors in the aqueous media must be high and the solution should exhibit high tendency to crystallize during evaporation or calcination steps.

ii. The wettability of the solution must be high, which means that solution must have film formation tendency. If not, then the solution should treated with proper surfactant or wetting agent to decrease the surface energy and enhance wetting.

iii. The solution must have an appropriate stability under ambient processing conditions/atmosphere.

iv. The solvent evaporation/drying and heat treatment/calcination processes must be carried out for obtaining dense, homogenous and reproducible coatings with sufficient properties.

There are two main solution based deposition techniques:

- *i.* Spray pyrolysis
- *ii.* Sol-gel processing

2.5.2.1. Spray pyrolysis

Spray pyrolysis is well known and industrially used coating technique with low cost and high mass production. Basically in this process, first, small sized solution droplets are generated on a hot substrate which subsequently decompose to the final product. These small sized droplet generation or atomization process can be carried out by pressure, nebulizer, ultrasonic or electrostatic methods. Each method shows different coating characteristics according to droplet size distribution, atomization rate, droplet velocity and growth kinetics. Specifically, drop size can be controlled by nozzle type and pressure. The high pressure decreases drop size and vice versa. Moreover, the chemical nature of the precursor materials directly affects structure, film formation behavior and morphology of the coatings. Schematic representation of spray pyrolysis technique is given in the Figure 2.15.

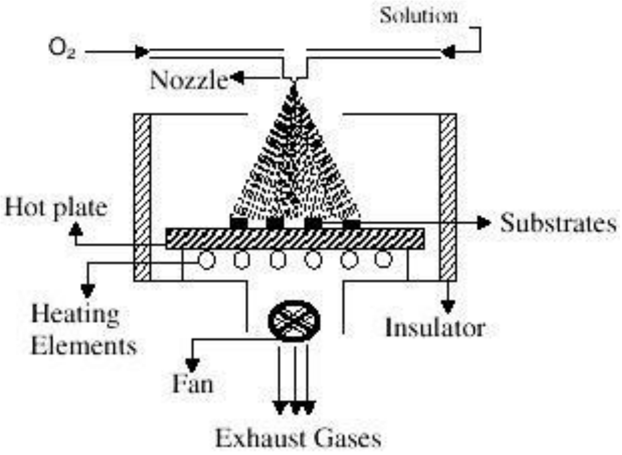

Figure 2.15 Schematic illustration of spray pyrolysis technique [61].

Another critical factor for controlling coating quality is substrate temperature. The substrate temperature must be high enough for decomposition of the solution droplets. If substrate temperature is too high, droplets would have high affinity to form a powder layer. The major advantages of this technique are; easy, low cost process, and lack of need any sophisticated equipments and it is possible to coat complex shapes with various sizes.

2.5.3. Sol-gel processing

In general, sol-gel process defines the transition of a liquid solution "sol" into a solid "gel" phase. The sol-gel process is a low temperature processing route for preparing complex oxides [62] and complex functional oxide nanostructures [63]. It is a multistep processing technique, involving both physical and chemical reactions which are hydrolysis, condensation, drying and densification [64]. This method is generally used for producing ceramic and glass materials. Different sized and shaped nano/micro particles and powders, fibers, membranes, porous materials and coatings are general products of sol-gel process. The schematic of the sol-gel method is shown in Figure 2.16.

The thin film coating procedure by sol-gel process covers three steps:

i. *Preparation of a sol*: hydrolysis and condensation reactions take place at around room temperature in a designed chemistry with controlled rates.

ii. *Coating*: deposition of sol onto substrate surface. Spray coating, dip coating and spin coating are the most common coating techniques.

iii. *Heat treatment*: in order to obtain dense and crystallized coatings heat treatment step is applied at relatively high temperatures. This step is also called as annealing, sintering or calcination (typically at around 500 ºC).

The major advantages of sol-gel processing are; relatively low processing temperatures needs in obataining oxide products, ability to produce multicomponent materials, high purity and stoichiometry control.

There are three main methods used to form thin films: spray coating, dip coating and spin coating.

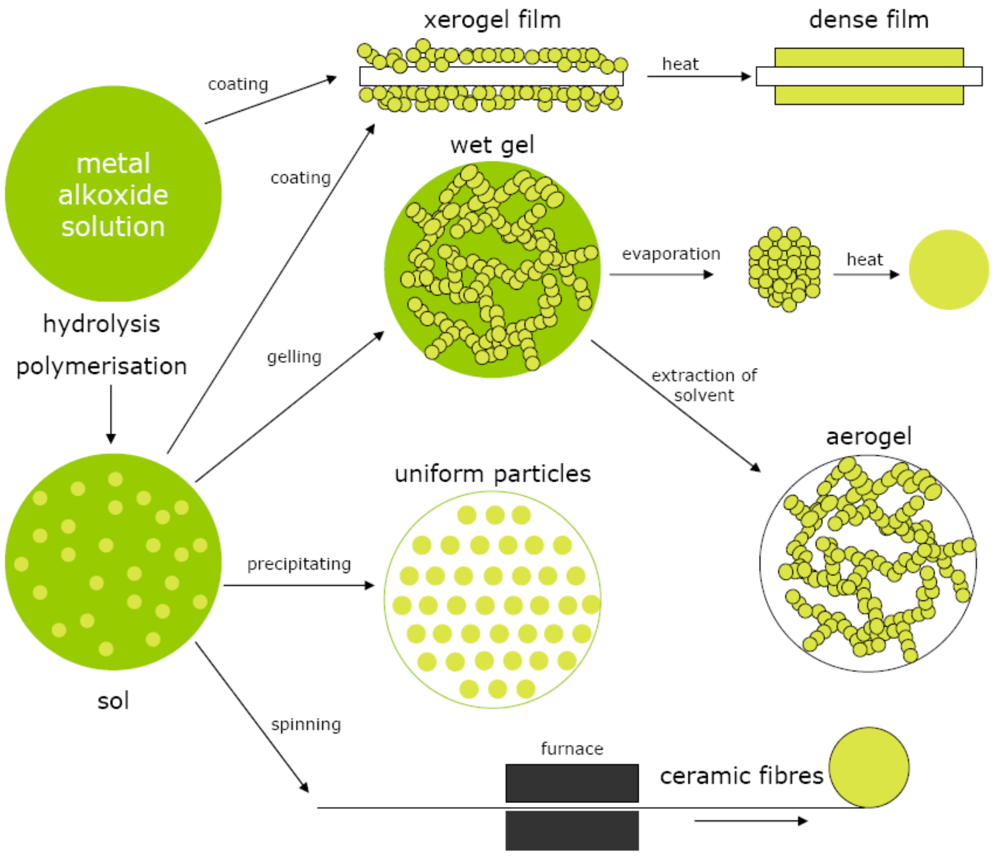

Figure 2.16 Schematic summary of sol-gel process [65].

2.5.3.1. Film formation methods for sol-gel route

2.5.3.1.1. Spray coating

Spray coating is extensively used and industrially applied sol-gel coating technique. Basically, sol is sprayed onto substrate surface with controlled scanning speed and spray pressure. The physical and chemical nature of the sol is key parameter which affected mechanical and optical quality of the coating.

According to these sol and processing parameters porous or dense coatings can be produced [66].

2.5.3.1.2. Dip coating

The dip coating is a well-known coating technique to fabricate homogenous thin films easily. It is a one step, simple, cheap technique and allows coating semi-curved shapes. This method does not require any sophisticated processing equipments or vacuum conditions.

The dip coating usually defined into three stages, which are shown in Figure 2.17:

i. *Immersion:* the substrate is dipped into coating sol with a controlled speed.

ii. *Hold time:* after dipping stage of the process. Substrate is holding in the sol to allow adequate penetration time for sol species.

iii. *Withdrawal:* substrate is withdrawn with a controlled speed to avoid vibrations, etc.

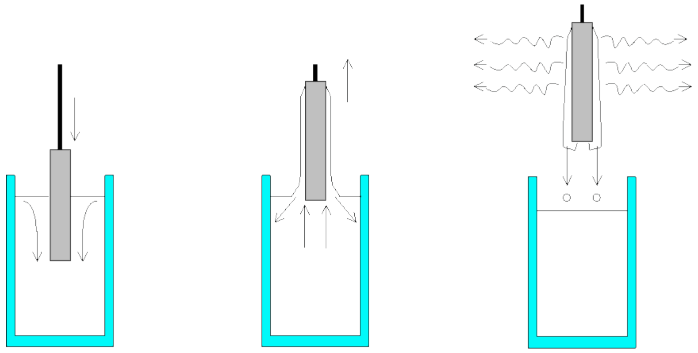

Figure 2.17 Schematic illustration of dip coating technique [67].

The quality of the coatings depends on both environmental and processing conditions. Temperature, relative humidity and environmental dust are some affected factors related with processing environment. In addition, thickness of the coatings can be adjusted by viscosity of the sol, solvent evaporation rate and withdrawal speed. The Landau- Levich equation is useful to determine thickness of the coatings [68]:

$$h = 0.94 \frac{(\eta v)^{\frac{2}{3}}}{\gamma^{\frac{1}{6}} (\rho g)^{\frac{1}{2}}} \tag{3}$$

Where h is coating thickness, η is the sol viscosity, v is the withdrawal speed, γ is the liquid-vapor surface tension, ρ is the density and g is the gravity. According to this equation it is easy to say that coating thickness is directly proportional to the withdrawal speed which means that, high withdrawal speed results with the thicker coatings.

The major advantages of dip coating method are; any size and curved substrates can be used, simple, low cost, low contamination risk and operation atmosphere can be arranged\changed. However, there are also some limitations in using this technique; for large substrates big containers might be required, i.e. large amount of coating sol should be prepared. This is not economical route for expensive precursor based sols. Additionally, it is improper method for one-sided coatings (coating is applied both layers of substrate).

2.5.3.1.3. Spin coating

Spin coating is used for many industrial and technological applications which based on centrifugal draining and evaporation of the deposited sol. Spin coating includes four stages; deposition, spin-up, spin-off and evaporation [69]. Schematic representation of spin coating process is given in the Figure 2.18.

i. *Deposition:* an excess amount of sol is deposited on the substrate surface. The sol should completely wet the surface *ii.* *Spin-up:* the substrate is rotated at high speeds for desired time. During this rotation period spiral vortices is formed and deposited sol spread on substrate surface by centrifugal force.

iii. *Spin-off:* in this stage acceleration of rotation speed keep constant and spinning reaches a defined rate. At this step viscous forces dominate the film formation behavior and edge effects are generally seen.

iv. *Evaporation:* in a regular sol formulation solvent is usually volatile and causes simultaneous evaporation which is the dominant coating thinning mechanism at this stage. After evaporation of the solvent green coating is started to transform a gel.

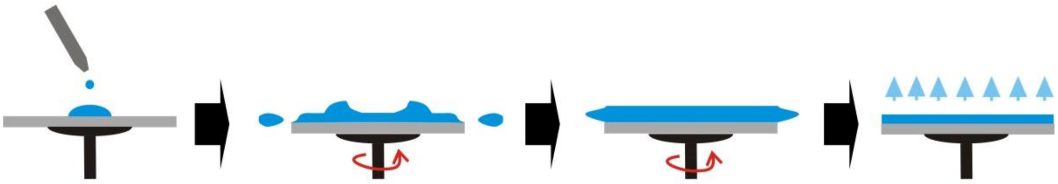

Figure 2.18 Schematic illustration of spin coating technique [70].

During spin-off step viscosity is not shear-dependent and does not change over the substrate [71]. This effect is due to net force equilibrium between the viscous forces (inward direction) and centrifugal force (outward direction). The thickness of coating layer after spin-off step can be expresses as:

$$h(t)=h_0/(1+4\rho\omega^2 h_0^2 t/3\eta)^{1/2} \tag{4}$$

where h_0 is the initial thickness, t is the time, ρ is the sol density and ω is the angular velocity.

When the sol viscosity and density are set as constant, coating thickness is inversely proportional to the spin rate:

$$h(t) \propto 1/\omega \tag{5}$$

As shown above spin rate and time are the most critical parameters in determining film thickness. Also some other factors affect the quality of the coatings, such as, environmental dust, temperature and processing atmosphere.

CHAPTER 3

FABRICATION OF PLAIN ITO THIN FILMS: EFFECT OF PROCESSING PARAMETERS ON OPTOELECTRONIC AND MICROSTRUCTURAL PROPERTIES

In this chapter, the effect of processing parameters on functional properties of plain sol-gel ITO thin films are presented. The main objective was to determine the effect of heat treatment temperature, spin coating parameters, number of coatings, sol molarity and aging on physical properties of ITO films. This chapter starts with the description of general properties of ITO and continues with a focus on sol-gel based ITO thin films. The physical and chemical features related with of processing parameters will be briefly explained. Then, the experimental procedures are explained. Finally, the effects of above mentioned processing parameters on ITO film properties, i.e. electrical, optical and microstructural are reported.

3.1. Structural properties of ITO

ITO has two crystal structures in its pure form. Both of these are similar to In_2O_3 crystal structure. It can be either in bixbyite crystal form or in corundum form. The representative structures are illustrated in Figure 3.1. The bixbyite crystal unit cell includes 40 atoms and two non-equivalent cation sites. As shown in Figure 3.1, there are empty positions for one fourth missing anions and two different six-fold-coordinated sites for the indium cations. One-fourth takes place in the location of trigonally compressed octahedra on *b* site, and the other three-fourths take place in the location of highly distorted octahedral on *d* site. There are empty positions for two anions; one is at the opposite vertexes of *b* sites and the other is at along the diagonal of *a* face of *d* sites. At these described sites, each cationic site can be considered as a cube. Along the four axes of <111>, the structural vacancies are located [72]. The formation of tin oxide in the cubic bixbyte structure of indium oxide is obtained through substitutional doping of In_2O_3 with Sn^{4+} and indium (In^{3+}) replaces with Sn^{4+} [73]. The corundum crystal structure of ITO is always obtained under high pressures (~10×10^4 MPa) and high temperatures (800 °C and excess) or both [74]. The lattice parameter changes in the range of 10.12- 10.31 Å depending on the extent of Sn doping and is close to the lattice parameter of In_2O_3 [75].

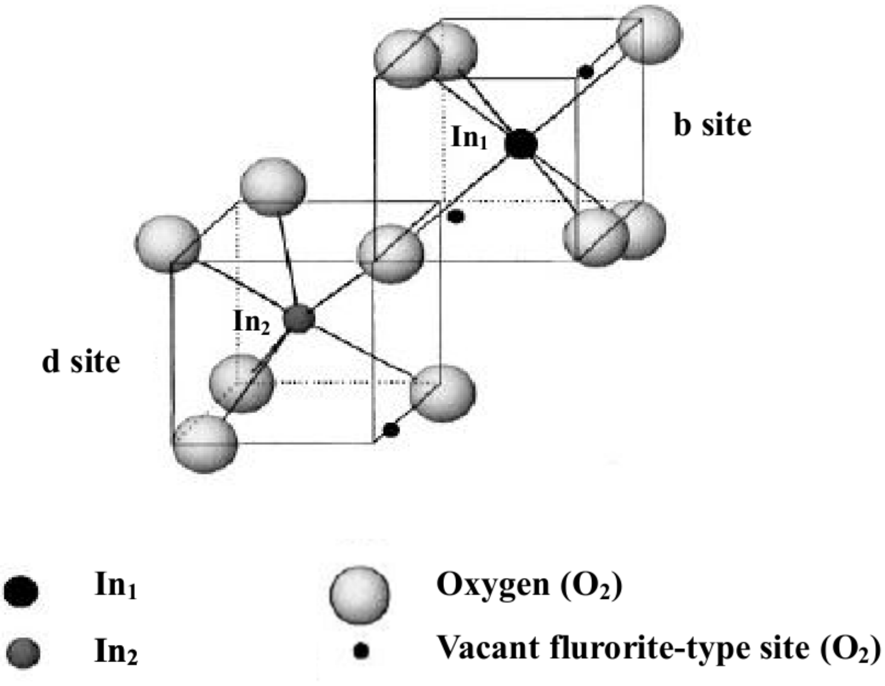

Figure 3.1 The representative atomic structure of In_2O_3 [72].

3.2. Optoelectronic properties of ITO

In_2O_3 is an n-type semiconductor and has relatively wide energy gap of 3.5 ~ 4.3 eV. SnO or SnO_2 is formed with a valence number of 2+ or 4+, respectively, when Sn is doped into In_2O_3. The final conductivity of doped ITO is influenced by the change in these valance numbers. Because of the lower valence number such as Sn^{2+} reduces the carrier concentration by creating a hole, conductivity is reduced. Different than the effect of Sn^{2+}, when Sn^{4+} cation (tetravalent cation) is doped, electron is provided to the conduction band (n-type). Due to the differences between the valance number of Sn^{4+} and In^{3+}, an electron charge-compensation will be obtained, as represented in the following equation:

$$xIn_2O_3 + xSn^{3+}_{2-x}(Sn^{4+} \bullet e)_x O_3 + xIn^{3+}$$

ITO with substitutional doping of Sn has narrower energy gap. Thus, the electrical conductivity of ITO is affected by Sn^{4+} concentration and increases as of the amount of Sn^{4+} increases. At the same time, due to the limited solubility of Sn in In_2O_3, doping is limited within the range of 6–8 at. % [76,77].

In addition, oxygen vacancies act as doubly ionized donors and contribute a maximum of two electrons to the electrical conductivity as shown in the following equation [78]:

$$O_O \rightarrow V_O^{\bullet\bullet} + \frac{1}{2}O_2(g) + 2e^-$$

Because of ITO has the wide band gap, it is reflective in the infrared light spectrum while transparent in the visible light spectrum [79].

Physical properties also affect the conductivity. As seen in Figure 3.2, the optical transmittance shows a great dependence on the thickness. Similarly, deposition conditions and the precursor composition strongly affect the optoelectronic properties of ITO films. In order to achieve high electrical conductivity, the deposited layer needs to include a high density of charge carriers, which are free electrons and oxygen vacancies. In the visible light spectrum, high electrical conductivity (which also means low sheet resistance) and high transmittance is balanced. As a result, sheet resistance of thin films can be smaller than 10 Ω/sq whereas their visible transmittance is higher than 80 %. Infrared (IR) reflectance is influenced by sheet resistance of the film and IR reflectivity increases at longer wavelengths. Consequently, sheet resistance should be higher than 30 Ω/sq to achieve IR reflectance higher than 80 % [80].

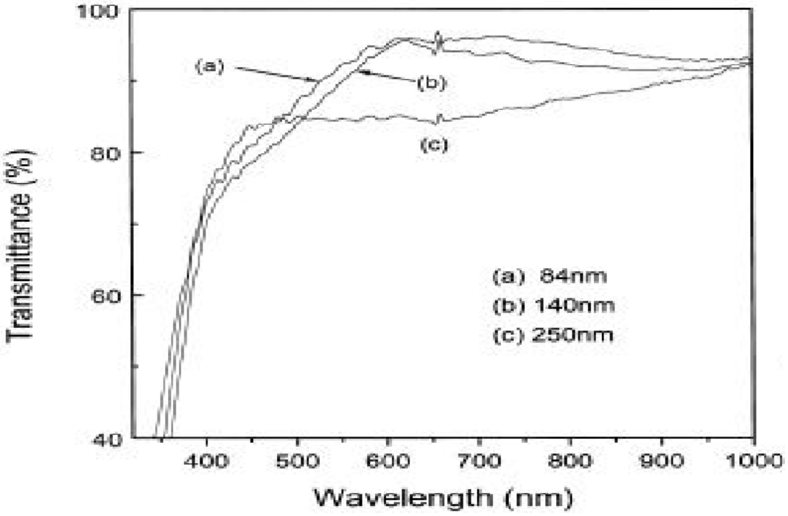

Figure 3.2 Optical transmittance spectra of ITO thin films at different thicknesses values [81].

3.3. Sol-gel processing of ITO thin films

3.3.1. Importance of starting chemicals (precursors)

In sol-gel process, oxides can be prepared using two main types of precursors. The first group is the *inorganic salts,* which can be represent as M_mX_n. M is the metal, X is an anionic group and *m* and *n* stoichiometric coefficients. The second group is the *organic alkoxides* with a chemical formulae of $M(OR)_n$, where *M* represents metal and *R* is an organic functional group [82]. These compounds can be hydrolyzed in aqueous or organic solvents and then form M-O-M type inorganic network by condensation [83]. Although metal alkoxides are mostly used as starting materials, it is difficult in practice to employ alkoxides due to their high sensitivity to moisture. However, metal salts are advantageous than metal alkoxides, because they are easy to handle and are more cost-effective. In hydrolysis process of metal salts, a proton from an aquoion of $[MO_NH_{2N}]^{Z+}$ is removed and form a hydroxo (M-OH) or oxo (M=O) ligands. Inorganic polymers with metal center, which are connected by oxygens or hydroxyls are formed by these condensation reactions. Some metal salts consist of chlorides, acetates, nitrates and sulfides, which have high solubility in water or organic solvents. In spite of the lower solubility of acetates in water or organic solvents compared to other metal salts, the metal ion can be stabilized by acetate ions in some cases by coordination of C=O groups [82].

Many solvents such as ethanol, methanol, isopropanol, acetyl acetonate [84], dehydrated isopropyl alcohol [85], 2-methoxyethanol can be used as alternative solvents for sol preparation. Proper combination of precursors and solvents are important in determining the quality of ITO thin films, since each solvent and precursor have different properties in terms of their solubility and evaporation behavior. 2-methoxyethanol has been suggested by Lee [86] as a solvent due to its high boiling point (124.5 °C). Meanwhile, viscosity of sol solution can be changed by the concentration of the precursor and thin film properties can be controlled by sol concentration. Both surface morphology and porosity of the films can be easily modified by the concentration for acetate-based sol formulations. It is also found that when acetate-based precursor was used as the starting salt, the thickness of ITO thin film can be increased from 36 nm to 247 nm as the concentration increased from 0.03 mol/L to 0.1 mol/L [87]. SEM images in Figure 3.3 shows the microstructure of the thin films and the change in grain size with different sol concentrations. As seen in the figure, as the sol concentration increases, the amount of solute increases resulting in an increase in the grain size. As a result of an increase in the amount of solute, larger electrostatic interaction between the solute particles is obtained, which increases the probability of contact between solute particles, increasing the grain size.

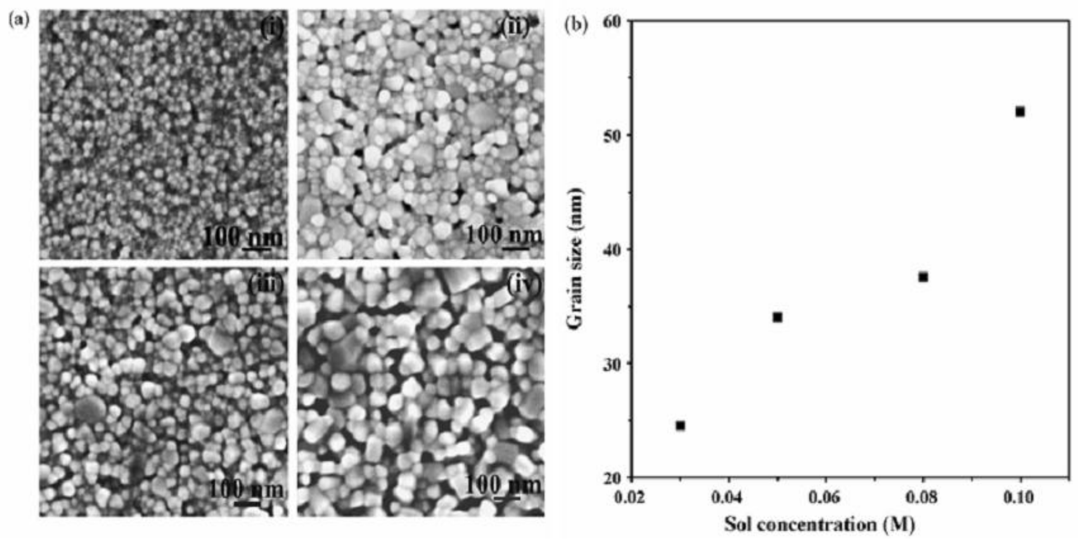

Figure 3.3 (a) SEM images of ITO films prepared with different sol molarities; (i) 0.03, (ii) 0.05, (iii) 0.08 and (iv) 0.1 M. (b) Change in grain size with sol molarity [87].

3.3.2. Sol composition: effect of tin concentration

Dopants such as tin [76,77,88,89], titanium [89], molybdenum [90] and fluorine [91] have been investigated in order to enhance the properties of In_2O_3 thin films. Among all dopant materials, Sn is most widely used one for production of In_2O_3 thin films. Resistivity of ITO thin films is investigated by Zhang et al.[91]. They prepared starting solution by mixing indium chloride and tin chloride dissolved in ethanol and deposited ITO thin films through dip coating. Electrical resistivities of these films as a function of Sn doping concentration is shown in Figure 3.4. It was observed that the resistivity of the thin films first decreased as the content of Sn increased to 10 from 5 mol % and then reached minimum at a Sn content of 10 mol % (In:Sn = 9:1). After that, the resistivity increased back again with increasing Sn content as shown in figure 3.4. When Sn substitunionally doped, unpaired electrons form because of the stoichiometric ratio mismatch. Thus, the Sn doping is considered as a type of the donor doping. These unpaired electrons are free to move and act as carriers. Therefore, the electrical conductivity of ITO is enhanced with increasing the Sn doping concentration. On the other hand, reduction in the electrical conductivity was observed with continuously increasing the concentration of the Sn doping. The reason for the change in the ITO thin film resistivity with Sn concentration is the segregation of the dopant ions to the grain boundaries especially when Sn concentration was higher than the critical value of 10 mol% (in present case) [92-94]. Many researches [92,95,96] have focused on the investigation of the effect of Sn doping concentration on the resistivity of ITO thin films. The optimal concentration was reported as 8–10 mol % [76,77]. Consequently, it is obvious that doping is an effective method to enhance the electrical conductivity of ITO thin films. However, concentration and the experimental conditions are critically important in obtaining satisfacting results.

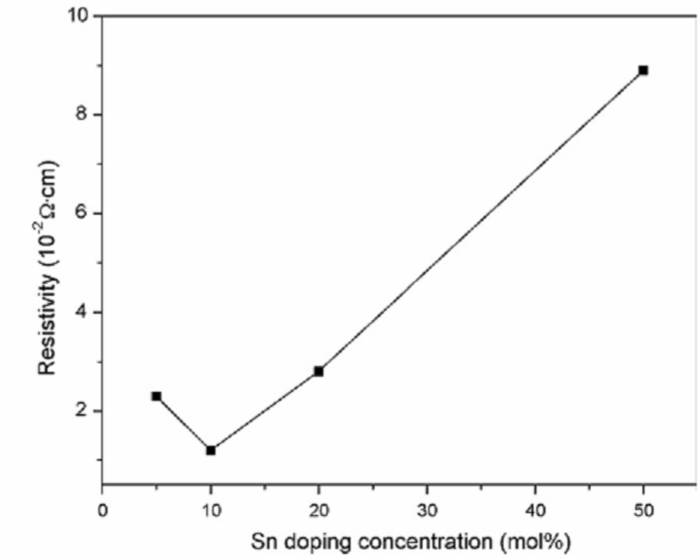

Figure 3.4 Electrical resistivity of ITO thin films with respect to Sn doping concentration [97].

3.3.3. Post coating process: thermal treatments

All sol-gel based thin films are strongly influenced by the post coating heat treatment. The reason is thermally-induced densification and crystallization taking place during heat treatment. Nishio et al. [98] reported that the electrical resistivity values of thin films (on quartz substrates) decreases down to 1.5×10^{-3} Ωcm with increasing heat treatment temperature to 800 ºC. Similar results were observed by Takahashi et.al. [99]. They found that the electrical resistivity of ITO thin films decrease by one order of magnitude through the increase in the heat treatment temperature from 400 to 700 ºC. This result was explained with increased carrier mobility from 1.3 cm^2/Vs (at 400 ºC) to 14 cm^2/Vs (at 700 ºC). The electrical resistivity of these films was decreased to $4x10^{-4}$ Ωcm after nitrogen heat treatment at 650 ºC. Similarly, Tahar et al. [100] have reported similar resistivity values ($3.3x10^{-4}$ Ωcm) for cadmium stannate films after heat treatment at 650 ºC [101]. However, in other work, the electrical resistivity decreased considerably at high heat treatment temperatures (600 ºC) and increased slightly with further increase to 700 ºC (Figure 3.5) [95,102]. A possible explanation was related with reducing characteristics of SnO_2. Since SnO_2 might reduce to SnO, meaning that Sn^{4+} transforms to Sn^{2+}, ionic conductivity might decrease. In addition, at high heat treatment temperatures, oxygen atoms will diffuse into the ITO lattice and as a result number oxygen vacancies-charge carrier concentration again decreases the conductivity [103].

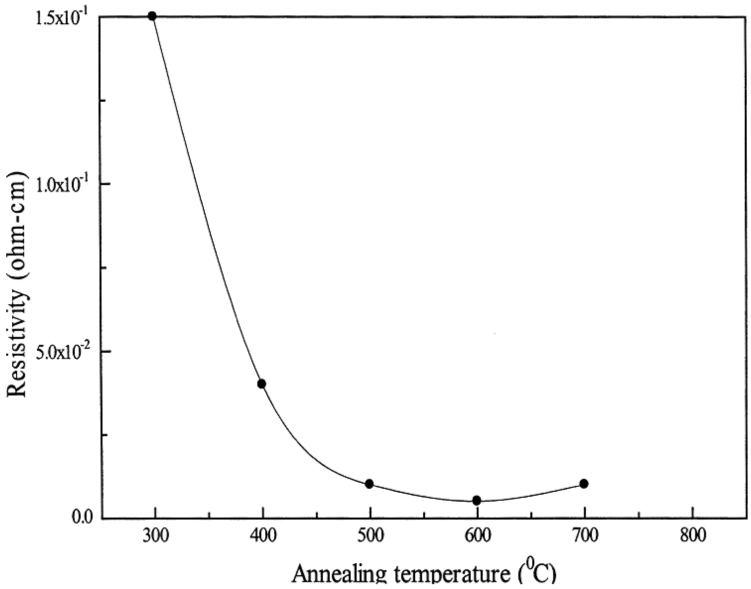

Figure 3.5 Effect of heat treatment temperature on the electrical resistivity of ITO thin films [104].

The heat treatment effect on ITO thin films produced using In- and Sn-chlorides was reported in [105]. The heat treatment temperature was set to 600 ºC (in air) for 30 min, and then a post treatment applied under N_2/H_2 atmosphere at 600 ºC for 1 h. The electrical resistivity decreased from $2x10^{-3}$ Ωcm to $2.5x10^{-4}$ Ωcm. It was also that the post treatment process increases carrier concentration from $2.5x10^{20}$ cm^{-3} to $9.1x10^{20}$ cm^{-3} and mobility from 20 cm^2/Vs to 30 cm^2/Vs. Moreover, for improving electrical performance of ITO thin films there are many different post treatment processes that can be applied. Wakagi et al. [106] reported effect of post electron plasma treatment on the sheet resistance of spin coated ITO thin films. The results showed that, the electrical resistivity decreases drastically following plasma treatment due to the decreased amount of organic impurities. Similar study was conducted by Kololuoma et al. [107]. This group studied the effect of argon plasma post treatment and found that after 75 min argon plasma exposure sheet resistance of the films drastically decreased from 600 Ω/sqr to 200 Ω/sqr.

The effect of heat treatment on the optical properties of ITO thin films was also studied extensively. It was found that, the maximum optical transmittance of thin films reached to 93 % after a heat treatment conducted at 600 ºC (Figure 3.6). Furthermore, optical properties of indium- tin chloride based- polyethylene glycol (PEG) stabilized sol-gel ITO thin films were also investigated. The transmittance of thin films increased by 3- 5 % within the wavelength range of 350- 700 nm due to the improved surface quality following PEG addition [108,109].

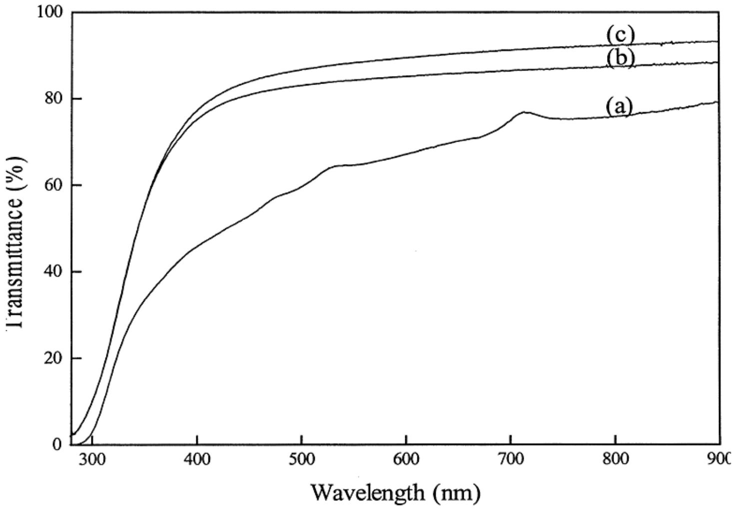

Figure 3.6 Optical transmittance of ITO thin films following heat treatment conducted at temperatures of (a) 400, (b) 500 and (c) 600 °C [104].

Beaurain et al. was investigated effect of heat treatment process on the grain growth kinetics of sol-gel derived ITO coatings prepared by metal salts [110]. The findings showed that grain size of the thin films after a heat treatment at 350 °C were about 8 nm and increased to 90 nm following a 550 °C treatment. This study showed a correlation between the resistivity and grain size.

3.3.4. Physical properties of the coating: film thickness

The effect of number of coatings on electrical properties of ITO thin films was studied by Li et al.. The results indicate that the sheet resistance was decreased with increasing number of coating cycles. The relation between sheet resistance and the number of coating layers was not linear due to physical nature of the monolayer film formation. The discontinuous nature of the film and poor surface coverage results in high porosity and poor crystallinity. The thickness of the thin films increased with multiple coating cycles owing to better wetting ability of the sols on the substrate. This causes a thicker layer deposit for each subsequent layer [111]. The lower sheet resistance of the thin films was related with the improved crystallinity and increased crystallite size. This effect decreased the grain boundary scattering, increased carrier lifetime and mobility [112]. Another explanation could be that the relative density of the thin film improved from 65 % to 87 % with increasing number of coating cycle from 1 to 5 [113]. This explanation was connected to two important factors: (i) sol filled the pores of previous coating layer, (ii) connected pores disappeared during heat treatment process (recrystallization).

3.4. Experimental studies

Based on previous knowledge some of the previoulsy mentioned parameters (section 3.3) have been investigated experimentally.

3.4.1. Materials

The chemicals used in the thesis and their sources and purities are listed in Table 3.1. All chemicals were used without any further purification.

Table 3.1 Chemicals list.

Chemical Name	***Source***	***Purity***	***Formula***
Indium chloride tetrahydrate	Sigma-Aldrich	97 %	$InCl_3·4H_2O$
Indium nitrate hydrate	Sigma-Aldrich	98 %	$In(NO_3)_3·xH_2O$
Tin chloride pentahydrate	Sigma-Aldrich	98 %	$SnCl_4·5H_2O$
Acetylacetone	Sigma-Aldrich	99 %	$CH_3COCH_2COCH_3$
Anhydrous 2-propanol	Sigma-Aldrich	99.5 %	$(CH_3)_2CHOH$
Ethanol	Sigma-Aldrich	99 %	CH_3CH_2OH

3.4.2. Cleaning procedure for glass substrates

All glassware (erlenmeyer, beaker, etc.) and glass substrates (soda-lime-silicate with nominal composition or SLS, 25x25 mm) were cleaned according to the procedure shown in Figure 3.7. In order to obtain a homogenous and uniform coating, glass substrates were first washed with detergent and deionized water (DI-water). Then the samples were sonicated in acetone at 60 ºC for 20 min and washed with DI-water to clean any trace of acetone that may remain on the substrate. After DI-water cleaning, substrates were sonicated in ethanol at 60 ºC for 20 min and DI-water cleaning was repeated. Final step was sonication of substrates in DI-water at 60 ºC for 20 min. All glass substrates and glassware were dried in a conventional open air drying oven at 90 ºC for 20 min prior to coating operation.

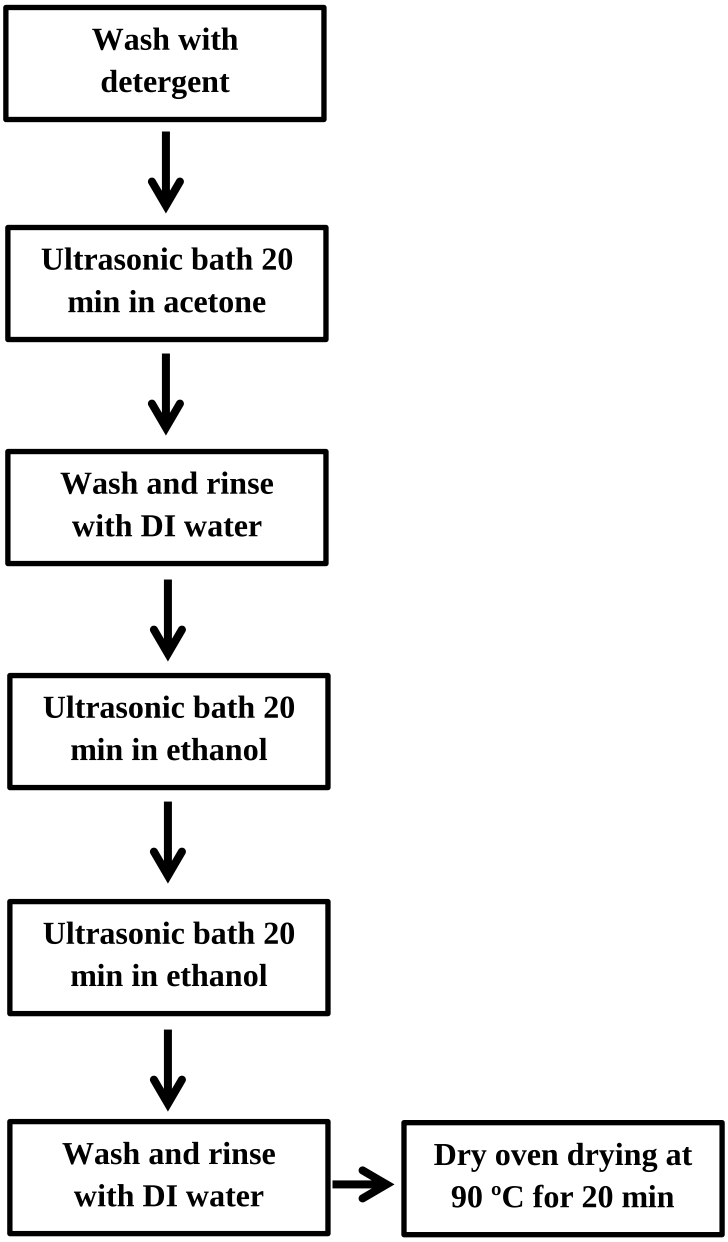

Figure 3.7 Cleaning procedure for glass substrates and glassware.

3.4.3. Preparation of ITO sols and deposition of the thin films

Generally, the precursor materials in sol-gel processing are organics and most of the time metal alkoxides. However, due to high cost of In and Sn organic compounds, inorganic metal salts such as indium nitrate or indium chloride and tin chloride can be used as alternative precursors for preparation of sol-gel ITO thin films. So, in this thesis metal salts were used as the starting chemicals.

ITO thin films were prepared by two different routes. In the first route ITO sols were prepared by $In(NO_3)_3 \cdot xH_2O$ and $SnCl_4 \cdot 5H_2O$ metal salts and aged at room temperature (25±1 ºC) for four days. In second route, again, ITO sols prepared by $InCl_3 \cdot 4.H_2O$ and $SnCl_4 \cdot 5H_2O$ metal salts then induced aged at relatively high temperatures, i.e. 60, 80, 90, 100 ºC. In both cases sols were deposited on pre-cleaned substrates.

3.4.3.1. Preparation (or synthesis) of naturally aged ITO sol

Figure 3.8 shows a flowchart for the experimental procedure. The sol-gel composition in this study was formulated to obtain 10 at. % Sn doping. The details in regard to the processing and preparation of coating solutions, the constituents and compositional ratios are also given in this flowchart (Figure 3.8). For preparation of the coating sol, 10.4 g $In(NO_3)_3.xH_2O$ was dissolved in 50 mL acetylacetone (AcAc) at 25 °C and the solution was refluxed at 80 °C for 3.5 h to ensure effective chelation. Meanwhile, 1 g $SnCl_4 \cdot 5H_2O$ was dissolved in 5 mL 2-propanol in another glass beaker with the help of a magnetic stirrer at 25 °C. Addition of the latter solution to $InCl_3$ solution was performed under continuous stirring. It should be noted that the viscosity of the sol should not be high to allow proper homogenization of the final resultant solutions. The coating sols were aged in ambient atmosphere at 25 °C for four days.

For investigating the effect of sol molarity on electrical, optical and structural properties of ITO thin films, different sol formulations were used. These different sol formulations and chemical constituent amounts are listed in Table 3.2.

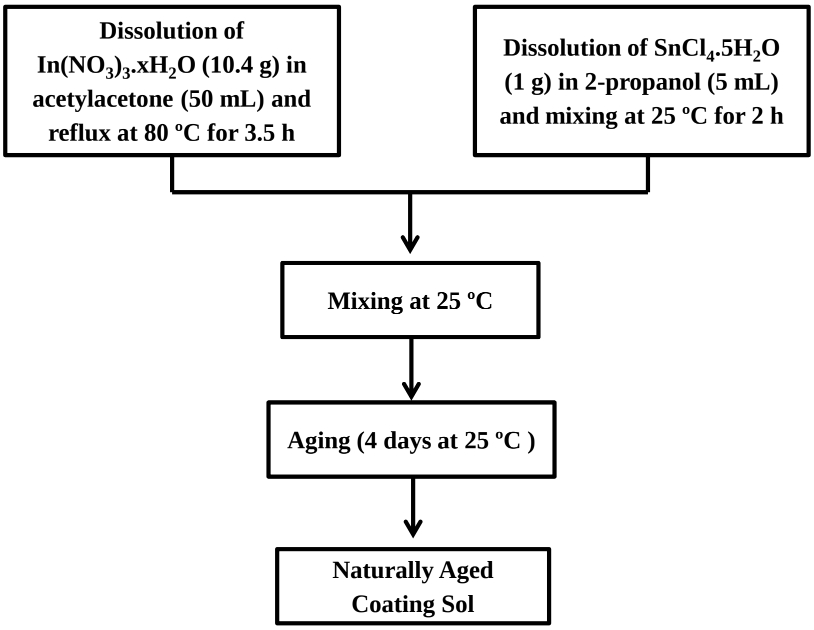

Figure 3.8 Processing route for naturally aged ITO coating sol.

Table 3.2 Formulations of naturally-aged ITO coating sols. (*: In+Sn:solvent)

	VARIABLE PARAMETERS		*FIXED PARAMETERS*	
ITO Sol Molarity* (M)	**$In(NO_3)_3{\cdot}xH_2O$ (g)**	**$SnCl_4{\cdot}5H_2O$ (g)**	**Acetylacetone (mL)**	**2- propanol (mL)**
0.1	0.3	0.035	10	1
0.2	0.6	0.07	10	1
0.3	0.9	0.105	10	1
0.4	1.2	0.14	10	1
0.5	1.5	0.175	10	1
0.6	1.8	0.21	10	1
0.8	2.4	0.28	10	1
1.0	3.0	0.35	10	1
1.2	3.6	0.42	10	1
1.4	4.2	0.49	10	1
2.0	6.0	0.7	10	1

3.4.3.2. Preparation of induce- aged ITO sol

Initially 8 g of $InCl_3\cdot4.H_2O$ dissolved in 45 mL of AcAc at 25 °C and then refluxed with 1 °C cooled water bath at 60 °C for 3 h. After refluxing, In:AcAc solution was cooled to 25 °C. In a separate beaker 1 g of $SnCl_4.5H_2O$ dissolved simultaneously in 5 mL of ethanol under rigorous stirring at 25 °C for 2 h. Finally, Sn:EtOH solution was added into In:AcAc solution to form premature ITO sol. The obtained sol was further stirred for 24 h and then induce aged for various durations (5, 8, 10, 13, 16 and 20 h) and temperatures (60, 80, 90, 100 °C). The detailed experimental flowchart is given in Figure 3.9. The details of studied induce aging parameters are given in Table 3.3.

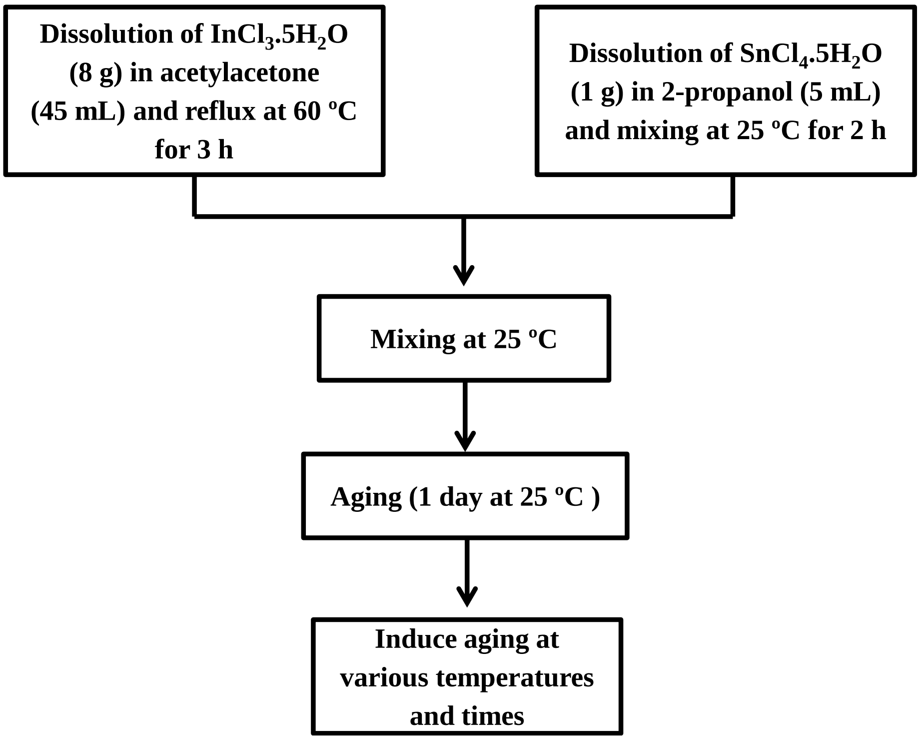

Figure 3.9 Processing route for induce- aged ITO coating sols.

Table 3.3 ITO coating sols prepared by different induce-aging paramaters.

FIXED PARAMETER	*VARIABLE PARAMETERS*	
ITO Sol Molarity (In+Sn:Solvent, M)	**Induce Aging Time (h)**	**Induce Aging Temperature (ºC)**
0.7	5	60
		80
		90
		100
	8	60
		80
		90
		100
	10	60
		80
		90
		100
	13	60
		80
		90
		100
	16	60
		80
		90
		100
	20	60
		80
		90
		100

3.4.4. Deposition of ITO thin films: coating procedure

The flowchart of the fabrication of ITO thin film is shown in Figure 3.10. A Laurell WS-400B-6NPP-LITE model spin coater was used to obtain both naturally and induce-aged ITO thin films on cleaned SLS glass substrates. Standardized coatings were fabricated at a spin rate of 3000 rpm for 30 s. Additionally, in order to investigate effect of spin rate and time some coatings were produced at various spin rate and time. Multiple spinning operations (1 to 10 cycles) were performed to obtain the final coatings. For each spinning step 200 µL of ITO sol (natural or induce-aged) was deposited on the substrate using a micropipette.

After each spin coating step, the wet coatings were put into a drying oven, and dried at 200 °C for 20 min. Finally, at the end of deposition, a heat treatment was applied to mature the coatings at 350, 450 or 550 °C for 1 h. The heating and cooling rate was adjusted to 5 °C/min.

A couple of processing parameters including; *i)* heat treatment temperature, *ii)* number of coating layer, *iii)* spin rate and time and *iv)* sol molarity investigated to elucidate the relationship between the processing parameters and electrical, optical, structural and morphological properties of the ITO thin films. The details of the studied processing parameters are shown in Table 3.4.

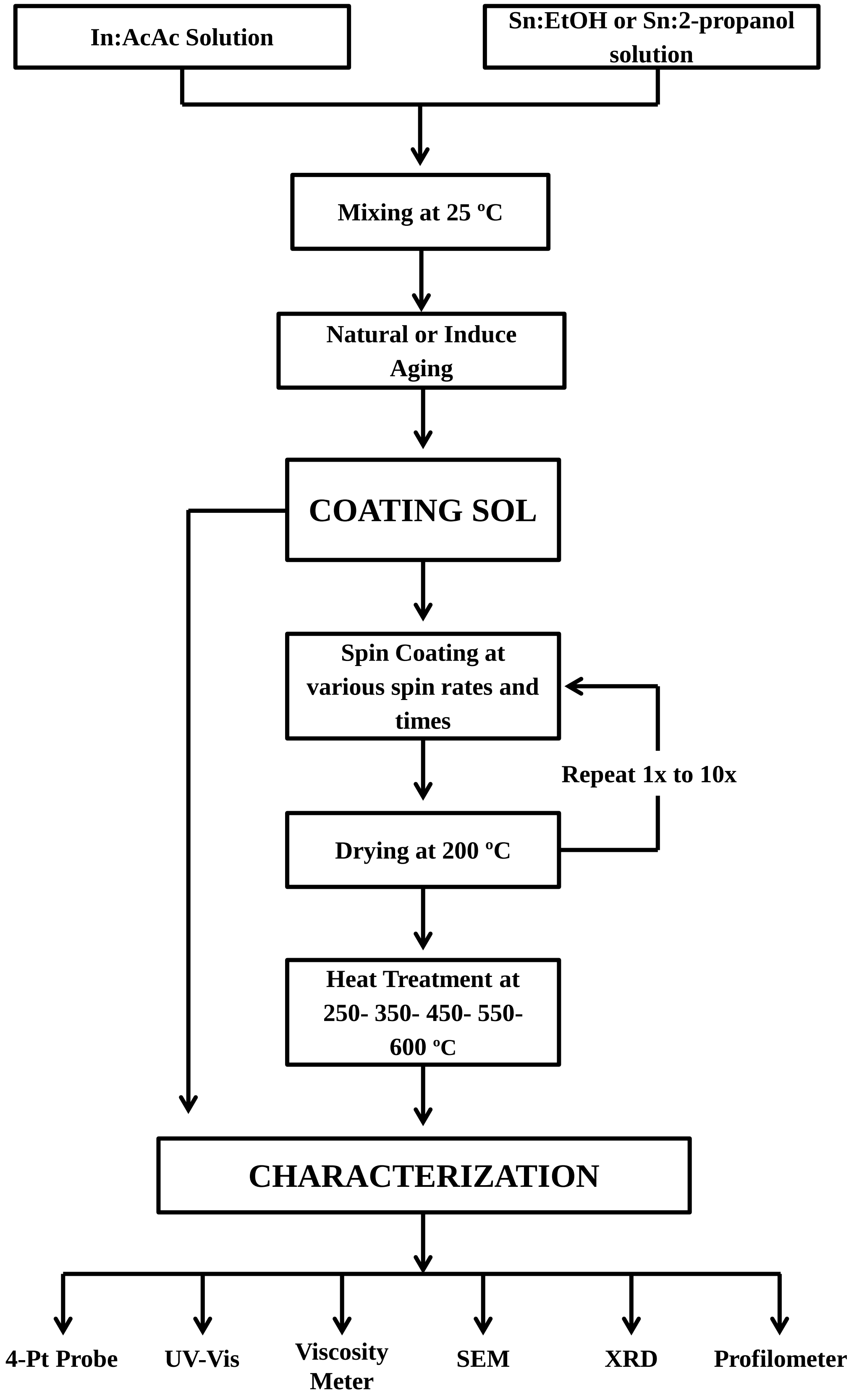

Figure 3.10 Fabrication and characterization procedure of sol-gel derived ITO thin films.

Table 3.4 The fabrication conditions of naturally aged ITO thin films.

		Heat Treatment Temperature (°C)			Number of Coating Layer					SPIN RATE (RPM)									SPIN TIME (s)									
		350	450	550	1	2	4	7	10	500	1k	2k	3k	4k	5k	6k	7k	8k	10	20	30	40	50	60	80	120	150	180
SOL MOLARITY (M)	0.1	X	X	X		X	X						X								X							
	0.2	X	X	X		X	X						X								X							
	0.3	X	X	X		X	X						X								X							
	0.4	X	X	X		X	X						X								X							
	0.5	X	X	X		X	X						X								X							
	0.6	X	X	X		X	X						X								X							
	0.7	X	X	X	X	X	X	X	X	X	X	X	X	X	X	X	X	X	X	X	X	X	X	X	X	X	X	X
	0.8	X	X	X		X	X						X								X							
	1.0	X	X	X		X	X						X								X							
	1.2	X	X	X		X	X						X								X							
	1.4	X	X	X		X	X						X								X							
	2.0	X	X	X		X	X						X								X							

3.5. Materials characterization

In this section, detailed information on the analytical characterization techniques is presented. X-ray diffraction (XRD) was used for phase analysis and determining the structural properties of ITO thin films. The surface morphology was examined by field emission scanning electron microscopy (FESEM or SEM), and the film thicknesses were determined using a surface profilometer. Optical transmittance analyses were conducted by a UV-Vis spectrophotometer. The rheology of coating sols was characterized in order to investigate effect of different sol formulations and aging parameters on the viscosity of the coating sol. Finally, electrical conductivity of the thin films was measured by 4-point probe electrical resistivity measurement set-up. The details are as follows.

3.5.1. X-Ray diffraction (XRD)

The chemical nature and phase evaluation of the sol-gel derived thin films were performed by X-ray diffraction (XRD) analyses using a Rigaku D/Max-2000 PC model diffractometer. The diffraction tests were performed for diffraction angle (2θ) between 20°-65°, at a scanning rate of 2°/min using Cu K_α radiation and an operation voltage and current of 40 kV 40 mA, respectively.

3.5.2. Field emission scanning electron microscope (SEM)

The microstructure of the thin films was examined using a FEI Quanta 400F model field emission scanning electron microscope (SEM). The samples employed in SEM investigations were coated with a 10 nm thick gold layer prior to examination.

3.5.3. UV-Vis spectrophotometry

The optical transmittance of the ITO thin films was measured using ultraviolet-visible (UV-Vis) spectroscopy (using Varian-Cary 100 Bio) in the wavelength range of 375 to 800 nm at room temperature. The uncoated glass substrates were used as blank reference for baseline determination.

3.5.4. 4-point probe electrical resistivity measurements

The sheet resistance values (in Ω/sqr) of the thin films were measured using a four-point probe conductivity measurement set-up (Jandel). The probe needle material was tungsten carbide with spacings of 1 mm, 1.27 mm and 1.59 mm. The sheet resistance values were measured at ten different locations on the same sample and the average values were reported.

3.5.5. Surface profilometer

Veeco Dektak M6 profilometer was employed for the coating thickness measurements of selected samples. Scan distance of the stylus was 10 mm, a span length enabling track of a step between bare and coated regions of partially coated PC substrates, which were specifically produced for thickness measurements. The average film thickness values were determined after three measurements at a scan speed of 50 s.

3.5.6. Viscosity measurements

Viscosity measurements of the ITO coating sols were done with Brookfield DV-E viscometer equipped with a disc spindle (SC4-18) and a small sample adapter was set at 25 °C by jacketed stainless steel cylinder. Before readings, sols were undergone shearing at shear rate of 100 rpm and readings were taken at 1 min intervals during 5 min.

3.6. The effect of processing parameters on the microstructure and optoelectronic properties of ITO sol-gel films

The ITO thin films were prepared via sol-gel spin coating method details are given *Section 3.4.4.* The effect of various processing parameters such as heat treatment temperature (annealing), spin coating process parameters (rate and time), number of coating layers, sol molarity, aging and heat treatment temperature on the optoelectronic performance and properties of thin films were investigated.

3.6.1. Effect of heat treatment temperature

Figure 3.11 shows the diffraction spectra of the ITO thin films obtained from “naturally-aged” sols heat treated at different temperatures. The films heat treated at 350 ºC were mostly amorphous. As expected, all the ITO coatings heat treated at 450 ºC or higher temperatures were crystalline. The same cubic bixbyite In_2O_3 crystal structure (JCPDS card no: 06-416) is seen regardless of heat treatment temperature. The XRD patterns revealed that the peaks (2θ degrees) at 30.6º, 35.6º and 51.1º respectively corresponded with the standard ITO pattern and these three intense peaks correspond to (222), (400) and (440) diffractions. It can be said that, especially intensity of the (222) peak was increased at high heat treatment temperatures, probably due to improved crystallinity of ITO thin film. No other phase(s) of Sn oxides or other relative compositions were found. However, there is a slight difference between peak positions to pure In_2O_3. This difference can be explained with the substitution of In ions by Sn ions. The substitutional Sn ions might expand the crystal lattice due to atomic size difference of the host and doping atoms. Another explanation can be connected with the strain effect of thin film. Due to thermal expansion coefficient mismatch between the film and the substrate, peak positions can change marginally.

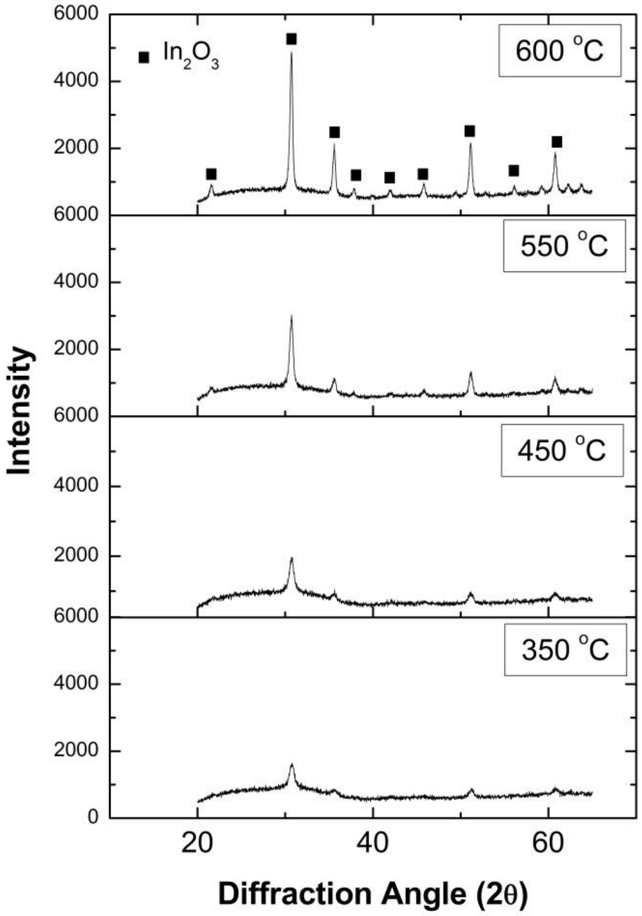

Figure 3.11 XRD diffractograms of ITO thin films obtained using naturally-aged sols after heat treatment at different temperatures.

Figure 3.12 shows the optical transmission spectra of the same thin films that were "naturally-aged" and heat treated at different temperatures. For the films heat treated at relatively lower temperatures (350 °C), the transmittance values for the visible range (400-700 nm) were around 70- 80 %. For well crystallized films that were obtained at higher heat treatment temperatures, such as 550 or 600 °C, these transmittance values are typically in the range of 88- 92 %. For the thin films formed at relatively low heat treatment temperatures i.e. 350 °C, a decrease in the transparency is observed with decreasing wavelength around UV region (wavelengths smaller than 300 nm). On the other hand, this change is much steeper for the thin films annealed at temperatures higher than 350 °C.

In addition, after heat treatment at 350 °C, ITO thin films turned to black, suggesting that some carbon related organic residuals still exist in the films and degrade the optical properties. Therefore, to obtain highly transparent ITO thin films, heat treatment temperature should be in the range of 450 °C to 600 °C. The residual organic groups from the solvents present in ITO thin films at relatively lower heat treatment temperature cause absorption in the visible range. As the heat treatment temperature increased further to 400 °C, transparency was increased due to elimination of these residual organics promoting the formation of ITO crystals. These results are consistent with the XRD patterns in Figure 3.12 suggesting the onset of crystallization at 450 °C. The increase in the optical transmittance with temperature could be attributed to increased structural homogeneity and crystallinity [114].

The absorption below 400 nm was most likely caused by the electron excitation from valance band to conduction band, corresponding to energy quanta comparable with the bandgap of Sn-doped In_2O_3 (approx. 3.5 eV). As heat treatment temperature was increased, there also a decrease in transmission values close to UV-range, i.e. below 350 nm.

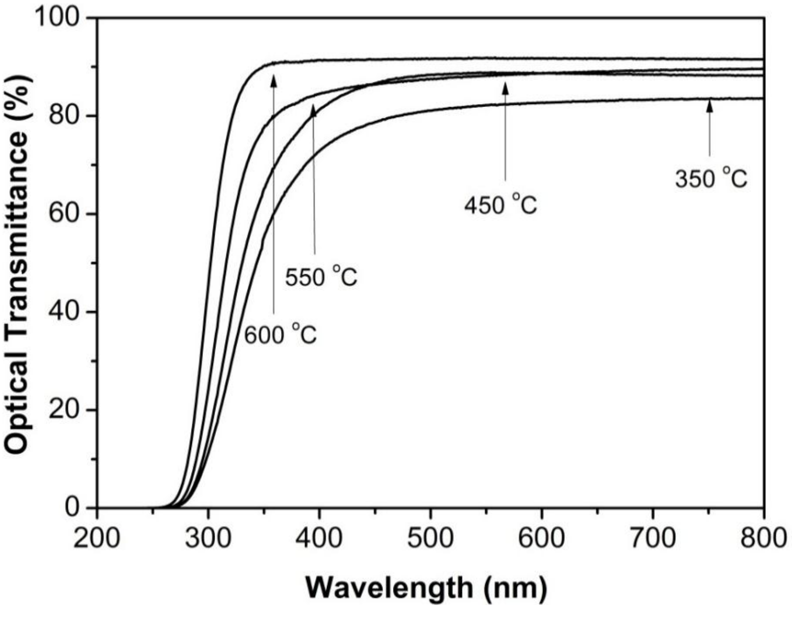

Figure 3.12 Optical transmittance spectra of ITO thin films prepared from naturally-aged sols after heat treatment at different temperatures.

Figure 3.13 shows the effect of heat treatment temperature on the sheet resistance of the thin films. The sheet resistance of the thin films reaches a minimum value for a heat treatment temperature of 550 °C. It is well known that by increasing the heat treatment temperature (in the range of 100 - 500 °C) the sheet resistance of ITO thin films decreases due to increased carrier concentration and also due to enhanced crystal growth leading to larger crystals [17, 18]. For a microstructure with large crystals, electron-grain boundary scattering decreases, which leads to higher carrier mobility and electrical conductivity. On the other hand, with increasing heat treatment temperature beyond 550 °C, the sheet resistance increases slightly. This is due to diffusion of the impurity ions from the SLS glass substrate into the ITO thin films. Even though the crystallinity improves with heat treatment, temperatures higher than 550 °C are expected to deteriorate the electrical conductivity, due to ion (Na^+, Ca^{2+}, etc.) exchange from underlying glass substrates [18]. In the rest of the study, only the optimum heat treatment temperature, i.e. 550 °C was used for calcination treatments.

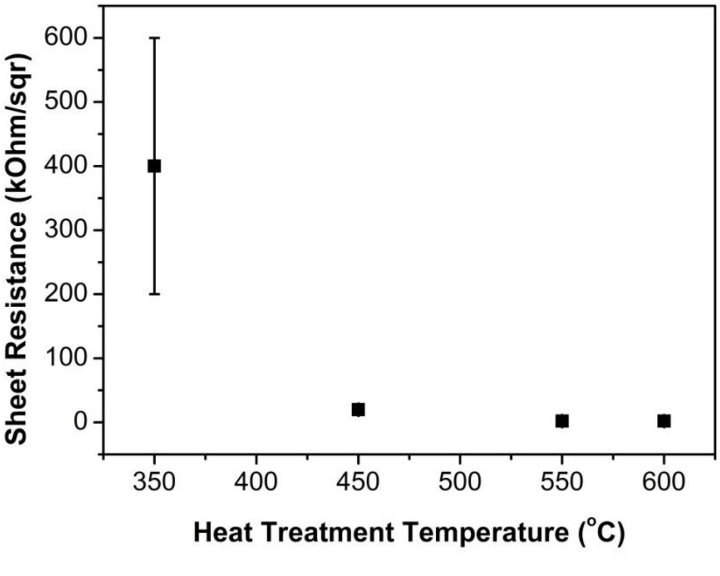

Figure 3.13 Sheet resistance of ITO thin films prepared from naturally-aged sol as a function of annealing temperature.

The effect of heat treatment temperature on the morphology of ITO thin film was revealed by SEM images shown in Figure 3.14. The low crystallinity and porous morphology of 350 °C heat treated thin film clearly seen. This porous microstructure is eliminated with increasing heat treatment temperature to 550 °C. These results were in agreement with the XRD results (Figure 3.11). Heat treatment improves the crystallinity and microstructures.

Two main mechanisms affect the mobility of the charge carriers in ITO thin films, which are ionized-impurity scattering and grain boundary scattering. As the heat treatment temperature was increased, the garin growth resulted in smaller grain boundaries and reduced grain boundary scattering. This leaded to improved transport of the electrons and also higher electrical conductivity.

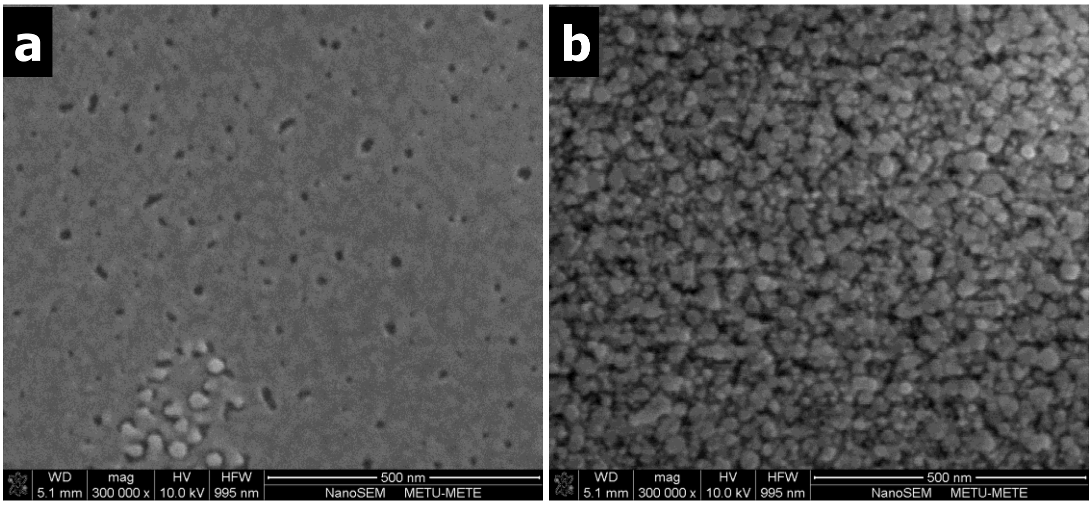

Figure 3.14 SEM images of ITO thin films heat treated at a) 350 and b) 550 °C.

3.6.2. Effect of spin coating parameters

Spin coating parameters that can change the thickness of thin films, which, in turn, will affect the optical and electrical properties of ITO thin films. Generally, the thickness of the thin films decreases with increasing spin rate and the relationship between spin rate and the thickness was given in a previous equation (*Section 2.5.3*). Additionally, spin time is another key parameter, which controls the solution flow mechanisms during spinning operation.

3.6.2.1. Effect of spin rate

The spin rate can change the film formation behavior and it controls/determines applied centrifugal force on deposited sol, velocity characteristics and turbulence of air between sol and air interlayer. So, the optimization of spin rate is crucial in fabricating high quality ITO thin films.

The XRD diffractograms of 4-layered ITO thin films, deposited at different spin rates are shown in Figure 3.15. The XRD analyses revealed that at all spin rates the detected peaks corresponded to the standard ITO pattern. It was also observed that the intensities of characteristic peaks decrease with increasing spinning speed. It is also well known that the spinning rate is inversely proportional to film thickness. The higher spinning rates resulted in thinner coatings. As the spin rate decreased, the (222) plane became sharper, indicating improved film crystallinity with thickness.

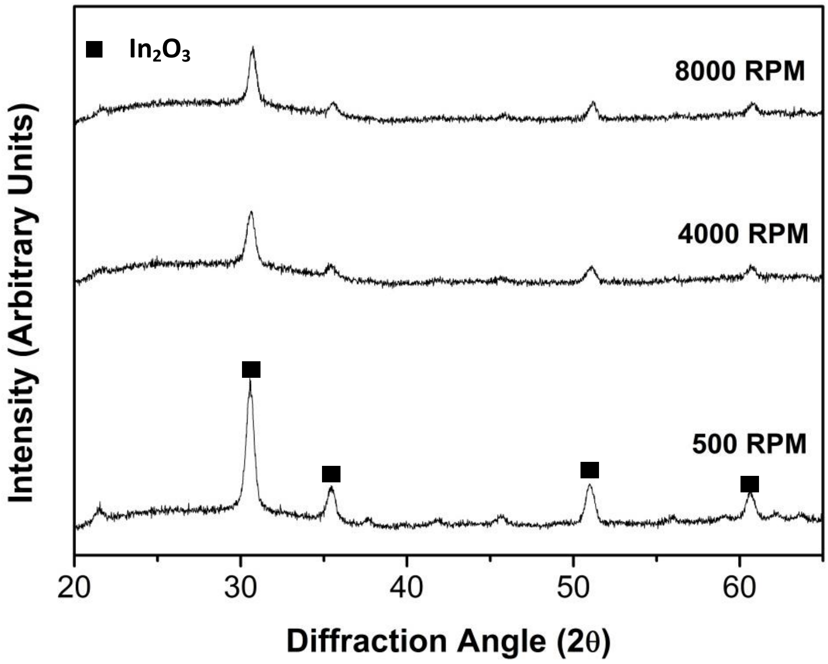

Figure 3.15 XRD diffractograms at the ITO thin films deposited at different spin rates.

Figure 3.16 shows the effect of spin rate on the optical properties of ITO thin films. The optical transmittance of ITO thin films changed with spin rate. The optical transmittance increased from 92 % (at 550 nm) for 500 rpm to 96 % for 3000 rpm and reached the highest value 99 % for the thin film spin coated at 8000 rpm. The optical transmittance continually increased with the increase in the spin rate. The relatively lower transmittance at a spin rate of 500 rpm might be due to thick film formation and non-homogenous pores within the thin film. Additionally, at low spin rates poor uniformity for the coatings and dark-yellowish contours were visually observed on the surface of thin films. This might be due to poor flow and lower degree of centrifugal force acting on the sol deposit during spinning, which results in relatively low optical transmittance. When the spin rate increases, with the help of centrifugal forces, the color contours disappear and more homogenous surface structure of thin films can be achieved. More homogenous film coverage eventually improves the optical quality of the film.

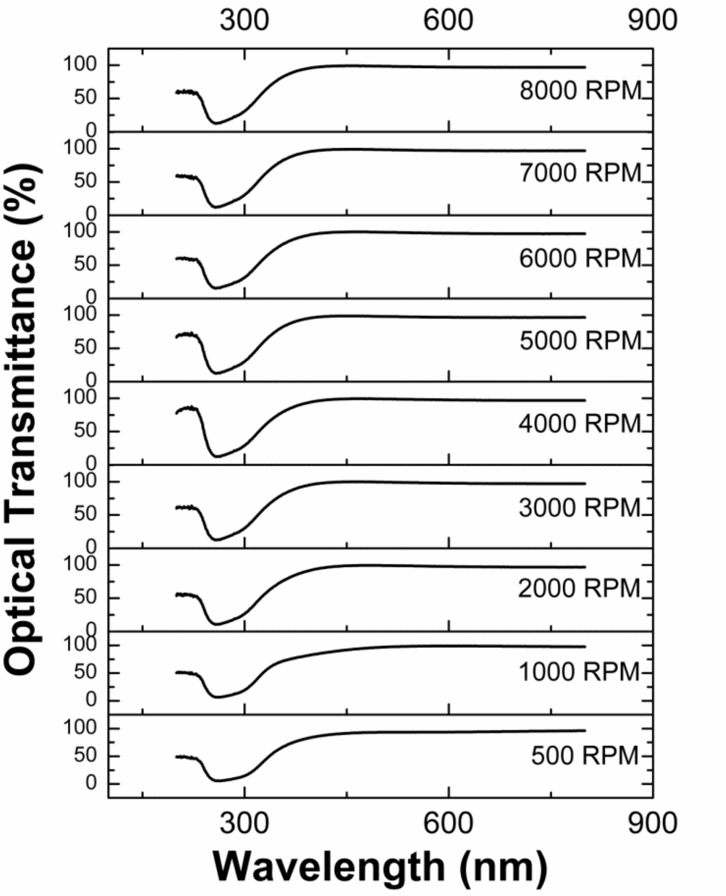

Figure 3.16 Optical transmittance of ITO thin films prepared using different spin rates.

The sheet resistance of the ITO thin films increased continuously with spin rate, as shown in Figure 3.17 The sheet resistance increased sharply from 0.8 kΩ/sqr to 2.3 kΩ/sqr when the spin rate was increased from 500 rpm to 4000 rpm and reached a maximum of 3.4 kΩ/sqr at 8000 rpm. This is most likely due to decrease in thin film thickness. Also high sheet resistance of thin films prepared by high spin rates can be due to the formation of smaller grains. Figure 3.18 shows the SEM micrographs of thin films prepared by 500, 1000, 5000 and 8000 rpm spin rates. There is a slight decrease in grain size with an increase in the spin rate and it was already mentioned earlier the small grain size negatively affect electrical conductivity of ITO thin films.

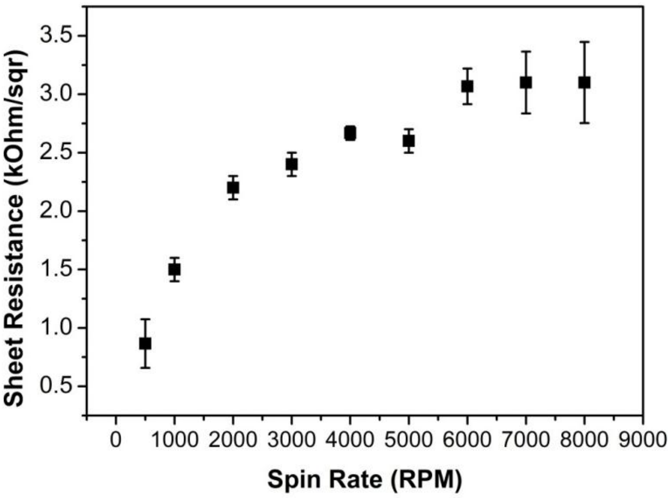

Figure 3.17 Sheet resistance of ITO thin films prepared using different spin rates.

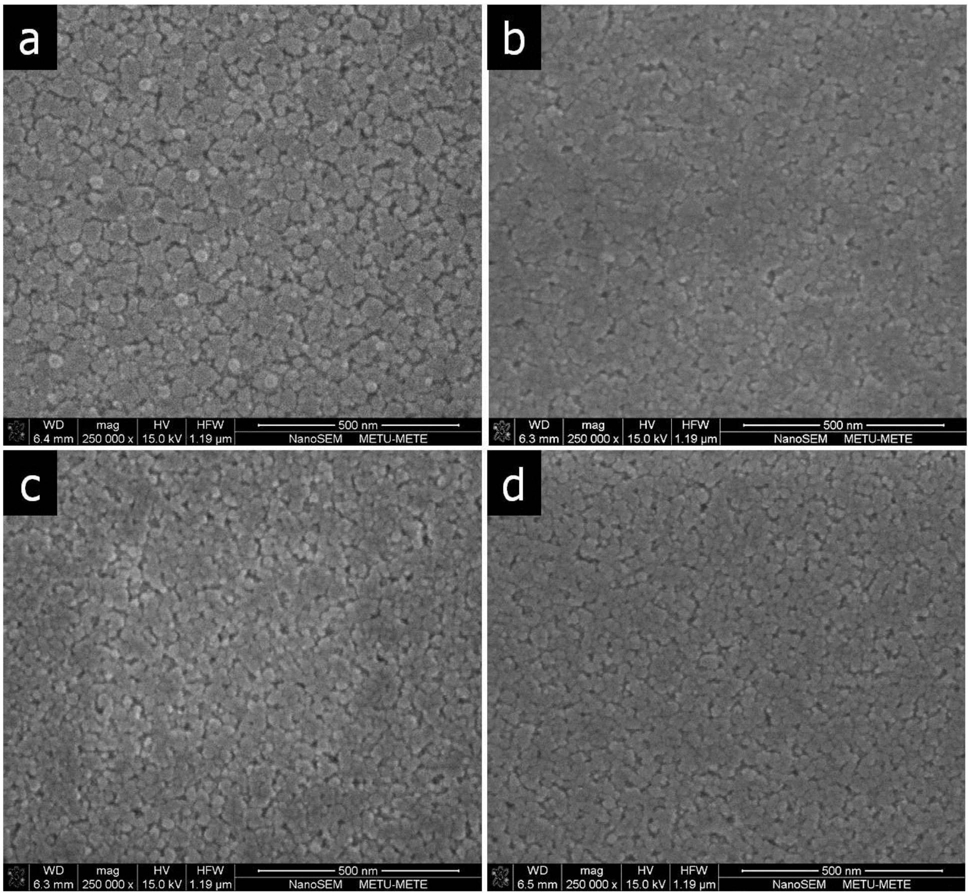

Figure 3.18 SEM micrographs of ITO thin films prepared with different spin rates of a) 500, b) 1000, c) 5000 and d) 8000 rpm.

3.6.2.2. Effect of spin time (duration)

Figure 3.19 shows the XRD diffractograms of the ITO thin films prepared at a spin rate of 3000. As can be seen from the figure no other phases beside In_2O_3 were detected. The diffractograms show that there is no significant change in the crystal structure with spin time. All of the diffraction patterns show similar features. It can be said that the spin time does not affect the crystal quality of the ITO thin films. Similarly, optical transmittance (Figure 3.20) and morphological (Figure 3.21) properties of thin films does not change with spin time. All of the coatings showed high optical transmittance (above 95 %). Additionally, SEM micrographs indicated identical morphology for all films deposited at different spin times.

However, electrical properties of ITO thin films were clearly affected by spin time. Figure 3.22 reveals that the sheet resistance of ITO thin films increased significantly with spin time. The lowest sheet resistance, 1.8 kΩ/sqr was obtained for the films spinned for 30 s, which was employed as the standard spin time for the rest of the experimental studies. Above 30 s, sheet resistance decreases down to 13 kΩ/sqr at 180 s spin time. This is probably due to reduced amount of deposited sol due to the presence of higher centrifugal forces during spin-off step. Long spin-off time may also cause effective and homogenous surface coverage. As a result of homogenous and defect free surface coverage optical, morphological and structural properties of thin films did not get affected by the spin time parameter directly. On the other hand, since the electrical conductivity is a function of film thickness, sheet resistance was increased.

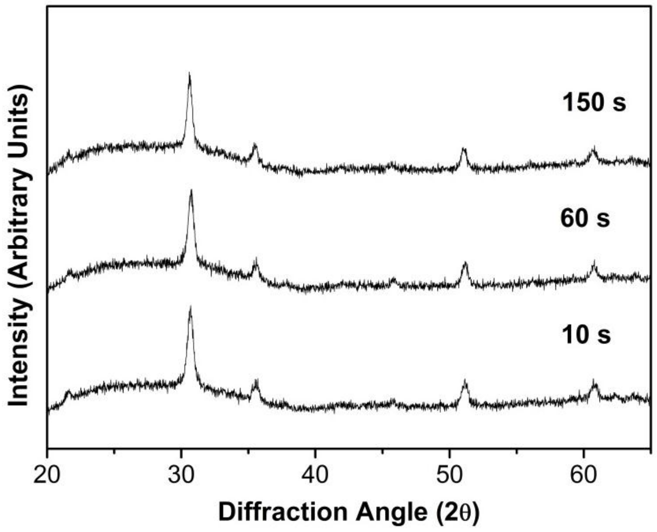

Figure 3.19 XRD diffractograms of ITO thin films prepared at different spin times.

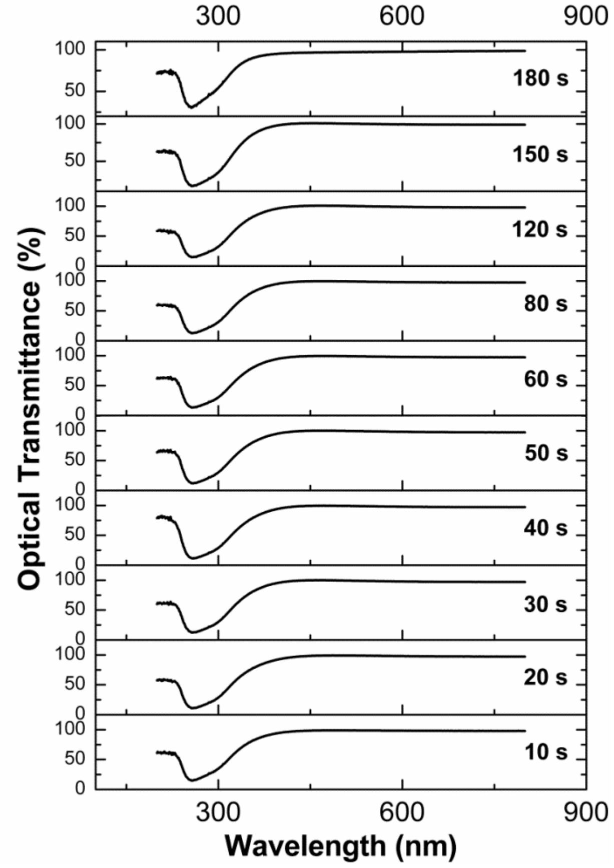

Figure 3.20 Optical transmittance of ITO thin films prepared at different spin times.

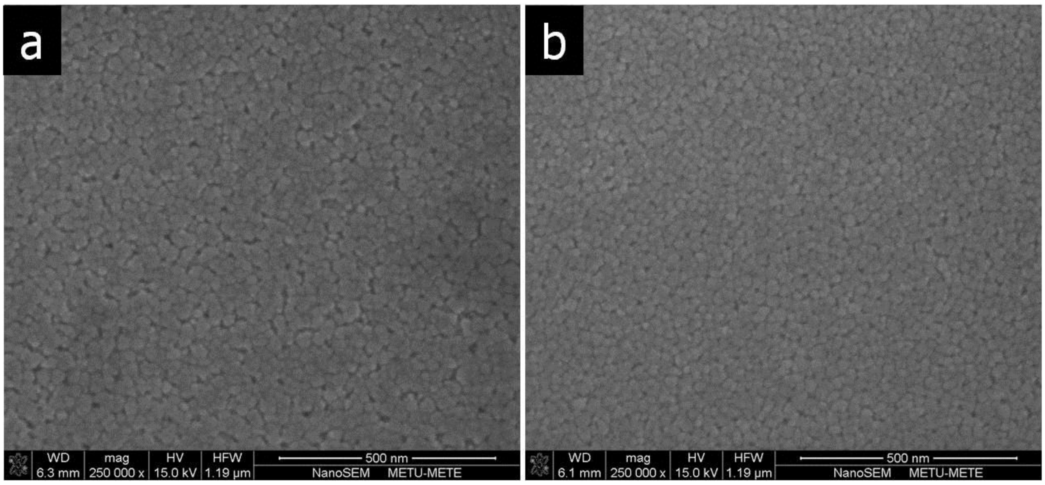

Figure 3.21 SEM images of ITO thin films prepared at different spin times of a) 10 and b) 180 s.

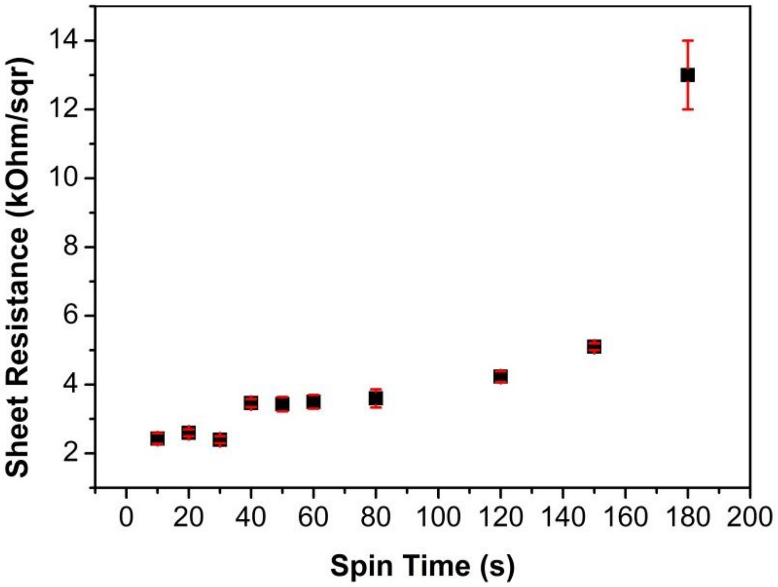

Figure 3.22 Sheet resistance of ITO thin films prepared at different spin times.

3.6.2.3. Effect of number of coating operation

Multilayered thin film coatings can also be formed for obtaining thicker coatings by repeating the spin coating process which includes subsequent spinning and drying cycles. The XRD diffractograms of ITO thin films formed by different number of coating layers are shown in Figure 3.23. It can be concluded that with higher number of coating operations, intensities for In_2O_3 increases due to formation of thicker films. In addition, when the number of coatings increased, the net duration of drying heat treatments increased which can additionally improve the thermally induced crystallization of ITO sols.

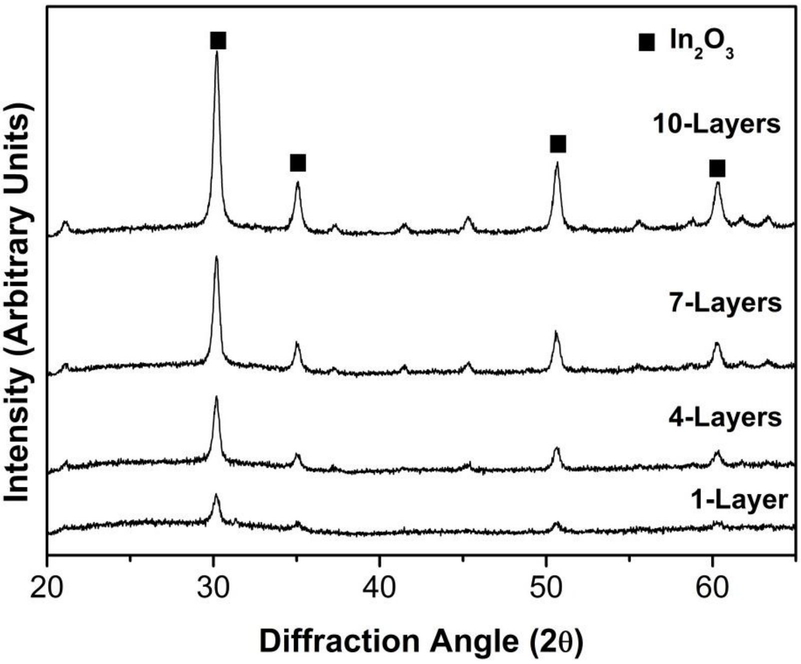

Figure 3.23 XRD diffractograms of ITO thin films prepared using different number of coating operations.

The optical transmittance of the ITO thin films as a function of the number of coating operations is presented in Figure 3.24. The optical transmittance of a single layered thin film was above 97 % in the visible range. However, the optical transmittance was decreased to around 60 % number of layers were increased to 10. The lower optical performance was a nature outcome of the increased film thickness.

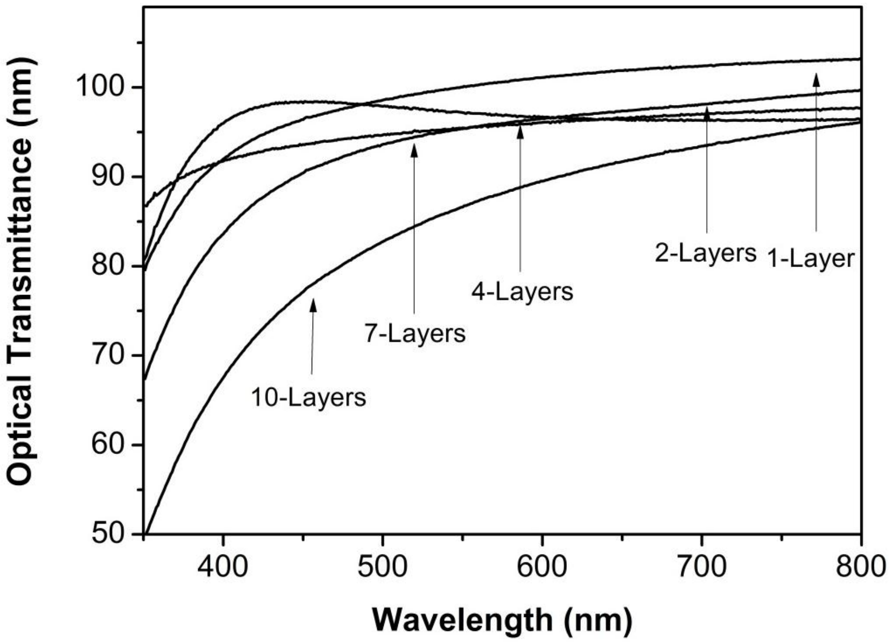

Figure 3.24 Optical transmittance of ITO thin films prepared with various number of coating operations.

Figure 3.25 shows the variation of the ITO thin film sheet resistance as a function of the number of coating steps. It can be seen that the sheet resistance decreased from 87 kΩ/sqr for single-layer coating to 0.8 kΩ/sqr for ten-layered coating. This is also attributed to an increase in the film thickness with the increased number of coating layers. In addition, the higher sheet resistance of the single layer coated thin film can be explained by the non-homogenous or discontinuous surface properties of film, i.e. insufficient coverage of the substrate or poor crystal quality and more pronounced alkaline ion diffusion from underlying glass substrate.

The sheet resistance of thin film was not changed linearly with increasing number of coating layers. This might be related with the wetting ability differences of bare substrate and pre-coated film layer. During the experimental studies, it was usually observed that the ITO sols were spreaded more easily on ITO coated surfaces, rather than bare glass substrate. This suggests that each subsequent layer was denser than the previous one due to enhanced wetting on precoating.

In summary, the effect of spin rate on the electrical sheet resistance might be due to increase of film thickness, but number of coating layer operation not only changes the thickness but also controls the density of ITO film. The effect of densification can be attributed to two factors: first, pores might be filled with subsequent coating steps. Second is related with the pore elimination during recrystallization. Some studies showed that presence of the dense crusts can heavily improve the thin film density in multilayer coatings [115].

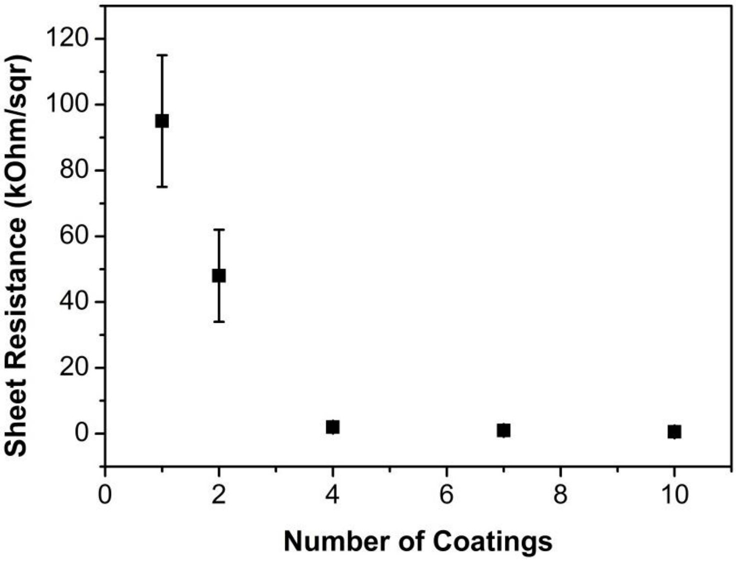

Figure 3.25 Sheet resistance of ITO thin films prepared with various number of coatings.

3.6.2.4. Effect of sol molarity

The optoelectronic performance of ITO thin films strongly depends on the coating sol molarity (In and Sn precursors:total solvent amount). So with this motivation the variations in structural, electrical, rheological and optical properties of the ITO sol-gel films with sol molarity has been investigated with a parametric approach. For this purpose, only 4-layered coatings calcined at 550 °C for 1 h were further investigated.

The effects of ITO sol molarity on the thickness, viscosity and crystallinity of 4 layered ITO thin films heat treated at 550 °C for 1 h are shown in Figure 3.26 and Table 3.5, respectively. It can be seen that the thickness, viscosity and crystallinity of the films were increased with the increase in the sol molarity. Figure 3.26 reveals that all the thin films were polycrystalline In_2O_3; whereas, only the coating prepared with low molarity (0.1 M) shows poor crystal quality. The low intensity and amorphous characteristic of low molarity thin films was greatly reduced and disappeared with increasing the molarity of the sol. From these results, it can be concluded that, with the increase of sol molarity the crystallinity of thin films increases within the concentration range srudied in this work, i.e. up to 2.0 M.

Table 3.5 Thickness and viscosity measurement results of ITO thin films prepared with various coating sol molarities.

Sol Molarity (M)	**Thickness (nm)**	**Viscosity @ 25 °C (cP)**
0.1	81±5	0.92
0.2	127±8	1.12
0.3	176±7	1.26
0.4	220±12	1.33
0.5	271±18	1.41
0.6	292±15	1.45
0.8	302±23	1.49
1.0	335±20	1.58
1.2	361±27	1.73
1.4	401±26	1.91
1.6	638±40	2.14
2.0	845±53	2.31

The thickness and viscosity results are in good agreement with the XRD findings. The thickness increased from 81 nm for 0.1 M sol to 302 nm for 0.8 M sol and reached the highest value of 845 nm for thin film prepared with 2.0 M coating sol. Similar trend was also obtained from viscosity measurements. The viscosity increased from 0.92 cP (0.1 M) to 1.49 cP (0.8 M) and reached the highest value of 2.31 cP for thin film prepared with 2.0 M coating sol. It is previously mentioned that, viscosity is one of the most important spin coating parameters *(Section 2.5.3),* which determines the thickness of the film. At low viscosity values, deposited coating sol easily flows on the surface of the substrate and with applied centrifugal forces a thin layer of coating can easily be formed. On the other hand, with increasing sol molarity due to an increase in the viscosity, sol shows relatively high resistance to centrifugal forces and thicker coatings can be formed. The low molarity coating sols were mainly composed of volatile solvents (such as acetylacetone and 2-propanol), which evaporate during drying. But with increasing molarity, the inorganic content increased and the thickness of the film increased. As a result of increased thickness of the films the crystal quality and characteristic peak intensities of thin films increased, when higher molarity (highly viscous) sols were employed.

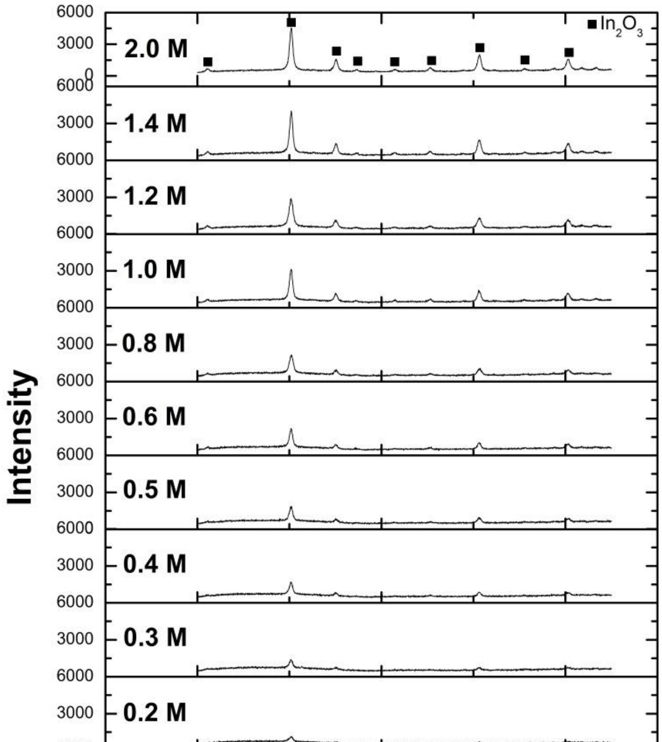

Figure 3.26 XRD results of ITO thin films prepared with various coating sol molarities.

The UV-Vis spectra of the ITO thin films prepared with various sol molarities are shown in Figure 3.27. The figure indicates that with increasing sol molarity the optical transmittance of thin films decreases. The optical transmittance at 550 nm decreased from 98 % (film of 0.1 M coating sol) to approximately 70 % for thin film prepared with 2.0 M coating sol. The thickness of the films heavily influenced the optical quality. When the sol molarity was low, i.e. around 0.1 or 0.2 M, the film thickness was about 80- 120 nm, which resulted in high optical transmittance. For high molarity sols, such as 1.6 or 2.0 M, because of the dominant effect of thickness (around 700 nm) transmittance decreased down to 70 %. In addition, another interesting finding based on UV-Vis spectral data was the difference in absorption behaviour. In 300- 400 nm wavelength region the absorption edge changes with changing sol molarity. At low sol molarities absorption edge of the coatings was narrow but with increasing sol molarity it get become broad and deep. This effect was mostly caused by the electron excitation from valence band to conduction band. This is in good agreement with the sheet resistance results. For highly conductive thin films, absorption edge becomes broader and deeper. Figure 3.28 shows the variation of the sheet resistance as a function of the sol molarity. The results show that the sheet resistance decreased from 57 kΩ/sqr (0.1 M) to 0.5 kΩ/sqr (2.0 M) when a highly concentrated coating sol was used.

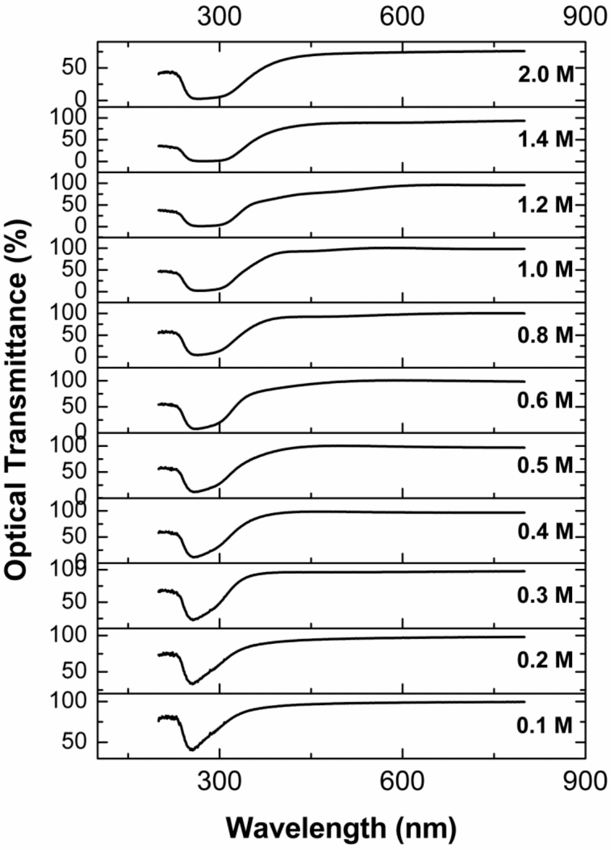

Figure 3.27 UV-Vis spectra of ITO thin films prepared with various coating sol molarities.

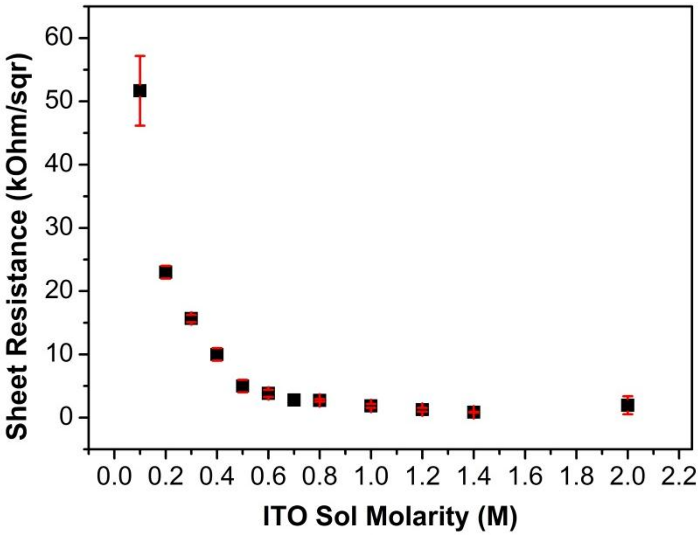

Figure 3.28 Sheet resistance of ITO thin films prepared with various coating sol molarities.

The molarity of the coating sol also affected the thin film morphology. Figure 3.29 show SEM micrographs of thin films prepared with 0.1, 0.2, 0.3, 0.4, 0.5, 0.6, 0.8, 1.0, 1.2, 1.4, 1.6 and 2.0 M coating sols. The insets are higher magnification (500000X) images of the same samples representing the change in the grain sizes of the films. At low sol molarities, highly smooth and small grain sized morphology was observed. However, with increasing sol molarity the surface morphology became relatively rough and grain size was gradually increased. High inorganic content of the high molarity sols might be led to increase the crystallite size during heat treatment

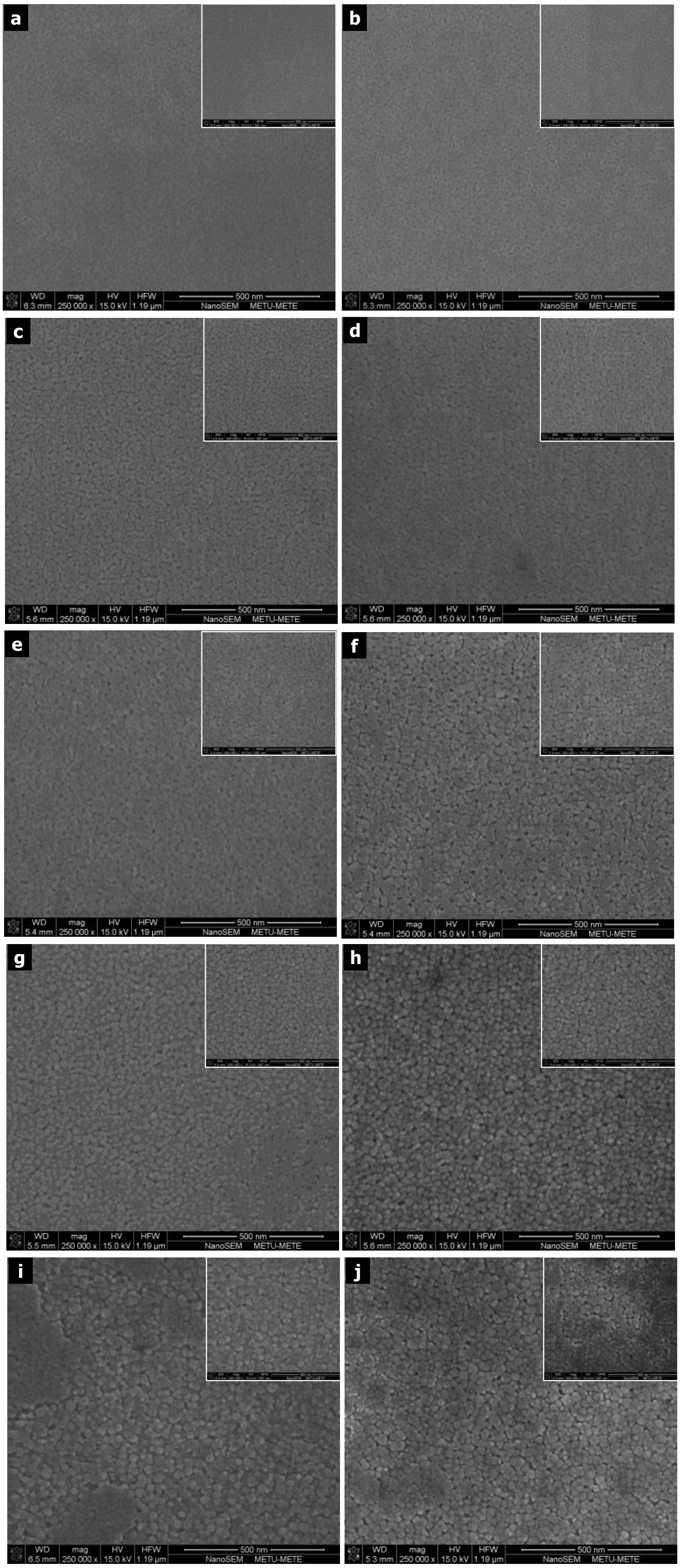

Figure 3.29 SEM images of ITO thin films prepared with various sol molarities.

3.6.2.5. Effect of induced-aging

A series of experiments were conducted to define the processing parameters required to obtain homogenous film coverage and to eliminate multiple coating steps. Thus, some experimental adjustments were carried out for the pre-coating step to physically modify the coating sol. Indium chloride-based coatings sols were cured at various temperatures for defined durations in the experiments. This applied process will be called as “induced-aging” in the following parts. Several aging time and temperature combinations have been investigated. However, only the data for the films aged at 80 °C (up to 48 h) is presented.

Figure 3.30 shows the XRD diffractogram of the ITO thin films obtained from induced-aged (at 80 °C for 3 h) and naturally-aged solutions after annealing at 550 °C (50 min. in ambient atmosphere). This figure shows that the thin films prepared from “induced-aged” sols have relatively intense and well defined diffraction peaks compared to those films prepared from “naturally-aged” sols. This can be explained with the improved in crystallinity of ITO thin films as a result of induced aging.

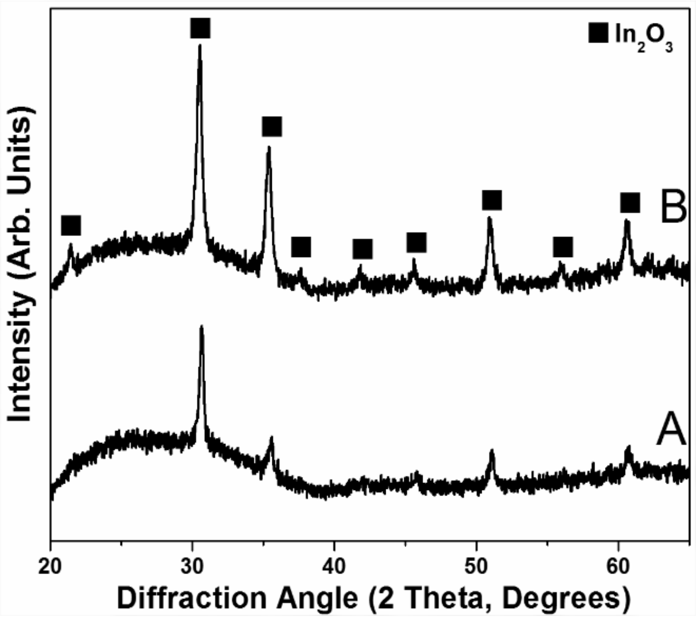

Figure 3.30 XRD patterns of ITO thin films prepared from (a) naturally-aged, (b) induced-aged sols annealed at 550 °C.

The aging process also affected the electrical properties of ITO thin films. Figure 3.31 shows the sheet resistance of ITO thin films as a function of aging duration. All samples were aged at 80 °C and calcined at 550 °C in ambient atmosphere for 1 h. It was observed that the sheet resistance of ITO thin films decreased significantly from 20 kΩ/sqr to 0.7 kΩ/sqr upon 3h aging. However, the sheet resistance increased to 25 kΩ/sqr after 48 h aging. The minimum sheet resistance was found to be 0.4 Ω/sqr for the sample subjected to induced aging at about 3 h, much lower than the typical values for "naturally-aged" sol derived films. The decrease in sheet resistance with increased induced-aging time may be explained with an efficient completion of sol-gel reactions leading complete polymerization of In_2O_3 network from partially hydrolyzed In–OH groups causing enhanced crystallization. The reason for increase in the sheet resistance for the films undergone to prolonged aging is unclear.

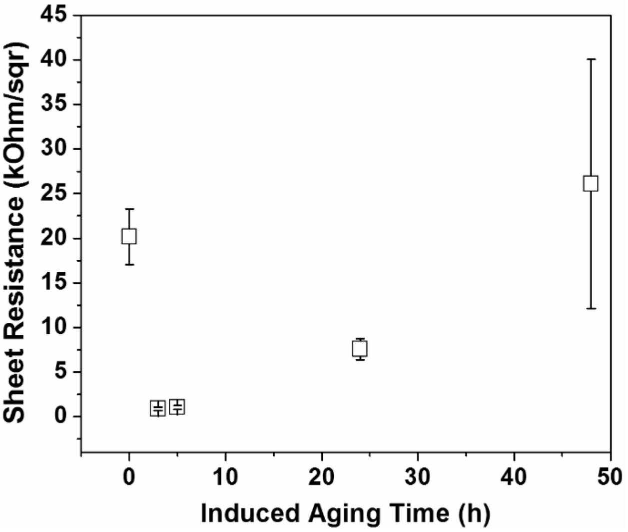

Figure 3.31 Sheet resistance of ITO thin films prepared from induce-aged sols as a function of aging duration (after annealing at 550 °C).

Figure 3.32 shows the SEM images of the thin films obtained from "naturally-aged" and "induced-aged" sols heat treated at 550 °C. The surface coverage for both thin films are similar; without any remarkable cracks and voids, indicating formation of uniform films on glass substrates. Meanwhile, both thin films have sub-micron size equaxed ITO crystals; but, structural arrangement were much more organized for the thin film obtained from “induced-aged” gel without any void-like faults. This morphological difference also provides some insights for observation of higher electrical conductivities for the ITO thin films of this processing route.

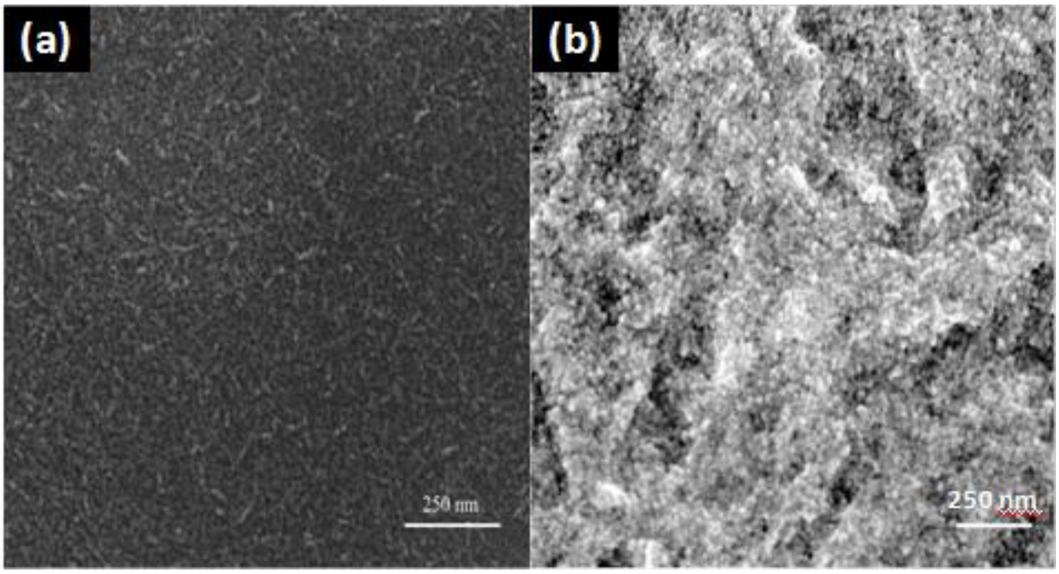

Figure 3.32 Surface SEM images of the thin films after annealing at 550 °C obtained from different sols a) formed by induced-aging, b) formed by natural aging.

Optical transparency is another important factor defining the overall performance of the ITO thin films. As mentioned earlier, thin films obtained from “naturally-aged” sols typically exhibited 90-97 % optical transmittance in the visible range. According to the related literature, 80% optical transmittance in the visible range is the limiting value for high performance TCO thin films. The highly conductive films prepared from induced aged (3 h) sol, on the other hand, showed relatively poor optical properties with an average optical transmission value of %86 in the visible range, which can be still considered acceptable for most of the technological applications of ITO thin films.

CHAPTER 4

FABRICATION OF ITO NANOPARTICLE INCORPORATED HYBRID ITO THIN FILMS

In this chapter, a relatively novel approach in processing sol-gel ITO thin films is presented. This is based on incorporation of ITO nanoparticles into the ITO-sols, obtained in the previous chapter. The main objective was to study the effect of such hybrid colloidal/sol-gel processing modification on physical properties of the resultant ITO films. This chapter starts with an overview on the stabilization techniques for dispersion of ITO nanoparticles in organic solvents. The physical and chemical origin of stabilization mechanism is briefly explained. Then, the colloidal stabilization results on ITO nanoparticle introduced suspensions are presented. Finally, the effect of such modification on ITO film performance properties; i.e. optoelectronic and microstructural are reported.

4.1. Introduction: Rationale for the hybrid thin films

As it was mentioned, ITO thin films characteristically offer low electrical resistivity, high optical transmittance and superior adhesion to the substrate. Sol-gel process is a promising technology to fabricate ITO thin films due to its low cost and processing easiness. However, electrical conductivity of sol-gel ITO thin films are usually poor compared to films prepared by vacuum based processing techniques, such as physical vapor deposition (PVD) and chemical vapor deposition (CVD). In order to solve this drawback, Toki et al. [116] investigated an alternative approach by dip coating of ITO sols including ITO nanoparticles for obtaining thin films. The function of ITO nanoparticles in sol is to promote crystallization at lower heat treatment temperature and improve electrical conductivity of thin films. They reported sheet resistance values in the range of 38 to 43 Ω/sqr. Similarly, Goebbert et al. [117,118] mechanically dispersed ITO nanoparticles in water-ethanol and organic dispersant system. The coatings were deposited on silica substrates by dip coating process. After heat treatment in reducing atmosphere, a resistivity value of $3.4x10^{-3}$ Ωcm was obtained. Hong and Han [119] demonstrated that 100 nm thick films can be formed by spin coating of ITO sol with 0.6 wt. % ITO nanoparticles. The important finding of this study was the demonstration of the decrease in crystallization temperature (around 35 ºC) of amorphous ITO gel. However, these thin films showed a sheet resistance of $7x10^{3}$ Ω/sqr and optical transmittance of 83 %. This is strongly related with poor dispersion of nanoparticles. Al-Dahoudi and Aegerter [120] alternatively studied single step spin coating process using colloidal ITO nanoparticle suspension. These thin films showed sheet resistance of 320 Ω/sqr after heat treatment at 550 ºC and post treatment at 300 ºC. But, this low sheet resistance was directly attributed to the formation of thick layer, which cannot be used in practical technological applications such as touch screens.

In the light of these studies it can be said that *"dispersion of ITO nanoparticles"* is one of the important processing issues in order to adapt this to sol-gel based processing routes. In order to disperse ITO nanoparticles in the coating sol first step is stabilizing ITO suspension in an organic solvent. This can be done by two major approaches: *electrostatic* and *steric stabilization*. Generally, steric stabilization is preferred due to some difficulties in electrostatic stabilization in organic solvents. The electrostatic repulsive forces of pure ITO colloids are very weak and agglomeration of nanoparticles is a common problem [121-122]. However, with increasing/controlling zeta potential of particles (or surface charge) in suspension, effective repulsive forces can be generated.

4.2. Stabilization of oxide particles in aqueous solutions

4.2.1. Colloidal suspension

Colloidal suspensions are chemical mixtures which are different from solutions. A colloidal system may be in solid, liquid, or gas form, and consists of two separate phases. First phase is *dispersed phase,* which is also called internal phase and the second one is the *continuous phase,* which is also called dispersion medium [123].

There are two groups for classification of colloidal system:

- Since colloidal dispersions have high surface free energy, this kind of systems is thermodynamically unstable and irreversible. Therefore, it is not easily to reconstitute the colloidal dispersions after phase separation.
- True solutions of macromolecular materials (natural or synthetic) are thermodynamically stable and irreversible on the contrary to colloidal dispersions. Thus, reconstitution can be obtained after separation of solute [124].

4.2.2. The electric double layer

The electrical double layer is an electrical structure, which appears on the surface of a particle when it is incorporated into a liquid medium. This electrical structure consists of two layers of active ions. The first layer is consisting of a surface charge, which can be either positive or negative and overlaps with the surface of the particle. The second layer is in the liquid medium and electrically cover up the first layer. This layer can also be called as diffuse layer due to formation of free ions in the liquid, which affects the electrical attraction [125].

Lykema stated the reason for the formation of electrical double layer with non-electric affinity of charge determining for a surface [124]. This process leads to the formation of electrical surface charge which is generally denoted in describe C/m^2. The surface generates an electrostatic field which affects the ions located in the liquid medium. Both electrostatic field, and thermal motion of the ions creates an opposite charge, which screens the electrical surface charge. The net electrical charge of this diffuse layer equal to the surface charge; but, with opposite polarity, that makes the final electrical structure as neutral. Some of the counter ions might absorb near the surface and this build inner-sub layer is called as *Stern Layer*. The outer part of the screening layer is called as *Diffuse Layer.*

The tangential stresses can cause to the diffuse layer or at least part of it. There is a conventionally introduced slipping plane, which seperates the liquid from particle surface. The electrical potential of this separated plane is called as *zeta potential* (ζ- potential). The zeta potential is a very useful value for estimating the degree of electrical double layer charge. The characteristic zeta potential range is in between 25- 100 mV. If zeta potential reaches to zero this point is called as *"point of zero charge"* or "*isoelectric point"*. The isoelectric point of aqueous suspension is usually determined by the suspension or solution pH value [125].

4.2.3. Interparticle forces

In a regular suspension, colloidal particles or nanoparticles experience; *i) Van der Waals* forces due to dipole-dipole interactions, *ii) electrostatic repulsion forces* due to overlapping of the interaction of double layers, *iii) solvation forces* due to forces arising from interactions of the nanoparticles with the solvent molecules. Additionally, there are somewhat different forces arising adsorbing organic layers (*electrosteric or steric forces*).

4.2.4. Steric stabilization

One type of repulsive force is the steric force. This force can be created by the addition of surfactants or polymers, which get attracted to the surface of the particle via physical or chemical bonding and prevent the agglomeration of particles. When two sterically stabilized particles approach each other, the organic molecules interact and resist further approach. This mechanism is schematically illustrated in Figure 4.1 [126]. The surfactant coverage which is affected by the solvent type and the bond type formed at the surface has influence on the stabilization repulsive force [127].

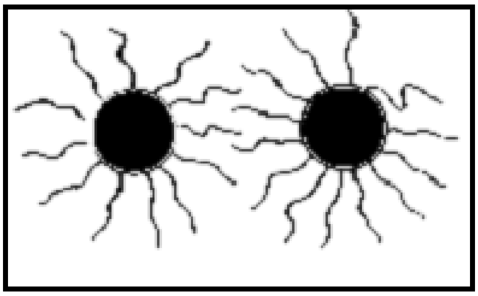

Figure 4.1 Schematic representaion of steric stabilization [47].

4.2.5. Electrostatic stabilization

Different mechanism can be applied to particles for electric charging which can be changed by controlling the pH value of suspension (called zeta potential) and by using appropriate dispersants. The particles have balanced charge while ions in liquid have the opposite charge with equal amount. An electrical double layer is formed by clustered ions around the particles. A schematic illustration of this phenomenon is shown in Figure 4.2. When the distance between particles increases, the electrical potential reduces exponentially resulting in obtaining uniform value in the double layer. Beyond the double layer, voltage difference called zeta potential is created between a short distances from the particle surface layer [126]. Double layers become closer and eventually overlap as two particles get closer each other. The zeta potential affects the strength of the electrostatic force. In order to prevent the agglomeration of particles, the zeta potential (more than 30 mV) should be higher than the van der Waals force between the particles. As a result, uniform dispersion can be obtained with high zeta potential value [127,128].

In production of ceramics or coatings through the conventional sol-gel methods, electrostatically stabilized sols can be used. Thus, sol-gel transformation is the important point of the nano processing [129].

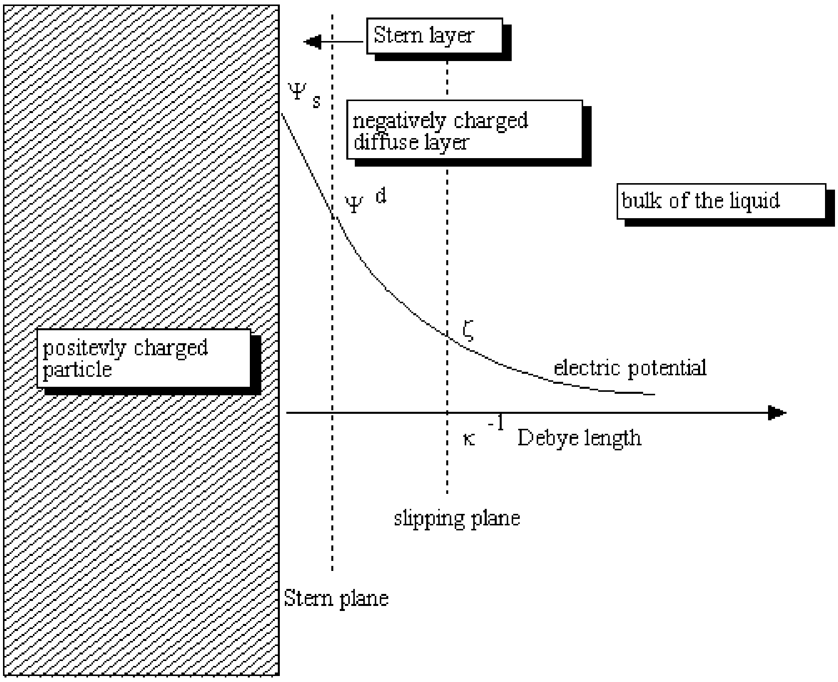

Figure 4.2 Detailed illustration of interfacial double layers [125].

4.3. General processing scheme to obtain well dispersed suspension

Dispersion of inorganic paticles in a liquid occurs in several stages. Initially wetting (i.e. liquid phase wets and spreads on the powder surface) occurs. Then agglomerates, if any, are broken down or fracturated into essentially primary units. Finally, the primary particles must remain dispersed in the liquid medium and reagglomeration must be prevented by some type of stabilization mechanism.

The algorithm, shown in Figure 4.3, demonstrates a general processing scheme to obtain a stable and well dispersed inorganic particle suspensions.

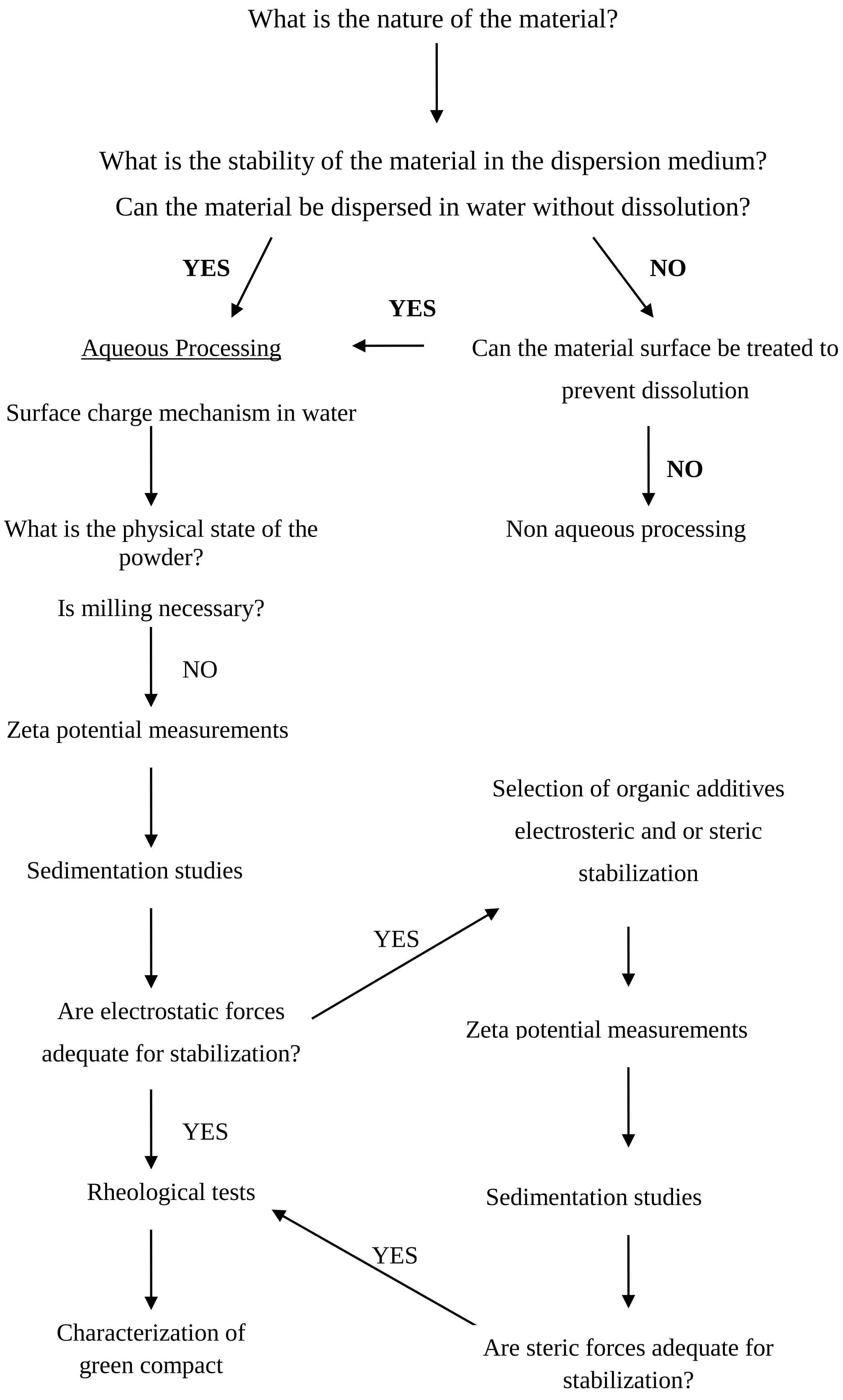

Figure 4.3 General processing algorithm to obtain stable and well dispersed nanoparticle suspensions [125].

4.4. Experimental studies on ITO-nanoparticle incorporated ITO-thin films

4.4.1. Materials

The chemicals used in this part of thesis and their sources/purity are given in Table 4.1. All listed chemical used without further purification.

Table 4.1 Chemicals list.

Chemical Name	***Source***	***Purity***	***Formula***
Indium tin oxide (ITO) nanopowder	Sigma-Aldrich	99 %, <50 nm	In_2O_3:Sn
Indium nitrate hydrate	Sigma-Aldrich	98 %	$In(NO_3)_3 \cdot xH_2O$
Tin chloride pentahydrate	Sigma-Aldrich	98 %	$SnCl_4 \cdot 5H_2O$
Acetylacetone	Sigma-Aldrich	99 %	$CH_3COCH_2COCH_3$
Anhydrous 2- propanol	Sigma-Aldrich	99.5 %	$(CH_3)_2CHOH$
Hydrochloric acid	Sigma-Aldrich	37 %	HCl

4.4.2. Cleaning procedure for glass substrates

To clean glassware and SLS substrates the experimental procedure given in the *Section 3.4.2* was used.

4.4.3. Preparation of ITO nanoparticle suspensions

As stated earlier, there are two ways for the stabilization of inorganic nanoparticles in liquid media; *i. electrostatic stabilization, ii. steric stabilization*. In the electrostatic stabilization, surface charges of particles are controlled by adjusting the pH of suspension in order to create repulsive forces between charged particles. In other words, the zeta potential is increased by adjusting pH for achieving stabilization. On the other hand, in steric stabilization, surface activating chemicals are used to minimize the physical interaction between particles. Particularly, the stabilization of ITO nanoparticles in alcohol-based systems is generally obtained by steric means. It is reported that the repulsive forces created between particles cannot overcome the van der Walls forces due to low dielectric constant of alcohol entities and these systems tend to agglomerate.

In this current study, only acetylacetone and propanol were used as organic solvent for nitrate based standard sol formulation. Dielectric constants of the respective chemicals at 25 °C (room temperature) were 23.1 and 20.1, for acetyacetone and 2-propanol, respectively. Since these two values are not significantly different, 2-propanol which is more cost-effective and less hazardous than acetylacetone was chosen as the continuous phase or solvent.

As it is stated above, steric stabilization is the general method for the stabilization of ITO nanoparticles (ITONP) in an organic solvent. However, this method is not selected in this study since addition of extra organics into the sol during stabilization can induce some additional problems. These organic groups can be excluded from the sol only the heat treatment, and this may cause the formation of pores resulting in characterization in the electrical and optical properties. For that reason, the electrostatic stabilization approach has been employed.

First, in order to investigate the electrical properties of ITO nanoparticles in organic solvent, depending on the pH value, the zeta potential measurement were performed. ITONP were added into 10 mL of 2-propanol containing beakers at fixed particle concentration of 0.001 M. And then, each suspension was prepared by adding $HCl_{(aq)}$ and/or $NaOH_{(aq)}$ solutions until a constant, pre-determined pH value was obtained. The studied pH values were pH 4, pH 5, pH 6, pH 7, pH 8 and pH 9. The curve of zeta potential change obtained from prepared suspension is shown in Figure 4.4. As can be seen from Figure 4.4 the zeta potential of nanoparticles increases with decreasing the pH of the suspension. Typically, the minimum required potential value to obtain a stable of colloidal system is ± 30 mV. It is a well-known fact that above this critical value, particles repulse each other due to the Coulomb forces and seperated suspensions can be formed, preventing agglomeration. The mentioned critical potential of ± 30 mV was achieved with the suspension, which is prepared at around pH 4. As a result, it is shown that ITONP can be dispersed in 2-propanol by electrostatic methods. Based on these findings, ITONP suspensions were prepared in 2- propanol (at pH 4) and these stable suspensions were employed in the subsequent studies.

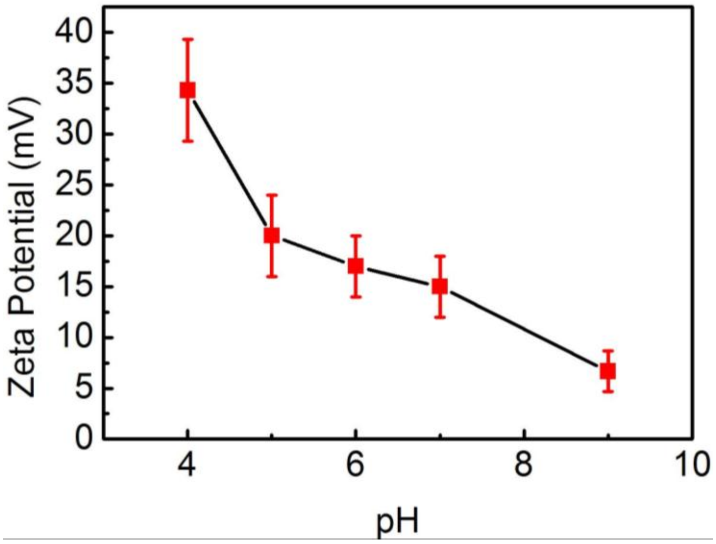

Figure 4.4 The change in the zeta potential of ITO nanoparticles in 2-propanol with diferent pH values. (The connecting lines are for visual aid).

4.4.4. Preparation of ITO nanoparticle incorporated ITO sol

Figure 4.5 shows the flowchart of preparation route of ITONP incorporated ITO coating sols. The molarity of ITONP suspension to be added was chosen as 0.001 M. However, hybrid coating mixtures containing different volumetric amounts of ITONP suspensions of different molarity were employed. The data shown in the flowchart also gives information about the hybrid coating concentration parameters. Sol preparation consist of following experimental procedures; first, $In(NO_3)_3 \cdot xH_2O$ (10 g) was dissolved in acetylacetone (50 mL) at 25 °C, and refluxed at 80 °C for 3 h. In reflux, solution was immerged into the water bath of 80 °C in order to keep the solution temperature constant and homogeneous.

Solution and water bath was continuously stirred with a magnetic stirrer and heated periodically by an electrical heater. During reflux process, color of the sol was first observed light yellow and became darker and eventually turned to dark brown. After refluxing, the sol was cooled to room temperature (25 °C).

Meanwhile, 10 mL propanol was poured into a 25 mL beaker and pH value of 2-propanol was adjusted to pH4 by adding $HCl_{(aq)}$ solution. 0.025 g ITONP (%99.9 purity) was added in 2-propanol:HCl solution. After ITONP addition, pH of the suspension was continuously measured and stirred with a magnetic stirrer at 800 rpm. Stabilization duration of suspension takes about 2 hours. After this process the color of the suspension became clear, which was light yellow at the beginning.

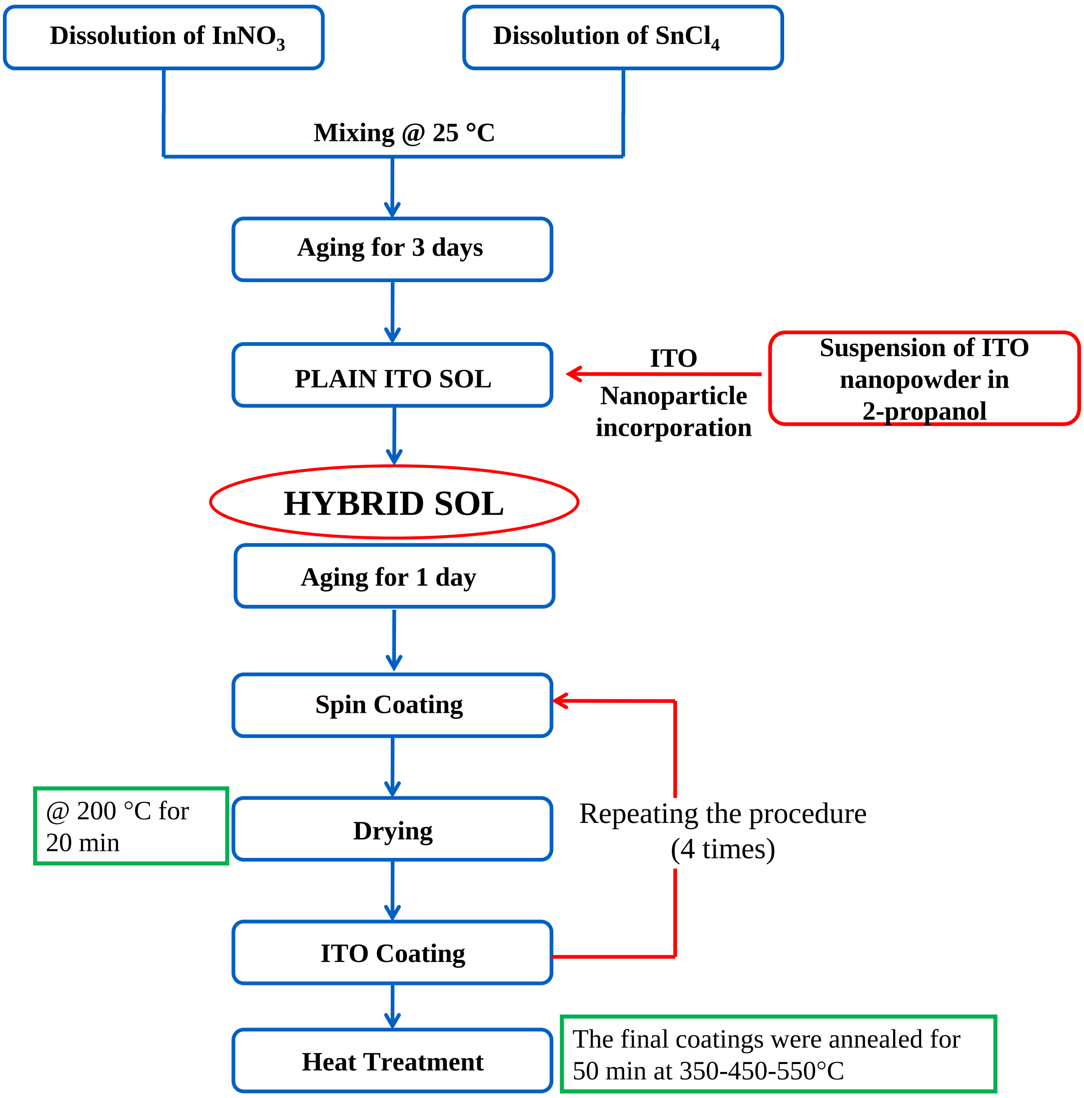

Figure 4.5 Preparation of ITONP incorporated ITO thin films.

The last step of the preparation of ITONP-added ITO sol was the addition of the ITONP suspension in ITO sol. For this process, in order to find optimum amount of ITONP incorporation, two different suspension deposition routes were followed (Figure 4.6). In first route, ITONP suspension prepared with a molarity of 0.001 M then various volumetric amounts of suspension was incorporated into the ITO sol. In the second route, ITONP suspensions were prepared with different molarities (0.002 to 0.2 M) and incorporated in ITO sol with a fixed volume of 100 µL. ITONP incorporation process was conducted while ITO sol was stirred at

800 rpm. After incorporation of ITONP suspension into ITO sol, the mixture was aged for 1 day at room temperature of 25 °C.

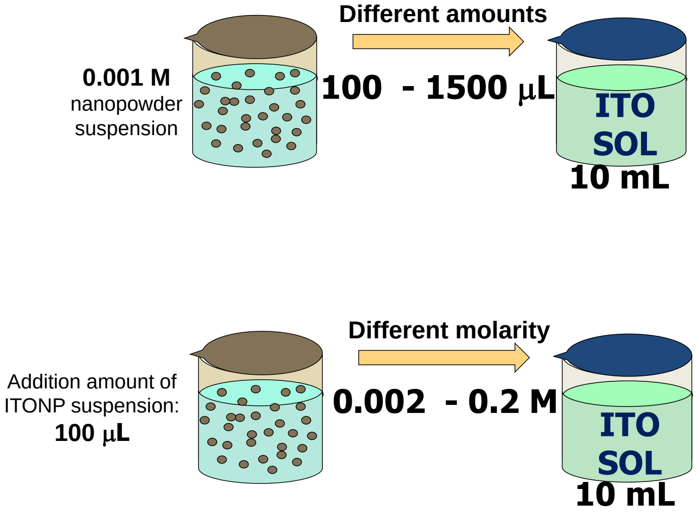

Figure 4.6 Schematic representation of ITONP incorporation into ITO sol.

4.4.5. Deposition of ITONP incorporated ITO thin films: coating procedure

The main objective of the experimental design based on molarity or volume of incorporated ITONP suspension was to determine the optimum mixture concentration resulting in an improvement in the functional properties. Two different sets of experiments were performed. The coating mixture formulations are summarized in Table 4.2 and Table 4.3. Table 4.2 shows the formation parameters, with respect to *volume* and Table 4.3 with respect to *molarity* of the ITONP suspension in the final mixture, respectively.

In preparation of the coating mixtures listed in Table 4.2, first ITO sol was prepared (according to the experimental protocol expalined in *section 3.4.3.1*). meanwhile, 0.025 g ITONP containing suspension stabilized in 10 mL of 2-propanol was prepared at pH 4. Then different volumetric amounts of (100, 200, 300, 500, 700 and 1500 μL) suspension was added into the 10 mL ITO sol. Finally, the hybrid mixtures were aged at room temperature for 1 day.

The preparation routine of the coating mixtures listed in Table 4.3 was similarly started with the preparation of unmodified/plain ITO sol (according to the experimental protocol explained in *section 3.4.3*). The different molarity (0.002, 0.004, 0.008, 0.015, 0.02, 0.03, 0.04, 0.05, 0.075 and 0.2 M) suspensions formed by dispersing proper amounts of ITONP in 10 mL of 2- propanol at pH4. Then, fixed volumetric amounts (100 µL) of suspensions were added into the 10 mL ITO sol. Finally, the hybrid mixtures were aged at room temperature for 1 day.

Spin coating technique was used for coating of ITONP-added ITO sol on SLS glass substrates. Laurell WS-400B-6NPP-LITE model spin coater was used for this process. During coating process, 120 μL volume of ITONP-added coating sols was poured on 25 x 25 mm glass substrates by a micropipette, then spinned at 3000 rpm for 30 s.

After the coating process, samples were dried at 175 °C for 10 min before applying subsequent coating. This process was repeated 4 times for each sample. Samples were finally heat treated at 550 ºC for 1 h.

Table 4.2 The preparation of coating mixtures with different ITONP suspension volumetric amounts.

Molarity of ITONP Suspension (M)	Incorporated ITONP Suspension Volume (μL)	Volume of ITO Sol (mL)
0.001	100	10
0.001	200	10
0.001	300	10
0.001	500	10
0.001	700	10
0.001	1500	10

Table 4.3 The preparion of coating mixtures with different ITONP suspension molarities.

Concentration ITONP Suspension (mol/L)	Amount of ITONP-Containing Suspension (µL)	Volume of ITO Sol (mL)
0.002	100	10
0.004	100	10
0.008	100	10
0.015	100	10
0.02	100	10
0.03	100	10
0.04	100	10
0.05	100	10
0.075	100	10
0.2	100	10

4.5. Materials characterization

Previsously described analytical techniques (*Section 3.5)* were employed in materials characterization with an additional technique, atomic force microscope (AFM). Details of this method is given below.

4.5.1. Atomic force microscopy

AFM was used to investigate the surface roughness ITONP-incorporated ITO thin films. The coating surfaces of selected samples were imaged using VeecoNanoscope V atomic force microscope in Tapping Mode using a silicon sharpened tip (nominal tip radius of 5–10 nm) at a scan rate of 1 Hz. Multiple scans of 1×1 µm size were captured at multiple locations on the same film surface in order to ensure representative images.

4.6. The effect of ITO nanoparticle incorporation on optoelectronic and microstructural properties of ITO sol-gel films

4.6.1. Effect incorporated ITO nanoparticle suspension volume

The XRD diffractograms of the ITO films obtained from hybrid mixtures listed in Table 4.2 are shown in Figure 4.7. The XRD findings show that with increasing amount of ITONP suspension addition, the crystal quality reduces as implied by lower intensity of the peaks. This is more obvious for the films obtained with highest ITONP incorporation (1500 µL).

Figure 4.8 shows the UV-Vis spectra of the same samples. All coatings have high optical transmittance and it is observed that ITONP addition did not significantly affected the optical performance of the coatings. Almost all coatings have optical transmittance of around 93 % in the visible light spectrum (≈400-700 nm). On the other hand, as seen in Figure 4.8, ITO thin films prepared with ITONP suspension addition of 100 and 200 µL have higher absorption edge in 300 nm wavelength. However, light absorption was reduced as the amount of ITONP addition increased.

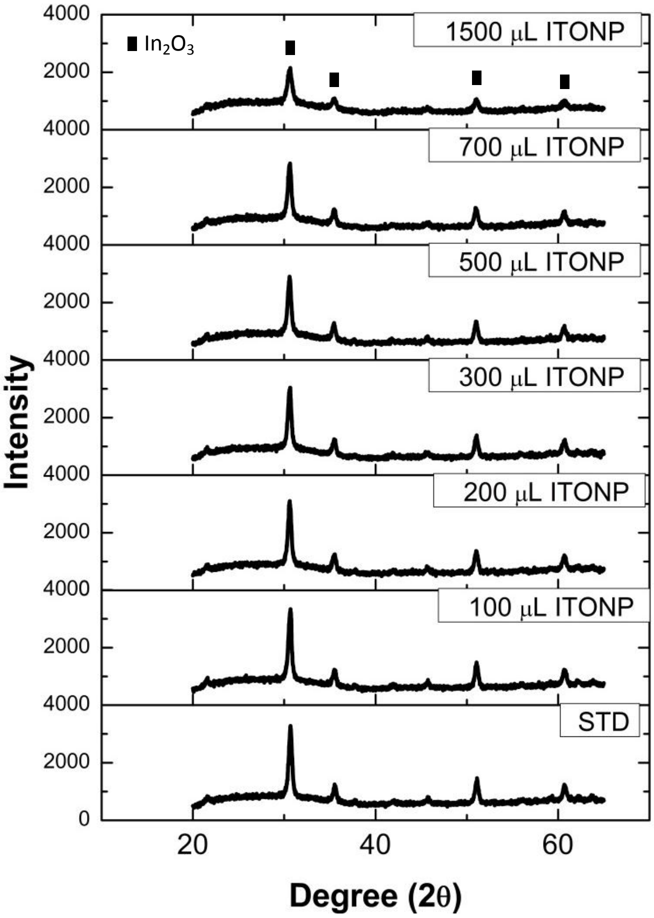

Figure 4.7 XRD diffractograms of ITO films prepared with various volumes of ITONP suspension addition into ITO sol.

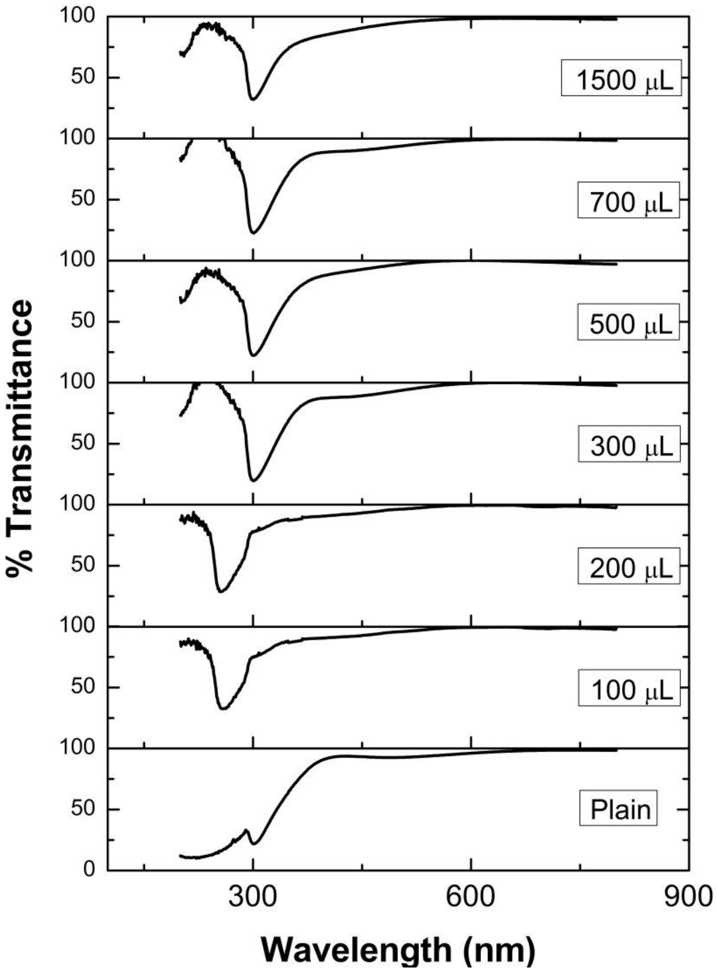

Figure 4.8 UV-Vis spectra of ITO films prepared with various volumes of ITONP suspension addition into ITO sol.

The sheet resistance of the hybrid ITO thin films are shown in Figure 4.9. The standart deviations were indicated by the error bars. As seen in related figure, sheet resistance of coatings prepared with standard ITO sol was found to be 1.5 kOhm/sqr, and decreased to 1.2 kOhm/sqr when the thin films prepared with 100 μL ITONP suspension incorporation. However above this critical value, sheet resistance increased with increasing incorporation volume of ITONP suspension, and a maximum resistivity of 3.5 kOhm/sqr was obtained for 1500 μL ITONP suspension addition. As a result, it is seen that electrical properties can be improved limitedly with small amount of ITONP suspension addition, and negatively affected above this critical value. The reason of poor electrical properties above the critical point might be due to the presence of Cl^- ions which was added in ITONP suspension as $HCl_{(aq)}$ in order to obtain elecrostatic stabilization. It is well known that, such ionic impurities adversely affect the electrical conductivity.

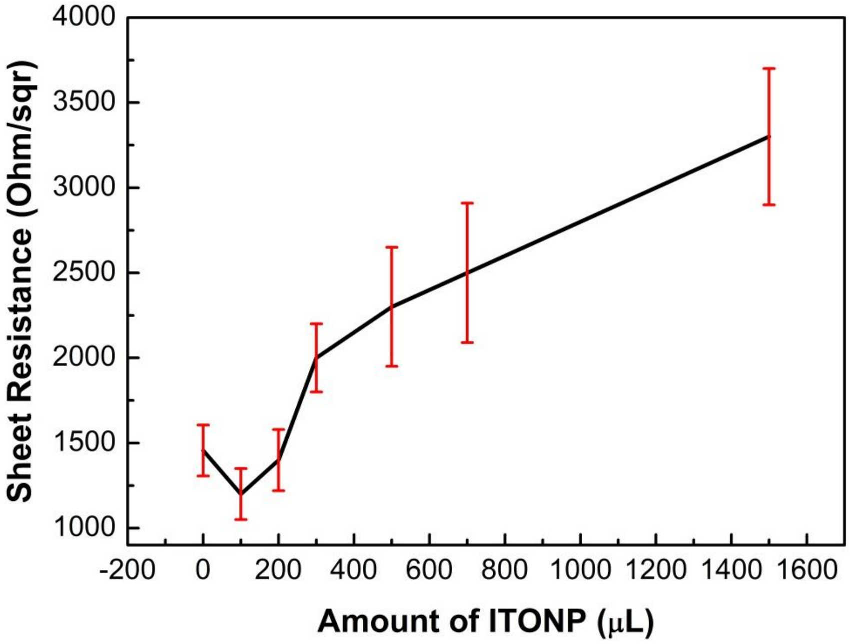

Figure 4.9 Sheet resistance measurements of ITO films prepared with various volumes of ITONP suspension incorporation into ITO sol. (The connecting lines are for visual aid).

4.6.2. Effect incorporated ITO nanoparticle suspension molarity

Figure 4.10 shows the XRD diffractograms of the films heat defined using the hybrid mixtures listed in Table 4.3. As seen in the figure, crystal quality of coating was improved using ITONP suspension with critical value of 0.008 M. However, performance of the coating with regard to crystallization properties was reduced with increasing the suspension molarity.

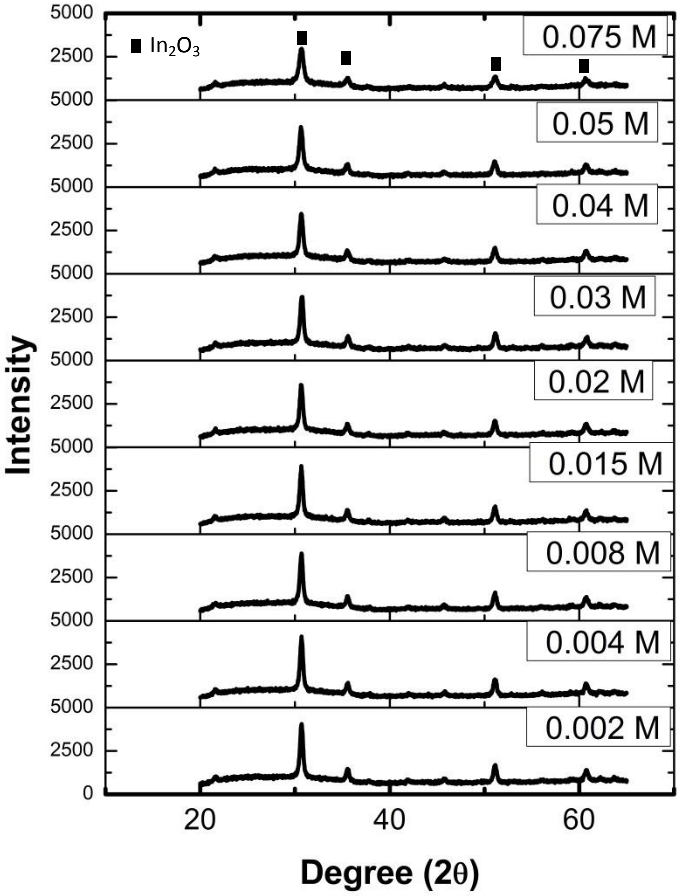

Figure 4.10 XRD diffractograms of ITO thin films prepared by the addition of fixed amount of ITONP suspension with various molarity.

Figure 4.11 shows the optical transmittance measurement of the second set of hybrid thin films (Table 4.3). For the films prepared by low molarity ITONP suspension addition showed optical transmittance values in the range of 88- 93 % in the visible range. However, with increasing ITONP suspension molarity, optical transmittance of thin films gradually decreased to 83- 85 %

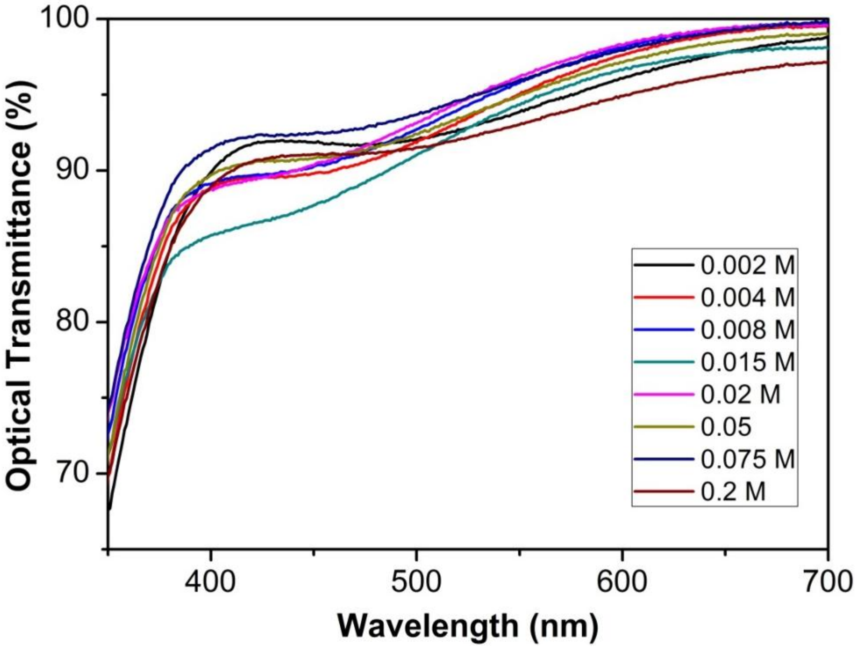

Figure 4.11 Optical transmittance of thin films prepared by a fixed amount of ITONP suspension with various molarity.

Figure 4.12 shows the change in sheet resistance of thin films of the thin films listed in Table 4.3. Sheet resistance of coatings prepared with plain/unmodified ITO sol was found to be 1.5 kOhm/sqr and decreased to 0.9 kOhm/sqr for the coating prepared with the incorporation 100 μL ITONP suspension into ITO sol at a molarity of 0.008M. However above 0.008M, sheet resistance decreased with increasing molarity of ITONP. The maximum sheet resistance was found to be 4 kOhm/sqr when the 0.2M of ITONP suspension was added. As a result, electrical properties was enhanced up to a critical addition of ITONP suspension additon which was considered as critical value, and electrical properties affected negatively above this point.

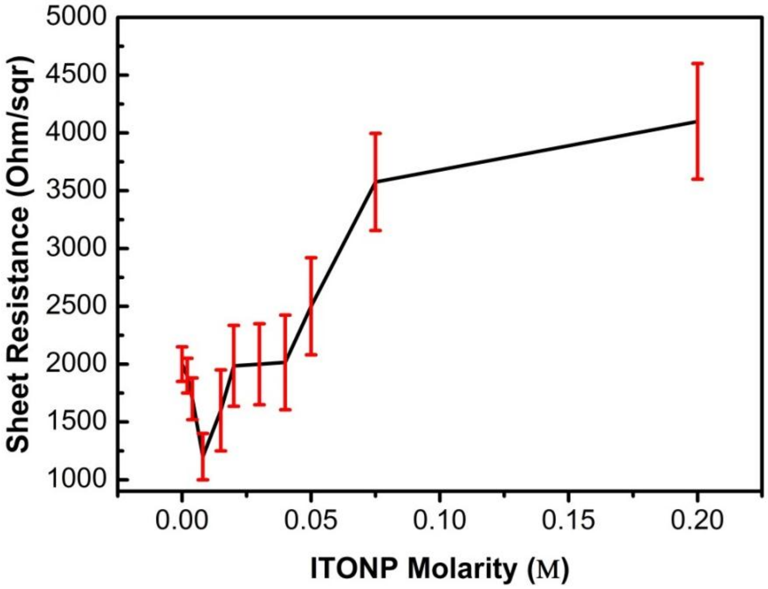

Figure 4.12 Sheet resistance of ITO films prepared with various molarities of ITONP suspension incorporation into ITO sol. (The connecting lines are for visual aid).

Figure 4.13 shows SEM images of films listed in Table 4.3. At high molarity ITONP suspension incorporation levels, such as 2.0 M, highly smooth and small grain sized morphology was observed. However, with decreasing molarity of ITONP suspension, the surface morphology becomes relatively rough and grain size gradually increases. This effect can be explained by ITONP incorporation. The incorporated nanoparticles might act as nucleation sites or seeds and allow the formation numerous number crystallites with small size.

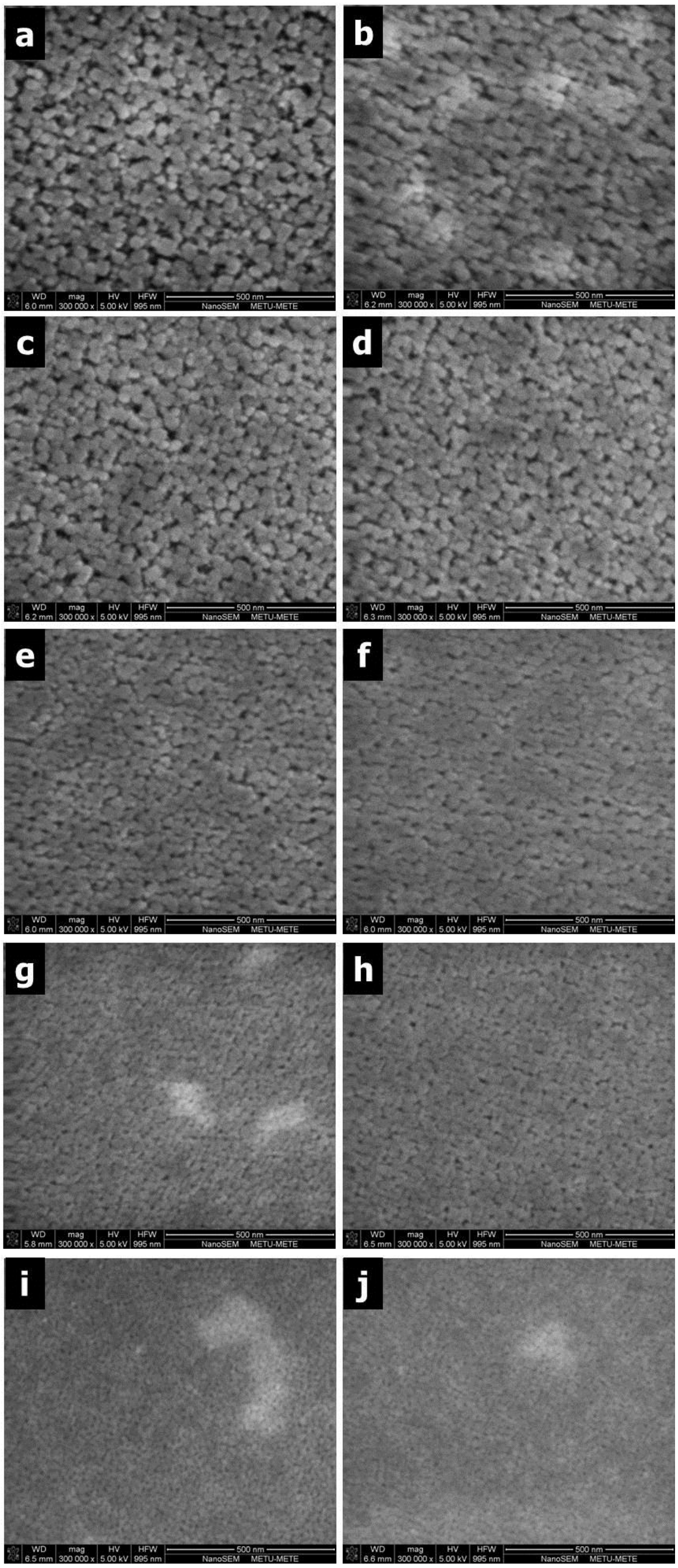

Figure 4.13 SEM images of ITO thin films prepared by various molarity ITONP incorporation into ITO sol. a) 0.002, b) 0.004, c) 0.008, d) 0.015, e) 0.02, f) 0.03, g) 0.05, h) 0.075, i) and j) 0.2 M.

Surface morphology of some representative thin films were also analyzed by AFM in order to support the results obtained from SEM. Another reason for performing AFM analysis was to investigate the grain size and surface roughness of thin films. Figure 4.14 shows the surface morphology of thin films prepared by various molarity ITONP suspension incorporated ITO thin films. It is seen that surface roughness was reduced with ITONP incorporation. Surface roughness of thin films was reduced to 1 nm with increasing the molarity of ITONP suspension to 0.2 M, while it was measured to be 3.4 nm for plain/unmodified ITO thin films. In other words, ITONP suspension with high molarity causes formation of nanoparticle which were currently crystals. Each nanoparticle acts as a seed and allows the new crsytal to grow on its surface during calcination process. As a conclusion, ITO thin films with very small grain size and low surface roughness can be prepared.

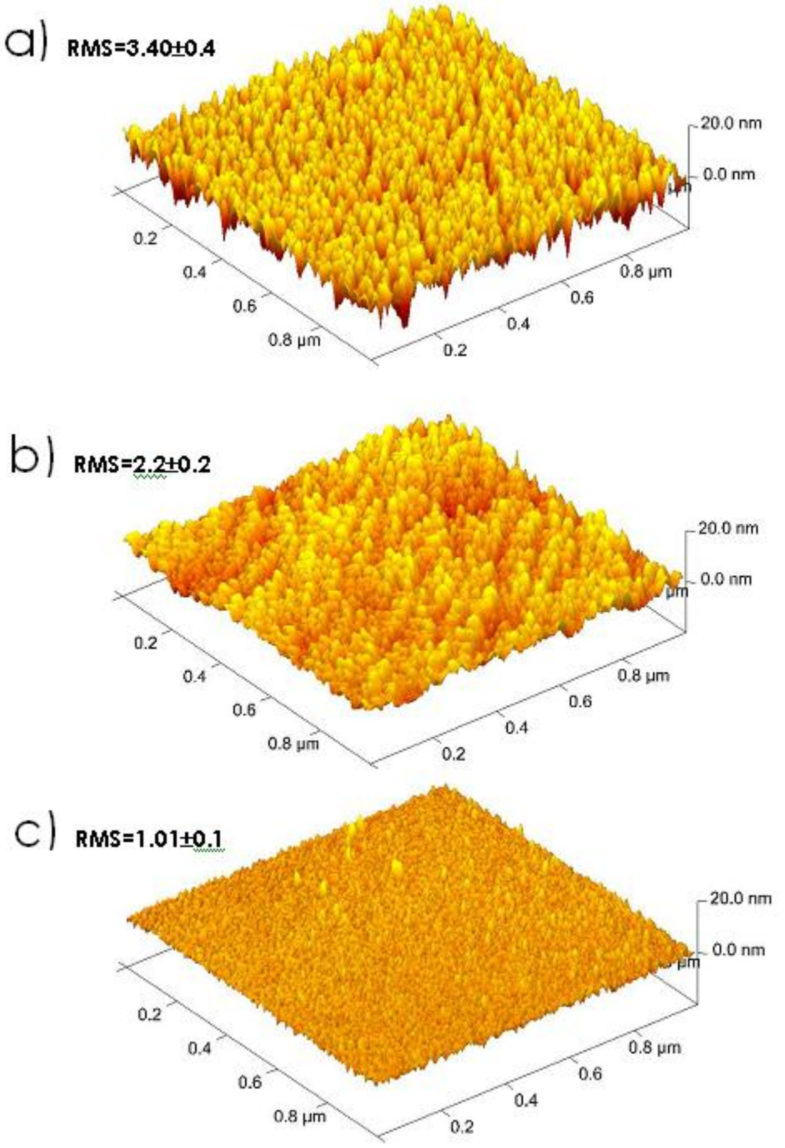

Figure 4.14 AFM images of thin films prepared with a) plain/unmodified ITO sol, b) 0.02 M ITONP, c) 0.2 M ITONP and heat treated at 550 °C. Surface roughness is reduced as molarity of ITONP suspension was increased.

CHAPTER 5

CONCLUSIONS

This thesis includes two parts: *i)* investigation of effect of sol-gel processing parameters on electrical, optical, microstructural and structural properties of plain ITO thin films, *ii)* investigation of the effect of ITO nanoparticle incorporation into ITO coating sol on electrical, optical, microstructural and structural properties of somewhat novel hybrid sol-gel ITO thin films.

i) Effect of sol-gel processing parameters on functional properties of plain ITO thin films

Indium tin oxide (ITO) thin films were successfully fabricated using nitrate-based or chloride-based indium precursors and tin chloride via sol-gel processing. The process parameters for fabrication of plain/unmodified ITO thin films was studied as a function of heat treatment temperature, spin rate, spin time, number of coating, sol molarity and sol aging. This detailed study was necessary in order to determine optimum fabrication conditions of sol-gel derived ITO thin films. XRD results revealed that, higher heat treatment temperatures in the range of 350 to 600 ºC results in ITO thin films of relatively high crystal quality. The minimum sheet resistance and maximum optical transmittance was achieved by heat treatment in air at 550 ºC for 1 h. The grain size was increased with increasing heat treatment temperature. The coating operation parameters also affect the final properties of ITO thin films. The electrical conductivity is related with the spin coating parameters. The sheet resistance of the ITO thin films increased continuously when the spin rate increased from 500 rpm to 8000 rpm, due to decrease in the film thickness. Films formed at low spin rates thin films showed poor optical transmittance due to poor surface uniformity and discontinuous microstructure, leading to dark-yellowish color contours. The optimized spin rate was determined as 3000 rpm. On the other hand, optical and structural properties of thin films did not clearly affected by spin time. However, sheet resistance was increased with increasing spin time. The optimized spin time was found as 30 s. Both, crystallinity and electrical conductivity of thin films were improved by increasing number of coating operations. However, the optical transmittance was decreased with increasing number of coating layers. The lower optical performance is due to increased film thickness. Additionally, the effect of coating sol molarity (precursors amount:solvent) on functional properties ITO thin films was investigated. The higher molarity for the coating sols resulted in lower sheet resistance and transmittance. The sols with molarities of 0.8 M and 1.0 M are better for fabricating good quality ITO thin films. The surface roughness and grain size were both increased when highly concentrated coating sols were used, as revealed by SEM investigations. Finally, an original thermal treatment –induce aging- was implanted to the coating sols prior to deposition. The results revealed that, optoelectronic and microstructural properties of ITO thin films improved by induce aging. The optimized induce aging time and temperature was set as 3h and 80 °C, respectively.

ii) Effect of ITO nanoparticle incorporation on functional properties of hybrid ITO thin films

In the second part of thesis ITO nanoparticle (ITONP) incorporated ITO thin films were fabricated using stabilized nanoparticle suspensions. A study was conducted to figure out the optimum ITONP suspension incorporation conditions. This was done by incorporating different volumetric amounts and molarities (ITONP:2-propanol) of ITONP suspensions into plain ITO sol. First, a colloidal chemistry analysis was performed to define the electrostatic stabilization condition for the ITONP suspensions. An acidic suspension pH (at around pH 4) provided well-dispersed suspensions. The functional properties of ITONP-incorporated (0.008 M and 100 µL) hybrid ITO thin films were compared to that of the plain ones fabricated with using same processing parameters and a significant enhancement was observed in the functional properties. The optoelectronic performance of ITO thin films were improved by 100 µL and 0.008 M ITONP suspension addition into

ITO sol. However, with increasing incorporated suspension volume or suspension molarity, performance of ITO thin films gradually decreases. The, surface roughness of ITO thin films prepared using nanoparticle added coating sols were found to be lower than the unmodified ones.

REFERENCES

[1] C.G. Granqvist, A Hultåker, Thin Solid films, 411, 1 (2002)

[2] K. Badeker, Annual Physics 22, 749 (1907)

[3] E. Leja, K. Budzynska, T. Pisarkiewicz, T. Stapinski, Thin Solid Films, 100, 203 (1983)

[4] N. Miyata, K. Miyake, K. Koga, T. Fukushima, Journal of Electrochemical Society, 127, 918 (1980)

[5] T. Pisarkiewicz, K. Zakrzewska, E. Leja, Thin Solid Films, 153, 479 (1987)

[6] E. Leja, T. Stapinski, K. Marszalek, Thin Solid Films, 125, 119 (1985)

[7] J. N. Avaritsiotis, R. P. Howson, Thin Solid Films, 77, 351 (1981)

[8] N. Ito, Y. Sato, P.K. Song, A. Kaijio, K. Inoue,Y. Shigesato, Thin Solid Films 496, 99 (2006

[9] C. A. Pan, T. P. Ma, Journal of Electronic Materials, 10, 43 (1981)

[10] D.S. Ginley, "Handbook of Transparent Conductors" Springer (2010).

[11] S. Lany and A. Zunger, Physical Review Letters, 98, 045501 (2007).

[12] H. Kawazoe, M. Yasukawa, H. Hyodo, M. Kurita, H. Yanagi and H. Hosono, Nature, 389, 939 (1997).

[13] A. Kudo, H. Yanagi, H. Hosono and H. Kawazoe, Applied Physics Letters 73, 220 (1998).

[14] M. Joseph, H. Tabata and T. Kawai, Japanese Journal of Applied Physics Part 2-Letters 38, L1205 (1999).

[15] T. Yamamoto and H. Katayama-Yoshida, Japanese Journal of Applied Physics Part 2-Letters, 38, L166 (1999).

[16] A. Tsukazaki, A. Ohtomo, T. Onuma, M. Ohtani, T. Makino, M. Sumiya, K. Ohtani, S.F. Chichibu, S. Fuke, Y. Segawa, H. Ohno, H. Koinuma and M. Kawasaki, Nature Materials 4, 42 (2005).

[17] G.Rupprecht, Z.Physics, 139, 504 (1954)

[18] V. Seshadri and G.A. Sotzing, Optical Science and Engineering 99, 495 (2005)

[19] F. Jonas and S. Kirchmeyer, Jahrbuch Oberflaechentechnik 62, 162 (2006).

[20] H. Okuzaki, Kobunshi Kako, Thin Solid Films, 54, 367 (2005).

[21] G. Eda, Y.Y. Lin, S. Miller, C.W. Chen, W.F. Su and M. Chhowalla, Applied Physics letters 92, 233 (2008).

[22] X. Wang, L.J. Zhi and K. Mullen, Nano Letters 8, 323 (2008).

[23] Jan Matthijn Dekkers, University of Twente Doctoral Dissertation, (1997)

[24] J. Karlsson and A. Roos, Thin Solid Films 392, 345 (2001)

[25] A. Stadler, Materials, 5, 661 (2012)

[26] H. Ohsaki and Y. Kokubu, Thin Solid Films 351, 1–7 (1999).

[27] www.electronics.frost.com (accessed on June 2012)

[28] www.electronics.frost.com (accessed on June 2012)

[29] K. Hara; H. Arakawa, in: Handbook of Photovoltaic Science and Engineering, A. Luque; S. Hegedus, (Eds.) John Wiley and Sons: New York, 663, (2003)

[30] B. O'Regan; M. Gratzel, Nature, 353, (6346), 737 (1991)

[31] K.Takahashi; M.Konagai, Amorphous Silicon Solar Cells, 102 (1983).

[32] C. Beneking; B. Rech; S. Wieder; O. Kluth; H. Wagner; W. Frammelsberger; R. Geyer; P. Lechner; H. Rübel; H. Schade, Thin Solid Films 351, (1-2), 241 (1999)

[33] http://www.ornl.gov/info/press_releases/photos/nanocone_solar_cell_illustr. jpg (accessed on June 2012)

[34] D. E. Williams, Sensors and Actuators B: Chemical 57, (1-3), 1-16 (1999)

[35] H.Gläser, Large Area Glass Coating, 1st english edition. Von Ardenne Anlagentechnik GmbH, Dresden (2000)

[36] http://www.captec-group.com/wp-content/uploads/iphone-11.gif (accessed on June 2012)

[37]http://www.zerobuildings.com/wpcontent/uploads/2010/12/electrochromatic_ window_dark_light.gif (accessed on June 2012)

[38] B. G. Lewis, D. C. Paine, MRS Bull, August, 22-27 (2000)

[39] R. Barber, G. Pryor, and E. Reinheimer, SID Digest of Technical Papers 28, 18 (1998)

[40] T. Saito, K. Kanna, T. Inoue, and S. Morikawa, SID Digest of Technical Papers, 26, 28 (1995)

[41] http://news.thomasnet.com/fullstory/EMI-Shielding-Film-suits-dynamic-flex-operations-465209 (accessed on June 2012)

[42] H. Kawazoe, H. Yanagi, K. Ueda, H. Hosono, MRS Bull. 25, 28 (2000)

[43] R. Gordon, MRS Bulletin, 25, 52 (2000)

[44] P. Drude, Annual Physics, 3, 369 (1990).

[45] F. Simonis, M. van der Leij & C.J. Hoogendoorn, Solar Energy Materials, 1, 221 (1979)

[46] N.Ashcroft, N.Mermin, Solid State Physics, Saunders College, Philadelphia, (1976)

[47] Naji Al-Dahoudi, Universität des Saarlandes Doctoral Dissertation, (2003)

[48] K.Chopra, S.Major, D.Pandya, thin solid films 102 (1983).

[49] Mathew Robert Waugh, University College London Doctoral Dissertation (2011)

[50] K.Chopra, I. Kaur, Thin Film Device and Applications, Plenum Press, New York (1983)

[51] A.Elshabini, F.Barlow, Thin Film Technology Handbook, McGraw-Hill, New York (1998)

[52] J.Anderson, M.Boudart, Catalysis:Science and Technology, 1, Springer-Verlag, Berlin (1981)

[53] D.Talbot, J.Talbot, Corrosion Science and technology, CRC Press, Boca Raton (1998)

[54]http://materials.web.psi.ch/Research/Thin_Films/Methods/Images/MOCVD_sc.jpg (accessed on June 2012)

[55] D.Glocker, S.Shah, Handbook of Thin Film Process Technology, Institute of Physic Publishing, Bristol (1995)

[56] M.Ohring, The Material Science of Thin Films, Academic Press, INC., San Diego (1992)

[57] http://www.umms.sav.sk/index.php?ID=415 (accessed on June 2012)

[58] H.Pulker, Coatings on glass, second revised edition. Elsevier Science, Amsterdam (1984)

[59] B. E. Aperathitis, M. Modreanu, M. Bender, Thin Solid Films, 450, 101 (2004)

[60] H.Schröder, Physics of thin films, Academic Press, New York (1969)

[61] http://ej.iop.org/images/0268-1242/19/6/019/Full/sst174196fig01.jpg (accessed on June 2012)

[62] C. J. Brinker, G. W. Scherer, Sol-gel Science, Academic Press, New York (1990)

[63] C. N. R. Rao, A. Muller, A. K. Cheetham, The Chemical of Nanomaterials, Vol. 2, Wiley-Vch Verlag GmbH & Co. KgaA, Weinheim, 372 (2004)

[64] A. C. Pierre, Introduction to the Sol-gel Processing, Kluwer Academic Publishers, 1, (1998)

[65] http://www.centexbel.be/solgel-treatment (accessed on June 2012)

[66] R. Schwartz, T. Schneller, R. Waser, C. R. Chimie, 7, 433 (2004)

[67] http://www.solgel.com/articles/nov00/Image247.gif (accessed on June 2012)

[68] L.Landau, B.Levich, Acta Physiochem 17, 42 (1942)

[69] C. Bornside, C.W. Macosko and L. E. Scriven, Journal of Applied Physics, 66, 5185 (1989)

[70] http://www.free-photos.biz/images/science/chemistry/solgel_spincoating.jpg (accessed on June 2012)

[71] C. J. Brinker, A. J. Hurd, P. R. Schunk, et al., Journal of Non-Crystalline Solids 147-148, 424 (1992)

[72] N. Nadaud, N. Lequeux, M. Nanot, Journal of Solid State Chemistry, 135, 140 (1998)

[73] J. Fan and J. Goodenough, Journal of Applied Physics, 48 (8), 3524 (1977)

[74] C. T. Prewitt, R. D. Shannon, D.B. Rogers, Inorganic Chemistry, 8, 1985 (1969)

[75] P. Nath and R. F. Bunshah, Thin Solid Films, 69, 63 (1980)

[76] S. M. Kim, K. H. Seo, J. H. Lee, Journal of the European Ceramic Society, 26, 73 (2006)

[77] C. P. Udawatte, K. Yanagisawa, S. Nasu, Journal of Solid State Chemistry, 154, 444 (2000)

[78] J. S. Lee and S. C. Choi, Journal of the European Ceramic Society, 25, 3307 (2005)

[79] L. Gupta, A. Mansingh and P. K. Srivastava, Thin Solid Films, 176, 33 (1989)

[80] R. H. Tahar, T. Ban, Y. Ohya, Journal of Applied Physics, 83, 2631 (1998)

[81] J. W. Bae, H. J. Kim, J. S. Kim, Surface and Coatings Technology, 131, 196 (2000)

[82] S. Sakka, Handbook of Sol-gel Science and Technology: Volume I Sol-gel Process, Kluwer Academic Publishers, London, 60-76 (2004)

[83] C. Brinker, G. Frye, A. Hurd, Thin Solid Films, 201, 97 (1991)

[84] S. B. Majumder, M. Jain, P. S. Dobal, Materials Science and Engineering B, 103, 16 (2003)

[85] S. Bandyopadhyay, G. K. Paul, R. Roy, Materials Chemistry and Physics, 74, 83 (2002)

[86] J. H. Lee, B. O. Park, Thin Solid Films, 426, 94 (2003)

[87] M. Dutta, S. Mridha, D. Basak, Applied Surface Science, 254, 2743 (2008)

[88] J. G. Na, Y. R. Cho, Y. H. Kim, Journal of American Ceramic Society, 72-4, 698 (1989)

[89] K. L. Chopra, S. Major and D. K. Pandya, Thin Solid Films, 102, 1 (1983)

[90] E. Elangovan, A. Marques, A. Pimentel, Vacuum, 82, 1489 (2008)

[91] J. N. Avaritsiotis, R. P. Howson, Thin Solid Films, 77, 351 (1981)

[92] S. R. Ramanan, Thin Solid Films, 389, 207 (2001)

[93] W. Tang and D. C. Cameron, Thin Solid Films, 238, 83 (1994)

[94] M. Ohyama, H. Kozuka, T. Yoko, Journal of American Ceramic Society, 81, 1622 (1998)

[95] M. J. Alam and D. C. Cameron, Thin Solid Films, 377-378, 455 (2000)

[96] E. Shigeno, K. Shimizu, S. Seki, Thin Solid Films, 411, 56 (2002)

[97] X. Zhang , W. J. Wu, T. Tian, Materials Research Bulletin, 43, 1016 (2008),

[98] K. Nishio, T. Sei, T. Tsuchiya, Journal of Materials Science. 31, 1761 (1996)

[99] Y. Takahashi, S. Okada, R.Tahar, K.Nakano, Journal of Non-Crystalline Solids 218, 129 (1997)

[100] R. Tahar, T. Ban, Y. Ohya, Y. Takahashi, Journal of American Ceramic Society 84, 85 (2001)

[101] R. Tahar, T. Ban, Y. Ohya, Y. Takahashi, Journal of Applied Physics 83, 2139 (1998)

[102] M. J. Alam, D. C. Cameron, Surface and Coatings Technology, 142-144, 776 (2001)

[103] M. Gross, A. Winnacker, P. Wellmann, Thin Solid Films, 515, 8567 (2007)

[104] M. J. Alam and D. C. Cameron, Thin Solid Films, 377-378, 455 (2000)

[105] R. Ota, S. Seki, M. Ogawa, T. Nishide, A. Shida, M. Ide, Y. Sawada, Thin Solid Films 411, 42 (2002)

[106] M. Wakagi, K. Chahara, K. Onisawa, Y. Kawakubo, T. Kichikawa, T. Satoh, T. Minemura, Thin Solid Films 411 (2000)

[107] T. Kololuoma, J. Rantala, Electronics Letters 36, 172 (2000)

[108] J. Zhang, K. H. Au, Z. Q. Zhu, S. O’Shea, Optical Materials, 26, 42 (2004)

[109] C. Su, T. K. Sheu, Y. T. Chang, Synthetic Metals, 153, 9, 9 (2005)

[110] J. Liu, D. Wu, Zeng. S, Journal of Materials Processing Technology, 209, 3943 (2000)

[111] Z. H. Li, D. Y. Ren, Trans. Nonferrous Metallurgy Society of China, 16, 1358 (2006)

[112] H. M. Zhou, D. Q. Yi, Z. M. Yu, Thin Solid Films, 515, 6909 (2007)

[113] K. Daoudi, B. Canut, M.G. Blanchin, Thin Solid Films, 445, 20 (2003)

[114] S. S. Kim, S.Y. Choia, C. G. Park, H.W. Jin, Thin Solid Films, 347, 155 (1999)

[115] J. P. Chatelon, C. Terrier and J. A. Roger, Semiconductor Science and Technology, 14, 642 (1999)

[116] M. Toki and M. Aizawa, Journal of Sol-gel Science and Technology, 8 717 (1997).

[117] C. Goebbert, R. Nonninger, M. A. Aegerter, and H. Schmidt, Thin Solid Films, 351, 79 (1999).

[118] R. Nonninger, C. Goebbert, H. Shmidt, R. Drumm, and S. Sepeur," Patent DE 19849048 (2000)

[119] S. J. Hong, J. I. Han, Current Applied Physics, 6S1, 206 (2006)

[120] D. S. Cheong, D. H. Yun, D. H. Kim, K. R. Han, Journal of Korean Ceramic Society, 48-6, 516-519 (2011)

[121] L.Wang,W. Sigmund, F. Aldinger, Journal of American Ceramic Society 83 (4), 697 (2000)

[122] D.H. Napper, J. Steric Stabilization, Colloid Interface Science 58, 390 (1977)

[123] Lyklema, J. Fundamentals of Interface and Colloid Science, 2, 3208, (1995)

[124] D. Shaw, J. Introduction to Colloid and Surface Chemistry, 4th Edition, (1992)

[125] J. H. Adair, E. Suvaci, J. Sindel: In Encyclopedia of Materials: Science and Technology , (Elsevier Publishing) The Netherlands , 8996-9006.

[126] R.Hunter, Zeta Potential in Colloid Science, Academic Press, New York, (1981)

[127] H.Müller, Universität Potsdam Doktoral Dissertation (1997)

[128] R.Greenwood, K.Kendall, Brit. Ceramic Trans. 97, 174 (1998)

[129] H.Schmidt, R.Naß, D.Burgard, R.Nonniger, Materials Research Society Symposium Proceedings, California, 520, 21 (1998)